Technology Demonstrations Project:

Environmental Impact Benefits with "TX Active" Concrete Pavement in Missouri DOT Two-Lift Highway Construction Demonstration

National Concrete Pavement Technology Center

CP Tech Center

Final Report I
October 2012

IOWA STATE UNIVERSITY

Institute for Transportation

About the National CP Tech Center

The mission of the National Concrete Pavement Technology Center is to unite key transportation stakeholders around the central goal of advancing concrete pavement technology through research, tech transfer, and technology implementation.

Disclaimer Notice

The contents of this report reflect the views of the authors, who are responsible for the facts and the accuracy of the information presented herein. The opinions, findings and conclusions expressed in this publication are those of the authors and not necessarily those of the sponsors.

The sponsors assume no liability for the contents or use of the information contained in this document. This report does not constitute a standard, specification, or regulation.

The sponsors do not endorse products or manufacturers. Trademarks or manufacturers' names appear in this report only because they are considered essential to the objective of the document.

Non-Discrimination Statement

Technical Report Documentation Page

1. Report No. DTFH61-06-H-00011 Work Plan 22	2. Government Accession No.	3. Recipients Catalog No.
4. Title and Subtitle Technology Demonstrations Project: Environmental Impact Benefits with "TX Active" Concrete Pavement in Missouri DOT Two-Lift Highway Construction Demonstration		**5. Report Date** October 2012
		6. Performing Organization Code
7. Author(s) Tom Cackler, James Alleman, John Kevern, and Joel Sikkema		**8. Performing Organization Report No.**
9. Performing Organization Name and Address National Concrete Pavement Technology Center Iowa State University 2711 South Loop Drive, Suite 4700 Ames, IA 50010-8664		**10. Work Unit No. (TRAIS)**
		11. Contract or Grant No.
12. Sponsoring Organization Name and Address Federal Highway Administration U.S. Department of Transportation 1200 New Jersey Avenue SE Washington, DC 20590		**13. Type of Report and Period Covered** Final Report I
		14. Sponsoring Agency Code DTFH61-06-H-00011 Work Plan 22

15. Supplementary Notes

Visit www.cptechcenter.org for color PDF files of this and other research reports.

16. Abstract

This research effort evaluated the environmental impacts and benefits obtained from concrete paving materials blended with photo-chemically-active titanium dioxide (TiO_2). The project was completed in combination with a full-scale Missouri Department of Transportation (MoDOT) two-lift paving demonstration project in the St. Louis, Missouri urban area. Two innovative photo-catalytic concrete paving materials have been studied during this project, including: a) a photocatalytic concrete mainline pavement and b) a photocatalytic pervious concrete shoulder pavement. The mainline pavement material was applied using a two-lift paving strategy, where the lower, base-level layer was constructed with less expensive materials (e.g., a low cementitious-content base lift), and the thinner top wearing course was then overlaid immediately with concrete containing photocatalytically active cement. The included photocatalytic concrete paving material is marketed under the trade-name TX Active. The second shoulder pavement element involved a similar, photocatalytic concrete material also containing the titanium dioxide additive, although in this instance the TiO2 was blended into a pervious (rather than conventional) concrete for the roadside shoulder pavement material. Together, this set of innovative mainline and shoulder paving materials, including both a two-lift photocatalytic mainline pavement and a photocatalytic pervious shoulder pavement, is believed to represent one of the most technically advanced and environmentally-friendly concrete pavement systems ever employed in the US. Field-scale assessment of this innovative highway involved both passive and active air quality NO and NO_2 testing, respectively using integrative Ogawa samplers and a 2B Technologies ozone titration analyzer. This field-scale assessment also involves water-quality testing of mainline and shoulder pavement runoff.

17. Key Words		18. Distribution Statement No restrictions.	
19. Security Classification (of this report) Unclassified.	**20. Security Classification (of this page)** Unclassified.	**21. No. of Pages** 117	**22. Price** NA

Form DOT F 1700.7 (8-72)   **Reproduction of completed page authorized**

TECHNOLOGY DEMONSTRATIONS PROJECT: ENVIRONMENTAL IMPACT BENEFITS WITH "TX ACTIVE" CONCRETE PAVEMENT IN MISSOURI DOT TWO-LIFT HIGHWAY CONSTRUCTION DEMONSTRATION

Final Report I
October 2012

Principal Investigators
Tom Cackler
James Alleman
John Kevern

Authors
Tom Cackler, James Alleman, John Kevern, and Joel Sikkema

TABLE OF CONTENTS

LIST OF FIGURES

viii

LIST OF TABLES

Acknowledgments

EXECUTIVE SUMMARY

General Synopsis

This research effort was developed to evaluate and establish the environmental impacts, and projected benefits, obtained from concrete paving materials blended with photo-chemically-active titanium dioxide (TiO_2). The project was completed in combination with a full-scale Missouri Department of Transportation (MoDOT) two-lift paving demonstration project in the St. Louis, Missouri urban area.

Two innovative photo-catalytic concrete paving materials have been studied during this project, including the following:

- A photocatalytic concrete mainline pavement
- A photocatalytic pervious concrete shoulder pavement

The first such mainline pavement material was applied using a two-lift paving strategy, where the lower, base-level layer was constructed with less expensive materials (e.g., a low cementitious-content base lift), and the thinner top wearing course was then overlaid immediately with concrete containing photocatalytically active cement. The included photocatalytic concrete paving material is marketed under the trade-name, TX Active (Figure 1).
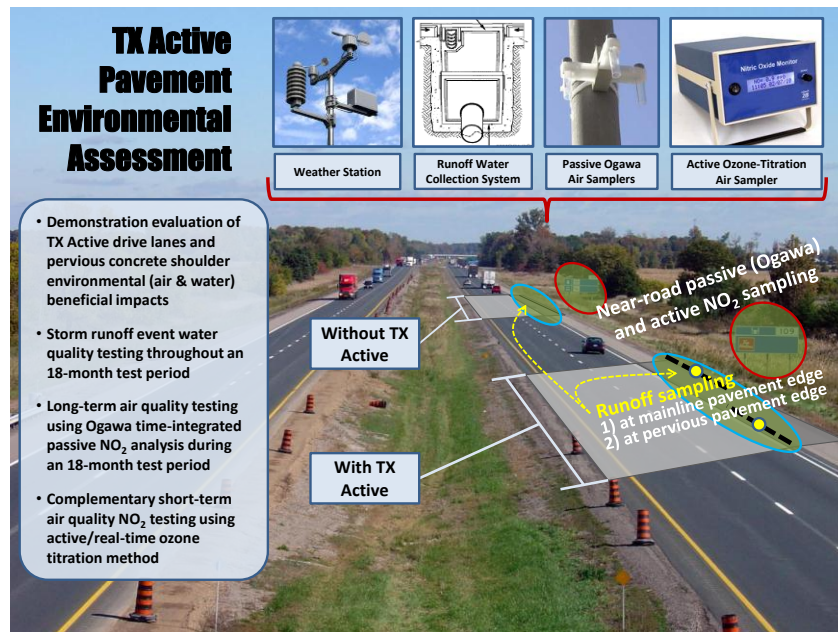
Figure 1. Qualitative Schematic of Photocatalytic Oxidation of NO and NO2 by Concrete Pavement Containing TiO2

The second shoulder pavement element of this research effort involved a similar, photocatalytic concrete material also containing the titanium dioxide additive, although, in this instance, the

TiO_2 was blended into a pervious (rather than conventional) concrete for the roadside shoulder pavement material. Together, this set of innovative mainline and shoulder paving materials, including both a two-lift photocatalytic mainline pavement and a photocatalytic pervious shoulder pavement, is believed to represent one of the most technically advanced and environmentally-friendly concrete pavement systems ever employed in the US.

Our research efforts accordingly focused on two complementary environmental research aspects connected with the use and behavior of these innovative materials, including both air-quality and water-quality benefits observed with this full-scale photocatalytic concrete paving study. In both cases, physically adjacent control paving sections (sections without the TiO_2 present) were similarly instrumented and tested for direct quantitative comparison between the observed air- and water-quality levels.

In terms of the projects activity timeline, construction of the highway was begun during the Summer of 2011 and completed in the following Summer of 2012. Public access to the highway was allowed on July 14, 2012. Continuous passive gas-phase testing (using Ogawa analyzers) of nitrogen oxide levels was completed for two months prior to the opening of the road. As such, as of this reports date in late August 2012, the highway has been in use for approximately one month. The existing field results presented within this Final Report I will consequently be further validated using continued air- and water-quality monitoring extending over the coming year (e.g., from September 2012 through August 2013). The associated details with the involved air- and water-quality testing efforts are explained in the following sections.

Air Quality Testing

This testing effort was intended evaluate the abatement of vehicle nitrogen dioxide (NO_2) emissions in relation to a photo-catalytically-induced TiO_2 conversion. Prior laboratory and real-world studies on a limited, full-scale mainline paving, based outside the US, primarily with TiO_2 pavers have been completed and show that the presence of the photo-reactive titanium dioxide catalyst provides for the beneficial oxidation of nitrogen dioxide (e.g,. Cassar, 1997; Murata, 1999; Cassar et al., 1999a and b; Ehses, et al., 2001; Cassar, et al., 2003; Lackoff, 2003; Beeldens, 2004; Vallee, et al., 2004; Bygott, et al., 2007; Gignoux, 2010; Guerrini, et al., 2010). Prior atmospheric near-road NO_2 testing has shown significant reduction, at levels reported to be 40 to 50%. This conversion is expected to subsequently create a nitrate product which physically adsorbs to the pavement, and which is then washed off during rainfall, snowmelt, etc. periods as a liquid-phase runoff residual.

An underlying regulatory motivation for this study is that the US EPAs National Ambient Air Quality Standard (NAAQS) for nitrogen dioxide has been recently changed, adding a new one-hour 100 ppb standard in addition to the previously established 53 ppb annual requirement. This change reflects escalating USEPA concerns related to individuals challenged with elevated exposures in near-road environments. Residents living near highways, students studying in schools near highways, etc., can experience short- or even long-term NO_2 exposures considerably higher than encountered by at-large community populations. At-risk individuals within this environment include those with asthma as well as children and elderly residents with

diminished respiratory capacity. A related regulatory requirement of this latter change will also be that near-road nitrogen dioxide levels must be measured starting this coming January 2013 in large urban areas (e.g., greater than 500,000 populations) to confirm NAAQS compliance.

Therefore, our overall study was intended to validate these TiO_2-derived benefits here in the US, in relation to an overarching new motivation to reduce vehicle NO_2 emission levels in urban highway environments subject to high-level annual daily traffic levels.

Two different methods were used to measure on-site atmospheric NO_2 levels, including one active and one passive procedure. The passive strategy involved an Ogawa procedure where a chemical complexing agent, triethanolamine (TEA) sorbs NO_2 from the near-road air zone on an extended, time-integrative timeframe (e.g., covering time periods between one and seven days). Ogawa testing is conducted at both the conventional and TX Active pavement zones, and these results represent our primary tool for measuring changes in NO_2 removal between the TX Active and control testing sites.

For the purposes of this project, our hypothesis with planning the involved air quality testing effort has been that Ogawa passive testing would both be more appropriate given the methods analytically integrative strategy, as well as the fact that the Ogawa method is considerably more affordable over the extended timeframe of our extended testing period (i.e., compared to a more sophisticated, and far more complicated, active chemiluminescent testing approach).

Our second, active analytical method for on-site NO_2 testing involved a newly developed testing protocol recommended for this study by the US EPAs Rich Baldauf (Baldauf, 2011). By comparison, prior real-world TX Active performance testing has traditionally focused on the use of yet another active, chemiluminescent testing protocol, which has been the method-of-choice for prior testing studies of near-road NO_2 levels.

Our projects innovative strategy, however, is based on the use of a new continuous ozone-titration method, where the depletion of ozone by total NO is determined using UV absorbance. Total NOx testing with this instrument is made possible by using a heated molybdenum pre-processing converter, which oxidizes NO_2 to NO, and a cyclic pumping scheme that sequentially switches between NOx and NO testing. Further details regarding this "active" method can be found at www.twobtech.com/.

Water Quality Testing

This testing effort is intended to determine whether the same photocatalytic mechanism for smog reduction might further improve stormwater runoff quality by decomposing vehicle-emitted pollutants. These compounds would predominantly be expected to include organic hydrocarbons (e.g., engine and transmission oils) and glycol-type antifreeze contaminants. Long-term sample collection using autosamplers for highway runoff, however, is not particularly well suited to these compound-specific analytical goals, since hydrocarbon- and glycol-type samples tend to

degrade rather quickly. Therefore, chemical oxygen demand (COD) and dissolved organic carbon (DOC, using filtered total organic carbon testing) are used as surrogate quality indicators.

Based on the expected NO_2 to NO_{3-} photocataylic conversion, our testing program has been arranged to conduct nitrate tests on the runoff liquids in order to provide a secondary indication of the aforementioned NO_2 removal phenomenon in relation to air-quality benefits. This nitrate testing establishes whether this release is taking place, or whether this nitrate product might be more permanently adhered to the reactive concrete paving materials.

Our chronological plan for these water-quality tests involves runoff samples taken over the course of a ~year-long period study, using a stormwater channeling and sampling collection system built into the pavement shoulder, and will also include parallel sets of comparative (i.e., with and without TiO_2) sample pavement sections. In both cases, these sample contaminant levels offer a complementary means of characterizing the circumstance of TiO_2-sustained impacts.

Pavement Coupon Testing

Bench-scale assessment of representative pavement coupon samples using the aforementioned active ozone-titration testing method provides a means of directly determining the specific reactivity of TX Active materials under controlled conditions. In addition, our lab testing intermittently used parallel chemiluminescent testing to cross-validate the ozone-titration method. This comparative testing regime, therefore, provides an overall means of validating our confidence with using the active, ozone-titration method for on-site testing.

Removable coupons of TX Active pavement were also embedded into the surface of the highway at the same locations at which air quality sampling is being conducted. These coupons were removed on a chronological basis during the study and returned for subsequent lab testing (i.e., bench-scale analysis of specific [per area basis] NO_2 reduction rates), by which the aging of, and temporal decrease in, photocatalytic reactivity with this pavement has been measured and tracked. Nine such coupons were placed at each of the three TX Active sampling sites along the highway test section (i.e., for a total set of twenty-seven coupons), and two each coupon samples are being removed and replaced at each location on a quarterly basis.

Additional Complementary Site and Meteorological Testing

This projects air- and water-quality plus sample pavement coupon testing efforts have been complemented with an additional set of site-specific physical measurements, including traffic makeup and density, ambient wind (i.e., speed and direction), solar radiation intensity, ambient temperature, and pavement albedo reflectivity measurements which complement the analytical process of quantitatively evaluating the overall data to establish the magnitude of observed environmental benefits.

Upcoming Project Activity

Lastly, this projects air- and water-quality monitoring program extends into the upcoming Summer 2013, by which a multi-season assessment shall have been completed. This upcoming data and evaluation will then be disseminated with a Final Report II publication expected in late Summer 2013.

OVERVIEW OF UNIQUE RESEARCH PROJECT FEATURES

This research effort has several highly unique aspects, as explained with the following narrative overview:

Unique aspect of two-lift pavement mechanism
This project represented one of only a limited number of full-scale demonstration applications for a two-lift paving strategy in the US (i.e., see Grove and Taylor, 2009).

Unique aspect of photocatalytic concrete mainline paving
This project also represented the first-ever full-scale pavement study of Essrocs TX Active concrete pavement material in the US, and one of less than a handful of such full-scale studies worldwide (e.g., with the previous most significant tests completed in Italy and France).

Yet another unique aspect of this project is that it was believed to represent one of the first ever full-scale TX Active mainline pavement applications on a higher-speed highway, as opposed to the prior full-scale studies (e.g., in Bergamo, Italy or the Vanves area of Paris, France) where the road setting was situated in an inner-city, slower-speed location.

Unique aspect of photocatalytic concrete pervious shoulder paving
This project represented the first-ever full-scale demonstration application of a photocatalytic pervious concrete shoulder-paving concept.

Unique air-quality testing aspects in relation to photocatalytic concrete pavement
This project provided full-scale air-quality results focused on the mechanism of vehicular nitrogen dioxide emission abatement using TiO_2 within the near-road environment, of which there are fewer than a handful of similar prior worldwide tests conducted on full-scale concrete paving sections.

This project is one of less than a handful of full-scale, let alone at any scale, by which an assessment of nitrogen dioxide abatement via TX Active paving has been completed using a time-integrated analytical method (i.e., via Ogawa-type passive diffusion sampling with a triethanolamine adsorbent). Here in the US, a prior test planned for Ogawa testing was developed by the US Army in Fort Belvoir, Virginia, but the completion of this project could not be confirmed. Passive NOx testing was conducted in another UK study in 2007 (Bygott et al., 2007), but in this case the tested TX Active surface was a painted, southerly facing wall surface rather than a horizontal, far-larger surface area pavement.

Uncertainty admittedly exists within the literature regarding near-road monitoring methods and results for highway NOx/NO_2 presence and fate. However, our project was not intended to improve understanding of short-term fluctuations. Instead, our experimental testing plan was developed to determine the overall cumulative effectiveness of TX Active concrete relative to a control section on a moreso long-range timeframe. Average measurements over a time period allowed for a better correlation to control sections. Our passive samplers were believed to be

well-suited to this type of work and are comparable to reference methods (Hagenbjörk-Gustafsson et al., 2009; Mukerjee et al., 2009b; Sather et al., 2007).

With understanding that our time-integrative approach represents a new strategy to monitor near-road pollutants, our passive air measurements with Ogawa samplers are effectively verified using a 2B Technologies Inc. active testing ozone depletion method.

Extensive parallel testing of crystalized nitrate buildup on TX Active concrete coupons is also being conducted during this project as a direct assessment of the involved photocatalytic NO_2 conversion and possible age-related reduction in photo-catalytic behavior. This research effort also represents a first-ever assessment of this phenomenon on a TX Active pavement…to our understanding. Nitrate buildup was, however, previously measured on a TX Active wall surface in the UK (Bygott et al., 2007).

Unique water-quality testing aspects in relation to photocatalytic concrete pavement
This project represents the first full-scale assessment of water-quality impact benefits observed in relation to the use of TX Active concrete paving.

This project also involved the first full-scale, let alone at any scale, assessment of runoff nitrate levels as a confirmative indicator of air-phase NO_2 conversion, sorption, and runoff release.

Unique water-quality testing aspects in relation to pervious concrete pavement
This is the first time pervious concrete has been used for stormwater management on a highway.

This also is the first time an internal curing agent has been used to eliminate plastic curing of pervious concrete.

PROJECT GOALS

The goals for this project were as follows:

- Characterize the NO_2 removal levels of the TX Active mainline and shoulder paving materials on a direct basis relative to conventional concrete pavement…using Ogawa time-integrated NO_2 analyses over routine one-week testing periods, as well as "active" testing using both chemiluminescent and ozone-titration analytical methods

- Evaluate pavement coupon samples in the laboratory in order to ascertain baseline performance levels, as well as measuring aging impacts on the TX Active material specimens as tested with older coupons

- Measure and ascertain the NO_2 removal levels of the TX Active pavement on an indirect basis via nitrate runoff measurements relative to conventional concrete pavement

- Measure and ascertain the water-quality related improvements provided with TX Active pavement relative to conventional concrete pavement, using COD, DOC/TOC, and TSS as key water quality indicators within runoff liquids

- Evaluate aging-related (e.g., in relation to weathering, deteriorating, etc. conditions of the TX Active surface, etc.) and seasonal-related (e.g., relative to weather conditions, angle of sunlight incidence, wind direction, wind speed, duration and intensity of solar radiation, etc.) variations in the latter TX Active contaminant removal levels

- Correlate the average daily traffic (ADT) levels for these test highway sections with the latter observed results

- Correlate wind speed, wind director, and ambient air temperature levels on these test highway sections in relation to the latter observed results

- Establish standard civil engineering material properties of these two-lift pavements

BACKGROUND

This proposed full-scale study involves the use of a concrete material marketed under the trade name TX Active by Essroc Inc., a subsidiary of the Italcementi Group headquartered in Belgamo, Italy.

Today, this material is used in a variety of architectural and engineering applications, ranging from surface coat applications on churches (Figure 2), wall and roof surfaces, office buildings, artistic structures (Figure 3), sidewalk and street pavers, to concrete pavement.

Figure 2. Jubilee Church in Rome, Italy (http://students.egfi-k12.org/wp-content/uploads/2009/10/jubilee11.jpg)

Figure 3. Water-symbol pylons mounted on the new I-35 bridge in Minneapolis, Minnesota (http://minnesota.publicradio.org/display/web/2008/09/24/substantial_completion/?refid=0)

The history of titanium dioxide use as a photochemical reactant in relation to environmental contaminants originally dates back to the mid 1970s (see Fujishima and Honda, 1975), and over the next twenty years was extensively researched (e.g., Hoffman, et al., 1995). Patents connected with the so-called smog eating capabilities of a titanium dioxide blended concrete material surface were secured by Italcementi in the late 1990s (see referenced Patent-Italcementi listings for 1999, 2000, and 2004), and published observations which confirmed this phenomenon were then reported starting around 2000 to 2003. The specific concept of using TiO_2-blended concrete materials as either pavers or mainline pavement for NO_2 abatement appears to date back in terms of publications to the early 2000s. Over the last seven to ten years the published literature on this material has progressively escalated, with the most recent 2010 publications covering full-scale experimental paving projects, and full-scale NO_2 observations in Paris and Italy (Gignoux, 2010).

4

Full-scale TX Active applications have included both a 2,000 m^2 wall and a 35,000 m^2 low pollution pavement (Rousseau, et al., 2009a and b). Experimental NO$_2$ removal results appear, as shown here, have ranged from about 30% at the pavement near-surface zone to about 12% as measured at a height of approximately two meters above the pavement.
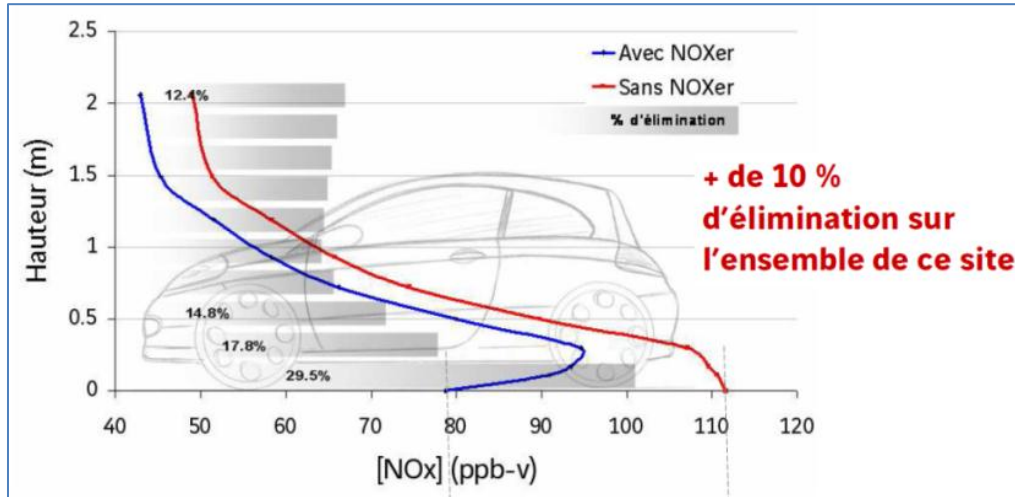
Figure 4. Qualitative Schematic of NOx Photocatalytic Oxidation and Removal at Varying Heights Above TX Active Pavement (Reference: Rousseau, et al., 2009)

The Environmental Protection Agency (EPA) has cited stormwater runoff as the single biggest contributor to surface water impairment (USEPA, 2012c). The clean water act has been revised to include non-point pollution and provide an enforcement mechanism through the National Pollutant Discharge Elimination System (NPDES) permit process. Municipalities are undertaking large, system-wide changes to reduce high contaminant sources such as combined sewer overflows and inadvertent water/sewer cross connections. However, a majority of stormwater runoff is produced from impervious rooftops and pavements. Roof-produced stormwater is relatively clean. Pavement produced stormwater contains oils and greases, suspended solids, and nutrients attached to the suspended solids, in addition to metal contribution from vehicles. Since 1999 the United States has undergone a fundamental change to the way stormwater is handled. Stormwater Best Management Practices (BMPs) are deployed on to help reduce the overall stormwater volume and provide pollutant reduction from construction sites and permanent infrastructure.

BMPs are loosely grouped into structural and non-structural techniques. An example of a non-structural technique includes street cleaning. Structural techniques include small rain gardens, large bio-retention areas, detention/retention ponds, and in-line interceptors. Structural BMPs can provide a stormwater volume reduction or only pollutant removal. Most structural BMPs require some additional land area for implementation, reducing site utilization. One structural BMP category that does not reduce site utilization is permeable pavements. Permeable pavements are pavement systems with a high permeability surface which allows rapid water exfiltration into a subsurface detention/retention area. The volume of the detention/retention area and residence time can be modified without affecting the surface area required. Permeable

pavements include pervious concrete, porous asphalt, interlocking precast pavers, and a variety of proprietary systems.

Pervious concrete is produced by balancing voids present in poorly-graded coarse aggregates with enough cementitious paste for adequate load-carrying capacity (Kevern et al., 2009). Typically 20% water-permeable voids produce sufficient strength (>3000 psi, 21MPa) and infiltration capacity (>500 in./hr, 1200 cm/hr). Strength, durability, and permeability are all controlled by the amount of voids. High void mixtures have good permeability, but poor strength and durability. Low permeability mixtures have good strength and durability, but can clog easily.

LITERATURE REVIEW

Pavement containing the photocatalyst TiO_2 exhibit unique properties, which result in the oxidation of both organic and inorganic pollutants, including NO_X. These pavements can serve as a new NO_X pollution mechanism for U.S. stakeholders, thereby improving the sustainability of the transportation sector. Photoreactor studies have determined relationships between $[NO_X]$ reduction and the multiple environmental factors. Field monitoring has provided documentation that the pavement causes $[NO_X]$ reduction when used in paving blocks, concrete, and spray coatings. While the body of literature is substantial, future research must use strengthen the link between photoreactor and field studies, determine the environmental variables with the greatest impact on $[NO_X]$ reduction, and develop models to facilitate selection of roadways for which maximum $[NO_X]$ reduction can be achieved.

Introduction

Titania serves as the common name for titanium dioxide (TiO_2) and fictions often-used name for the queen of the fairies. This dual meaning provides an uncanny allusion to the compounds nearly magical photocatalytic degradation of a broad set of organic and inorganic pollutants. In the 1960s, Akira Fujishima and Honda (1972) carried out the first research yielding the potential for practical applications. Their study found that light ($\lambda < 415$ nm) induced a photocurrent between TiO_2 and platinum electrodes immersed in an aqueous solution, resulting in oxygen and hydrogen evolution. Following this discovery, initial research focused on enhancements to water decomposition and by 1977 researchers began studying environmental applications. Frank and Bard (1977) employed TiO_2 as a photocatalyst to oxidize cyanide ions, which frequently occur as a by-product of industrial processes. In this study, a samples cyanide concentration was reduced by up to 54% when illuminated by a xenon lamp for 30 min in the presence of TiO_2. When samples were placed in sunlight for two days in excess of 99% removal was observed. These new findings channeled interest towards environmental applications that address aqueous and airborne pollutants.

Photocatalytic degradation of nitrogen oxides (NO_X) from on-road motor vehicles by pavement containing TiO_2 has generated a substantial amount of research interest as an environmental application of this compound. NO_X—the sum of nitric oxide (NO), nitrogen dioxide (NO_2), and other oxides of nitrogen—are produced by high-temperature combustion processes. NO_X emissions result in a variety of detrimental effects to both respiratory systems and the natural ecosystem. In addition, NO_X contribute to the formation of tropospheric ozone when reacted with volatile organic compounds (VOCs) in the presence of sunlight (USEPA, 2011a). Although NO accounts for approximately 95% of NO_X emissions, this pollutant is freely oxidized to NO_2 in the atmosphere; therefore, United States Environmental Protection Agency (USEPA) assumes all NO_X in emissions estimates to be in the form of NO_2 (USEPA, 2001). NO_2 is toxic when inhaled at high concentrations and can cause respiratory ailments (e.g., respiratory infections, bronchitis, and emphysema) at part-per-billion by volume (ppbv) levels of exposure (USEPA, 2011b). Within the United States, on-road motor vehicles account for 34% of NO_2 emissions (USEPA, 2001) **Error! Reference source not found.**. An estimated 35 million people (i.e., more than 10% of the U.S. population) live within 100 m (300 ft) ofmajor sources of on-road

vehicle emissions and are exposed to elevated concentrations of NO_X (Thoma et al., 2008). Furthermore, multiple health studies have linked an increase in the observation of negative health effects with the proximity of people to major roadways (Brauer et al., 2002; Brunekreef et al., 1997; Finkelstein et al., 2004; Garshick et al., 2003; Kim et al., 2004).

Conventional efforts to mitigate transportation sector air pollution focus on alternative vehicles and fuels, transportation policy, and emissions control technologies. These strategies have reached a point where additional improvements in air quality will require novel approaches and significant expense. Advances in photocatalytic concrete pavements provide a new pathway to improve the sustainability of transportation by reducing the negative impacts associated with vehicle emissions. Photocatalytic reactions cause oxidation of a variety of organic and inorganic pollutants. Notably, the photocatalytic property of these pavements causes oxidation of NO_X. To foster research in photocatalytic degradation of motor vehicle pollution by pavement containing titanium dioxide, the following sections examine the field and identify research needs. While these pavements catalyze oxidation of variety of organic and inorganic pollutants, this review places focus on reactions with NO_X.

Regulatory drivers and Conventional Mitigation Strategies

Within the United States, efforts to minimize the atmospheric concentration of NO_X from on-road motor vehicles are driven by National Ambient Air Quality Standards (NAAQS) and vehicle emissions standards. Both of these regulatory classes receive their authority from the Clean Air Act (CAA) and subsequent amendments.

National Ambient Air Quality Standards

NO_2 is one of six principal pollutants regulated by National Ambient Air Quality Standards (NAAQS) because exposure can cause respiratory ailments (e.g., infections, bronchitis, and emphysema). NO_X also presents other environmental concerns; small particles formed by reaction of NO_X with moisture and ammonia cause lung damage and NO_X represents a critical step in formation of tropospheric ozone, yet another NAAQS criteria pollutant due to detrimental effects to natural ecosystems and the respiratory system. VOC emissions, while not regulated by NAAQS, are also of similar concern because NO_X and VOC reactions in the presence of sunlight generate ozone (USEPA, 2011a).

USEPA NAAQS establish primary standards, which protect public health, and secondary standards, which protect public welfare (Clean Air Act, 42 U.S.C. § 7409(b), 2008). 2010 revisions strengthened the NAAQS for NO_2 by supplementing the existing annually averaged 53 ppbv NO_2 primary and secondary standard with a primary standard that designates an area as nonattainment if the 3-year average of the 98th percentile of the annual distribution of the daily maximum 1-hour average NO_2 concentrations exceeds 100 ppbv (Primary National Ambient Air Quality Standards for Nitrogen Dioxide, 75 Fed. Reg. 6474, 2010).

With use of data from an existing network of area-wide NO_2 monitors (i.e., monitors located to measure NO_2 across a broad area), USEPA found one location in nonattainment of the 100 ppb standard (USEPA, 2010a). However, the 2010 final rule also requires installation of near-road NO_2 monitors by 2013. These monitor must be located within 50 m of a road segment that is selected on the basis of annual average daily traffic (AADT), but placement also requires consideration of "fleet mix, congestion patterns, terrain, geographic location, and meteorology" (USEPA, 2010b). In these near-road locations, NO_2 concentrations are 30% to 100% higher than area-wide concentrations (USEPA, 2010c). When developing the regulations impact assessment, USEPA did not have adequate data to predict which areas may violate the new 100 ppbv standard after these monitors are installed. The agency concluded "the possibility exists that there may be _many more_ (emphasis added) potential nonattainment areas than have been analyzed" (Primary National Ambient Air Quality Standards for Nitrogen Dioxide, 75 Fed. Reg. 6474, 2010).

A USEPA nonattainment designation has multiple and sometimes severe consequences. Within 18 months after an area within a state is designated nonattainment for NO_2, the state must submit a state implementation plan (SIP). This plan must detail the control techniques that the state will employ in order to both attain and maintain the NAAQS (Clean Air Act, 42 U.S.C. § 7510, 2008) . To aid SIP preparation USEPA issues information on control technologies—including data on installation and operation cost and emissions reductions—to the States (Clean Air Act, 42 U.S.C. § 7508(b)(1), 2008). Transportation often contributes substantially to criteria pollutant emissions. USEPA provides specific control measures to control these emissions including, improving public transportation, establishing lanes for high occupancy vehicles, and facilitating non-automobile travel (Clean Air Act, 42 U.S.C. § 7508(e), 2008). If a States implementation plan fails to meet the various requirements found in the CAA, the Administrator of USEPA can impose austere highway and offset sanctions. Highway sanctions allow the Administrator to bar the Secretary of Transportation from awarding title 23 projects or grants, with exception of those for which safety improvement is the principal purpose (Clean Air Act, 42 U.S.C. § 7509(b)(1)(A), 2008). For areas that USEPA designates as nonattainment, construction and operation of facilities that will emit criteria pollutants requires either an emissions reduction—or offset—from existing sources or construction in a location that will not contribute to the emissions that exceed the applicable standard. For an area that fails to attain NAAQS the Administrator can increase this offset of emissions reduction to increased emissions to a ratio of 2 to 1 (Clean Air Act, 42 U.S.C. § 7509(b)(2), 2008).

Motor Vehicle Emissions Standards

As noted, within the United States, on-road motor vehicles account for 34% of NO_2 emissions (USEPA, 2001) and an estimated 35 million people, who live within 100 m (300 ft) of major sources of on-road vehicle emissions, are exposed to elevated concentrations of NO_X (Thoma et al., 2008). The significance of these emissions, both in terms of the proportion of total NO_X emissions and health impact, has resulted in promulgation of tailpipe NO_X emissions standards by USEPA. Major categories of on-road vehicles include light-duty vehicles, light-duty trucks, and medium-duty passenger vehicles, heavy-duty highway compression-ignition engines and urban buses. For light-duty vehicles, light-duty trucks, and medium-duty passenger vehicles newer than model year 2004, USEPA has established 8 emissions categories (termed "bins").

NO_X emissions limits [at full useful vehicle life, 100,000-120,000 miles (approximately 160,000-190,000 km)] in these bins range from 0.00 to 0.20 g mi^{-1} (0.12 g km^{-1}) (USEPA, 2007). Auto manufacturers may sell vehicles that fall into any of the 8 bins, but the average emissions limit of all vehicles sold must fall below the bin 5 limit, 0.07 g mi^{-1} (0.04 g km^{-1}) (USEPA, 2012a). Heavy-duty highway compression-ignition engines and urban buses are regulated with a separate set of emissions standards. For model year 2010 and newer, NO_X emissions from these vehicles are limited to 0.2 grams per brake horsepower-hour (g bhp-h^{-1}) (0.27 g kW-h^{-1}) (USEPA, 40 CFR 86.007-11, 2012b).

For vehicles in the light-duty category, the present bin 5 emissions limit represents a 98% reduction from emissions prior to implementation of standards (USEPA, 2007). For heavy-duty vehicles, the noted limits are a 98% reduction from 1985 emissions limits (USEPA, 2012b). To achieve these levels of NO_X emission control requires advanced and expensive tailpipe control equipment. For example, retrofit installation of a selective catalytic reduction device on a heavy-duty vehicle diesel engine costs between $12,000 and $20,000 when installed with an oxidation catalyst or costs between $15,000 and $25,000 when installed with a diesel particulate filter (MECA, 2007).

Principles of NO_X Oxidation by Photocatalytic Pavement

In similarity with any other productive effort, the law of diminishing marginal returns governs the effectiveness of conventional NO_X mitigation strategies. Under conventional strategies, each additional dollar spent is used less efficiently because the spending results in smaller and smaller marginal reductions in ambient NO_X concentrations. In the case of ambient NO_X pollution, documented negative health effects for those who live in near-road microenvironments indicate that further reductions in NO_X should be sought. Having reached a point low marginal return, if policymakers operate under conventional strategies, achieving this goal will be expensive. In order to achieve desired health impacts in a manner that efficiently uses whatever funding is available, stakeholders must consider NO_X mitigation strategies that fall outside of the current paradigm and are governed by a separate input-output curve (i.e., dollars spent vs. NO_X reduction). Photocatalytic pavements are one of these new-paradigm strategies for motor-vehicle pollution abatement. This technology must be evaluated with further laboratory and field research.

Pavement-specific literature refers to NO_X degradation as the DeNOx-process. This process has one stage for NO_2, two stages for NO, and is illustrated in Figure 3. The process begins when NOx adsorbs on sites where $^\bullet OH$ is generated by exposed TiO_2. Adsorbed NO is oxidized to NO_2 by the $^\bullet OH$. NO_2, both adsorbed from the air and formed by oxidation of NO, is oxidized to nitrate (NO_3^-). It is possible for NO_3^- to be bound to pavement surface by an alkali, but it is most probable that this product is flushed by water from the surface (Husken et al., 2009). The high probability that NO_3^- will be washed from the surface can be attributed to another unique photo-induced TiO_2 property, superhydrophilicity. Under sunlight, water on the surface of a pavement containing TiO_2 spreads into a thin film with a contact angle of nearly zero degrees. This low contact angle allows water to penetrate between the pavements surface and adsorbed material. This penetration lifts and flushes this material from the surface (A. Fujishima and Zhang, 2006).

Concentration of reaction products (i.e., NO_2^- and NO_3^-) has not been measured in the field, but one report estimates a maximum concentration of 1.2 mg/L-N, a value far below USEPAs 10 mg/L-N standard for drinking water (City Concept, 2004; USEPA, 2009).
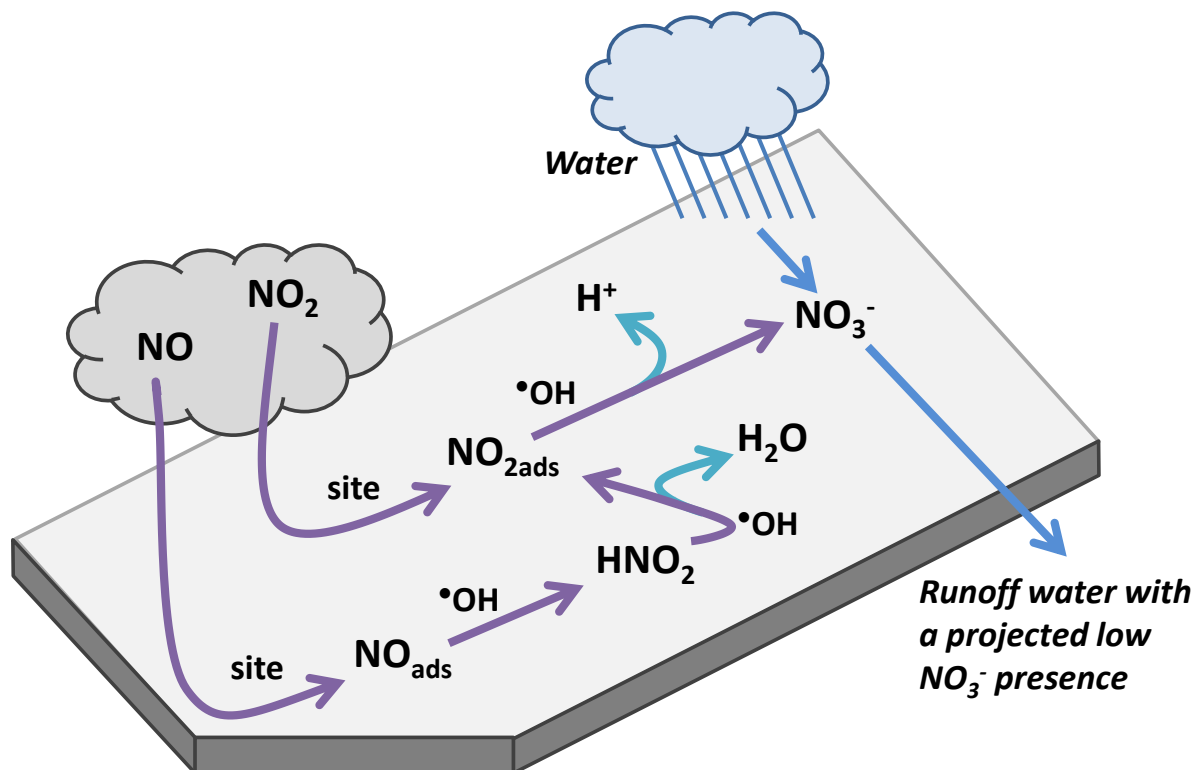
Figure 5. Photocatalytic oxidation of NO and NO₂ by concrete pavement containing TiO₂

Photocatalytic pavements represent a novel approach that may serve as a means to effectively mitigate NO_X pollution. Current research has not expanded beyond this pollution abatement effort. However, it should be noted that TiO_2-based photocatalysts degrade an extensive range of both organic and inorganic pollutants, which may well result in additional pollution abatement benefits (Beeldens et al., 2011).

The wide range of pollutants degraded by TiO_2-based photocatalysts dovetails with 1162 different air toxics found on the USEPAs Master List of Compounds Emitted by Mobile Sources because these compounds are known or suspected to cause cancer or other serious health and environmental effects (USEPA, 1994, 2006). For the USEPA, monitoring all mobile source air toxics is impractical. In their case, the following six criteria pollutants have been selected as indicators of air quality: carbon monoxide, lead, nitrogen oxides, ozone, particulate matter, and sulfur oxides.

Table 1 uses a similar approach to indicate the suitability of TiO_2 photocatalysts as a means to mitigate mobile source pollution.

Table 1. Emissions and TiO2-based photocatalytic reactions for mobile source pollutant indicators

Pollutant[1]	Estimated U.S. emissions from on-road vehicles (10^3 short tons) (USEPA, 2001)	Percent of total U.S. emissions from on-road vehicles (%) (USEPA, 2001)	Selected associated species	TiO$_2$-based photocatalytic reactions	Reaction references
Carbon monoxide	49,989	51	CO	$CO + O^{*2} \rightarrow CO_2$	(Hwang et al., 2003)
Lead	0.022	0.52	Pb(II)	$^\bullet R^3 + Pb(II) \rightarrow R_{OX} + Pb(I)$ (inhibited by oxygen, best suited for aqueous treatment)	(Murruni et al., 2008)
Nitrogen dioxide	8,590	34	NO$_2$, NO	$NO_2 + {}^\bullet OH \rightarrow NO_3^- + H^+$, $NO + 2{}^\bullet OH \rightarrow NO_2 + H_2O$	(Dalton et al., 2002)
Volatile organic compounds (VOCs)	5,297	29	C_4H_6, $C_6H_5CH_3$, C_8H_{10}, CH_2O, C_4H_9OH, $(CH_3)_2CO$, $CH_3(CH_2)_2CHO$	Multiple reactions possible	(Obee and Brown, 1995; Peral and Ollis, 1992)
Particulate matter (diameter <10 µm)	295	1.2[4]	N/A	N/A	
Particulate matter (diameter <2.5 µm)	229	3.4[4]	N/A	N/A	
Sulfur dioxide	363	1.9	SO$_2$, HOSO$_2$	$^\bullet OH + SO2 \rightarrow HOSO_2$, $HOSO_2 + O^{*2} \rightarrow {}^\bullet OH + SO_3$	(Y. Zhao et al., 2009)

[1] List excludes ozone because this species is not emitted directly. VOCs are listed instead because reactions between VOCs and NO$_X$ produce ozone.

[2] O* denotes an active oxygen species

[3] R denotes a radical species

[4] Total emissions includes both natural anthropogenic emissions

Notably, this table replaces ozone with VOCs because ozone is not emitted directly and VOCs are a precursor to tropospheric ozone. With exception of particulate matter, photocatalytic reactions have been reported for each pollutant. Furthermore, with exception of lead, each reaction occurs in the gas phase.

Overview of Heterogeneous Photocatalysis Mechanism

Photocatalytic pavements have unique properties, which result in the oxidation of both organic and inorganic pollutants (Beeldens et al., 2011). These properties arise because cements used in these pavements contain TiO_2, a photocatalyst. While other photocatalytic materials exists, investigation has identified TiO_2, with the anatase crystal structure, as the most effective (Ohama and Van Gemert, 2011). The unique photocatalytic oxidation properties of TiO_2 are chiefly due to generation of hydroxyl radicals ($^\bullet OH$) under UV-A illumination (i.e., wavelength range of 300 nm to 400 nm) (A. Fujishima and Zhang, 2006). As illustrated in Figure 4, when nanoscale TiO_2 particles absorb light with energy greater than the gap between valence and conduction bands (i.e., 1-3.3 electron volts), valence band electrons are excited and move to the conduction band (Tompkins et al., 2005). This electron movement produces electron-hole pairs. TiO_2 particles, which are n-type semiconductors, contain sufficient numbers of mobile electrons that generation of electron-hole pairs do not significantly upset thermodynamic equilibrium. Therefore, the energy from light can be stored without compromising TiO_2 particle integrity. Once produced, electron holes tend to recombine with an electron, eliminating the hole-pair and releasing the stored energy as thermal energy or radiation. However, if the electron hole migrates to the particle surface, oxidative reactions are possible. In the typical photocatalytic oxidation process, an electron from a hydroxyl ion fills the TiO_2 particles electron hole, creating a ($^\bullet OH$). This radical is highly reactive and can then oxidize various pollutant molecules (Akira Fujishima et al., 2000).

① Light with energy greater than band-gap energy (E_g) excites an electron (e^-) from the valence to the conduction band creating a valence-band hole (h^+).

② h^+ migrates to surface and oxidizes a hydroxyl ion (OH^-) to a hydroxyl radical ($^\bullet OH$).

③ To maintain neutral charge the excited electron migrates to the surface and reduces molecular oxygen (O_2) to a molecular oxygen radical ($^\bullet O_2^-$).
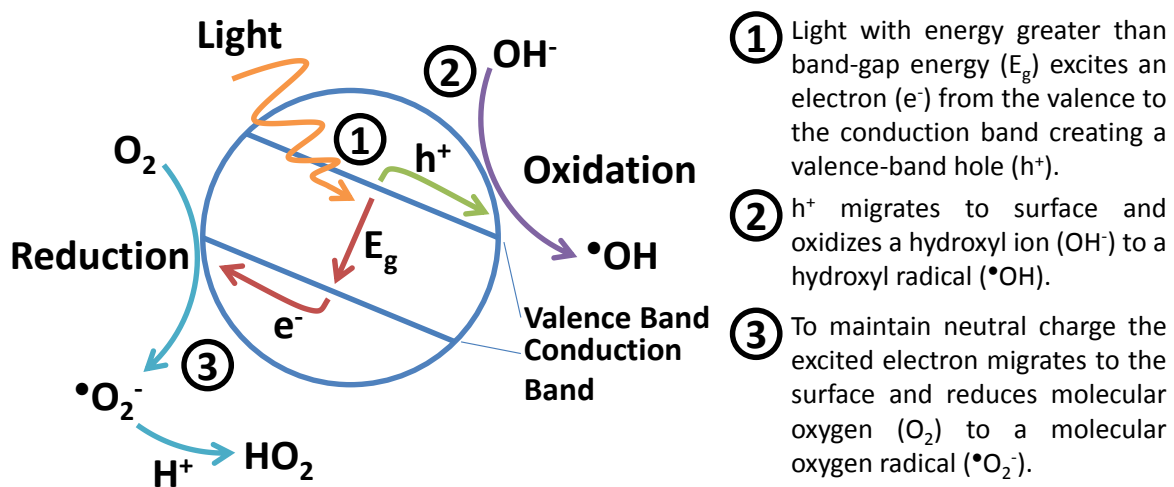
Figure 6. Photocatalytic oxidation steps (Adapted from Tompkins et al., 2005)

Photocatalytic oxidation causes the TiO_2 particle to gain electrons. A net gain of electrons threatens the continued usability of the particles for photocatalytic oxidation because a negative charge will develop if too many electrons are gained. This state has not been observed in practice. Research indicates that in many cases, a neutral charge is maintained when electrons leave TiO_2 particles via reduction of molecular oxygen to radical oxygen (also illustrated in Figure 4). The electron holes have a greater oxidizing power than the reducing power of excited electrons; therefore, reduction of molecular oxygen does not cancel out the TiO_2s oxidizing power. Of note, radical oxygen when reacted with hydrogen produces the hydroperoxyl radical, which also can oxidize certain molecules (A Fujishima et al., 1999).

Optimization of TiO_2 for use as a photocatalyst is the subject of ongoing research. Anatase has the highest photocatalytic activity levels of common TiO2 mineral forms due to comparatively higher surface area and surface density of sites available for photocatalysis (Herrmann, 1999). Although anatase TiO_2 displays a comparatively high level of photo-activity, it only absorbs UV light (which represents approximately 5% of sunlight). Enhanced photocatalytic activity could be obtained if the spectrum of light that TiO_2 absorbs is increased. Efforts to achieve this result have included coupling with semiconductors, doping with metal, preparing TiO2 that is oxygen deficient, and doping with non-metal anions (A. Fujishima et al., 2008). Non-metal anion doping shows the greatest potential to achieve development of visible-light photocatalytsts. Publications have reported that doping with nitrogen, carbon, sulfur, boron, phosphorus, and fluorine increases the spectrum of light that TiO2 absorbs to the visible range (A. Fujishima et al., 2008). These developments increase photocatalytic generation of $^\bullet OH$, thereby increasing photocatalytic degradation of various pollutants. Undoubtedly, future developments will also enhance photo-degradation of NO_X by pavement containing TiO_2.

Laboratory Evaluation of Photocatalytic Pavements

Evaluation of new technologies proceeds from laboratory to field stages. Photocatalytic pavements are no exception. Lab studies, with use of a flow-through photoreactor, constitute a significant portion of this technologys published body of literature. The sections that follow provide an overview of the experimental apparatus and testing approach used in this evaluation and summarizes results while noting areas needing future study.

Experimental apparatus and testing approach

Test methods to evaluate oxidation of nitric oxide by photocatalyic pavements are provided by international, Japanese, and Italian standards (ISO, 2007; JIS, 2010; UNI, 2007). Each standard provides a similar scope for a test method to determine removal of nitric oxide by photocatalytic ceramic materials. Although written to provide a standard testing approach for ceramics, the international standard is suitable for photocatalytic concrete. NO_X removal is determined by measuring the amount of pollutant removed from a test gas after it passes over a photocatalytic material housed within a flow-through photoreactor. The standard provides equations to determine the net number of moles of NO removed from the test gas by the sample; however, the bulk of publications report NO_X removal as calculated by the following equation:

$$NO_x \ removal \ (\%) \ = \frac{C_{NO_Xi} - C_{NO_X}}{C_{NO_Xi}} \times 100\%$$

The apparatus required to complete this determination are divided into the following groups: test gas supply, photoreactor, light source, and pollutant analyzer (see Figure 5 for schematic). The standard proposes the following operating conditions: 1.0 ppmv NO input concentration, 50% relative humidity, 3.0 L min^{-1} flow rate, 50 mm photoreactor width, 5.0 ± 0.5 mm air pathway height, and 5 h sample irradiation length. In order to test [NO$_X$] reduction under various environments, these conditions are frequently modified.
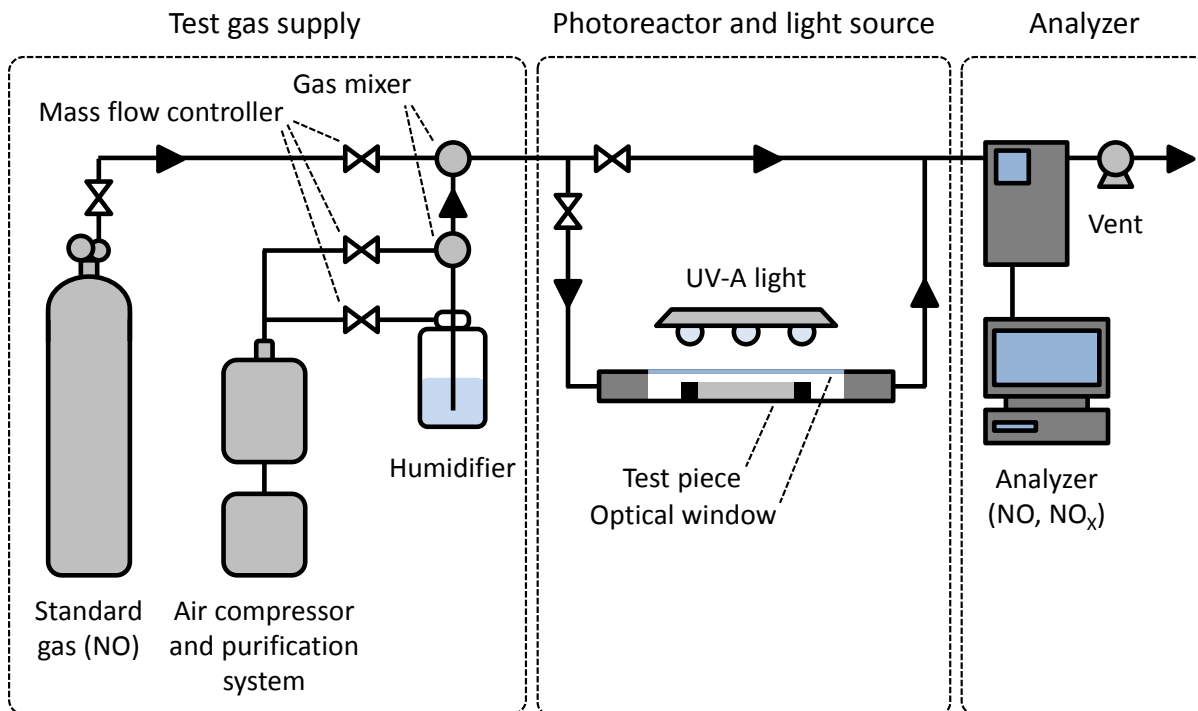
Figure 7. Schematic of experimental apparatus (adapted from ISO, 2007).

Photoreactor studies

To predict the performance of photocatalytic pavements under field conditions, researchers use photoreactor tests to measure [NO$_X$] reduction under various environmental, material, and operation conditions. The earliest publications varied environmental variables of irradiance, relative humidity, NO$_X$ concentration, NO$_2$/NO$_X$ fraction, and flow rate and the material variable, TiO$_2$ content. Table 2 presents a summary of these evaluations and the relationship between each independent variable and the resulting [NO$_X$] reduction. To achieve the maximum NO$_X$ removal efficiency at minimum cost requires further investigation. The following sections describe various environmental, material, and operation variables that impact NO$_X$ removal efficiency and identify areas that require additional study.

Table 2. Summary of photoreactor tests for mortars containing TiO2 (unless noted, values are presented with the reported number of significant digits)

Summary of photoreactor tests for mortars containing TiO_2 (unless noted, values are presented with the reported number of significant digits).

Independent variable	Values tested		Associated reduction (%)		[NOX]	Test conditions						Reference	Relationship between independent variable and NO oxidation	
	High	Low	High	Low	$\Delta_{High-Low}$	E (W m^{-2})	RH (%)	[NOX] (ppmv)	NO2/NOx	Q (L min^{-1})	TiO2 (% by binder weight)		Type (positive, negative, unknown)	Reason
Irradiance (W m^{-2})	12	0	87[d]	10[d]	77		50	1.0	0	3	NR	Murata et al., 2000	Positive	↑ rate of electron-hole generation with ↑ E
	13.1	0.3	25[d]	5[d]	20		50	1.0	0	3.0	NR	Hüsken et al., 2009		
	12.1	2.1	45.8	12.6	33.2		49.9, 49.6	1.04	0.52	3	5.9[i]	Ballari et al., 2011		
Relative humidity (%)	80	10	52[d]	87[d]	-35	6		1.0	0	3	NR	Murata et al., 2000	Negative	Water blocks pollutant adsorption at active sites
	80	10	13.6	32.3	-18.7	10.0		1.0	0	3.0	NR	Hüsken and Brouwers, 2008; Hüsken et al., 2009		
	80	30	14[d]	43[d]	-29	NR		0.41	0	NR	5	Dylla et al., 2010		
	69.0	10.2	37.9	84.6	-46.7	10.1		0.52	0	3	5.9[i]	Ballari et al., 2011		
NOX conc. (ppmv)	5.0[d]	0.05	44[d]	90[d]	-46	6	50		0	3	NR	Murata et al., 2000	Negative	Oxidation is limited by rate of •OH generation
	1.0	0.1	36.9	68.4	-31.5	10.0	50		0	3.0	NR	Hüsken and Brouwers, 2008; Hüsken et al., 2009		
	1.009	0.096	20.53	64.29	-43.76	10	50		0.01, 0.02	3	NR	Ballari et al., 2010		
	1.01	0.11	34.9	71.8	-36.9	10	50.0		0	3	5.9[i]	Ballari et al., 2011		
	1.3	0.1	38[d]	82[d]	-44	16	23,24		0	3	NR	Sikkema et al., 2012		
NO2/NOX	1	0	36.5	34.9	1.6	10.0	50.0, 49.8	1.01, 0.99		3	5.9[i]	Ballari et al., 2011	Unknown	Unknown
	0.70	0.0	41[d]	74[d]	-33	20	20	0.55		3	5	Dylla et al., 2011		

Q (L min^{-1})	5	1	22.1	66.6	-44.5	10.0	50	1.0	0		NR	Hüsken and Brouwers, 2008; Hüsken et al., 2009	Negative	↓ time of pollutant exposure at active sites with ↑ Q
	5	3	15.72	21.10	-5.38	10	50	1.018, 1.019	0.2		NR	Ballari et al., 2010		
	9	3	21^d	61^d	-40	NR	NR	0.41	0		5	Dylla et al., 2010		
TiO$_2$ (% by binder weight)	10	3	18.1	6.2	11.9	10	50	1	0	3		Hüsken et al., 2009	Positive	↑ rate of electron-hole generation with ↑ TiO2 content
	5	3	61^d	56^d	5	NR	?	0.41	0	3		Dylla et al., 2010		
	5	3	26.9	18.0	8.9	NR	50	0.41	0	9.0		Hassan et al., 2010a; Hassan et al., 2010b; Hassan et al., 2010c;		

d = digitized from figure NR = not reported, ↑ = increased, i = % by total weight, ↓ = decreased

Environmental Variables

Irradiance

Increased UV irradiance on a photocatalytic surface increases the rate at which electron holes are created. An increase in electron-hole generation results in increased production of hydroxyl radicals, which oxidize NO_X. Multiple publications report that the relationship between irradiance and pollutant oxidation can be divided into two regimes. These regimes are divided into a linear relationship below the regime division point and a non-linear relationship above this point (Herrmann et al., 2007; Jacoby et al., 1995; Kumar et al., 1995; Lim et al., 2000; Obee and Brown, 1995). Jacoby et al. (1995) explains that under the linear regime, electron holes are filled by reactions with species on the photocatalytic surface (e.g., OH^-) faster than by recombination with excited electrons; in contrast, under the non-linear regime, holes are filled by recombination at a faster rate than by reaction other species. Although these publications are in consensus that this regime is identifiable, reports of the regime division point irradiance value range from 10 to 250 W m^{-2} (Herrmann et al., 2007; Lim et al., 2000). Photocatalytic pavement studies, which investigated the relationship between irradiance and [NO_X] reduction, have not confirmed this linear regime at irradiance values ranging from 0.1-13.1 (Ballari et al., 2009; Husken et al., 2009; Y. Murata et al., 2000). For each of these studies, the relationship can be described by a power law ($R^2 > 0.98$ for each study). A linear relationship can only be assumed if measurements at low irradiance values are excluded; however the number of points that must be excluded to obtain a $R^2 > 0.95$ differs between studies, with the greatest value being 5 W m^{-2}. As reported by Grant and Slusser (2005), mean daytime UV-A irradiance from the most northern (Fairbanks, Alaska, latitude 65.1°N) and southern (Homestead, FL, latitude 25.4°N) locations of a United States Department of Agriculture (USDA) climate monitoring network ranged from 10.5 to 22.3 W m^{-2}. These values all fall in the area where the linear or nonlinear regime applies. However, in urban areas NO_X ambient concentration follows a diurnal pattern associated with traffic. Urban background monitoring in London, UK, found that NO_2 peaks both in early morning and late afternoon and NO, which oxidizes quickly to NO_2 during daylight hours, peaks in early morning (Bigi and Harrison, 2010). At these peaks, irradiance values are substantially lower than the mean daytime value. Improving the efficiency at which photocatalytic pavement mitigates atmospheric NO_X pollution requires greater photoactivity and additional laboratory study at these low irradiance values.

Relative Humidity

Photocatalytic degradation of NO_X by pavement containing titanium dioxide occurs when NO_X is oxidized by $^•OH$ (Figure 3). These $^•OH$ are generated by oxidation of an OH^- by an electron hole (Figure 4). Water vapor serves as the atmospheric source for OH^-. Intuition would thereby suggest that increased humidity would result in increased [NO_X] reduction. In actuality, the opposite is true. In addition to photocatalytic properties, materials containing TiO_2 also exhibit photo-induced superhydrophilicity (i.e., water on the surface has a contact angle of nearly 0°) (A. Fujishima et al., 2008). Adsorbed water vapor disperses over on the surface, blinding photocatalytically active sites (Beeldens, 2007). Data from photocatalytic pavement studies indicate a linear relationship with a negative slope (see Table 2). These studies all occurred at

room temperature, allowing comparison of the results by relative humidity. In contrast, field applications will exhibit substantial variation in temperature, which results in significant changes in the amount of water that can be present in the atmosphere. For field studies, specific humidity (the ratio of water vapor mass to total air mass) provides a better comparison. At 20°C, 10% and 80% relative humidity (the extremes of laboratory data) convert to specific humidity values of 1.44 and 11.6 g water (kg moist air)-1 respectively (at 101.1 kPa). As part of the rule making process, the USEPA used 2006-2008 data to determine ambient NO_2 concentration in the form of the 2010-promulgated NO_2 standard for counties within the United States. The five counties with the highest NO_2 concentration in this measurement form are as follows: Cook, IL, San Diego, CA, Los Angeles, CA, Erie, NY, and Denver, CO. With exception of Denver County, each of the listed counties frequently experience high specific humidity conditions. Any field application of photocatalytic concrete to mitigate NO_X pollution will need to be carefully tailored the environmental conditions.

NO_X Concentration

Photocatalytic pavement studies display a clear negative correlation is evident between inlet NO_X concentration and percent [NO_X] reduction (Ballari et al., 2010; Ballari et al., 2011; Husken and Brouwers, 2008; Husken et al., 2009; Y. Murata et al., 2000; Sikkema et al., 2012). Herrmann (1999) reports that reaction kinetics fall into a low-concentration first-order regime and a high-concentration zero-order regime. Under the zero-order regime, the reaction rate is controlled by reactions between adsorbed molecules. As applied to [NO_X] reduction by photocatalytic pavements, the overall rate of [NO_X] reduction will remain constant as input concentration increases, therefore the percent [NO_X] reduction will decrease. As compared to the zero-order regime, the decrease in percent [NO_X] reduction is dramatic within the first-order regime because the availability of active sites for decreases with increased concentration. Many photoreactor studies follow the ISO method and thereby assess [NO_X] reduction at 1 ppmv. This value is an order of magnitude greater than even the highest value USEPA NO_2 standard and cannot be considered representative of environments where this technology may see application. Although photoreactor studies do evaluate the relationship between input concentration and [NO_X] reduction, data points are often evenly distributed between high and low concentrations. As research moves to field application, it will need to be complemented by photoreactor studies that place focus on [NO_X] reduction at low-concentration values.

NO_2/NO_x Ratio

USEPA emissions estimates used for national trends assume a NO_2/NO_X ratio of 1 because NO is freely oxidized in the atmosphere (USEPA, 2001). Within near-road environments assumed and measured NO_2/NO_X values for initial emissions in near-road environments fall between 0.05 and 0.31 (Wang et al., 2011). Photocatalytic pavement research has not established the relationship between NO_2/NO_X ratio and [NO_X] reduction. H. Dylla et al. (2011a) asserts a negative correlation. The data set from Ballari et al. (2011) does not support this claim, listing [NO_X] reduction of 34.9 and 36.5 at NO2/NOX ratios of 0 and 1 respectively. Settling these conflicts within the literature will require additional photoreactor studies that focus on near-road NO_2/NO_X ratios, which were identified in Wang et al. (2011).

Flow Rate

[NO$_X$] reduction within a specific volume of test gas increases proportionally to the residence time over a photocatalytic surface because greater time exists for pollutants to absorb and be oxidized at active sites. As a result, literature demonstrates a clear negative correlation between [NO$_X$] reduction and flow rate. In each case the relationship appears linear, but each publications supplies at most 3 data points (Ballari et al., 2010; Heather Dylla et al., 2010; Husken and Brouwers, 2008; Husken et al., 2009). Tested flow rates (1-9 L min^{-1}) do not vary substantially from the 3 L min^{-1} specified in the ISO (2007) standard. If the standards reactor dimensions are also used, air velocity over the photocatalytic surface would measure 0.2 m s^{-1}. Although considerable variation in wind velocity occurs within the field, in a relatively unobstructed environment, a reasonable expectation would set wind velocities at least an order of magnitude greater than the value specified by the standard (approximately 7 km h^{-1}). Wind velocity of this magnitude would significantly reduce the effectiveness of field applications of photocatalytic pavements, especially if the wind carried pollutants in a direction perpendicular to the roadway. Street canyons may represent an optimal location for photocatalytic pavements. The structures that border each side of these streets reduce natural ventilation and in many cases air pollution rises well above background concentrations (Vardoulakis et al., 2003). While this reduced airflow provides suitable site conditions for photocatalytic pavement, application of this technology within a street canyon must take into account decreased irradiance during periods when buildings obstruct sunlight.

Temperature

Available literature is vague in regards to the impact of temperature changes on NO$_X$ PCO performance. Assertions are general and in most cases state that [NO$_X$] reduction efficiency increases with higher temperature (Beeldens et al., 2011) and that only large differences in temperature (i.e., summer vs. winter) are significant (H. Dylla et al., 2011a). In addition to being vague, the literature also is contradictory and one source reports a decrease in oxidation rate with increased temperature (Chen and Chu, 2011). Cold temperature climates, such as those that occur in northern and continental areas of the United Sates, may substantially reduce the pavements air purification performance. To determine whether photocatalytic pavement can serve as a viable method to address air pollution in these climates, the influence of temperature on the rate of NO$_X$ PCO must be researched.

Material Variables RE: TiO$_2$ Content

Photocatalytically active sites occur on the surface of pavement where TiO$_2$ is exposed. An increase in the amount of TiO$_2$ contained in the photocatalytic material (often measured as a percentage of binder mass) results in greater NOX removal (Heather Dylla et al., 2010; M. M. Hassan et al., 2010a, 2010b; Marwa M. Hassan et al., 2010c; Husken et al., 2009). Although this positive correlation is supported by literature, the relationship is non-linear. Studies of VOC oxidation have found that grains catalytic activity diminish with increases in TiO$_2$ content and have proposed that optimal TiO$_2$ content falls between 1 and 5% (Strini et al., 2005; Watts and Cooper, 2008). This diminished return was attributed to catalyst aggregation and segregation that

resulted in a decrease in TiO_2 concentration at the materials surface. Due to the nature of this relationship, it is not apparent whether this benefit is justified by the unit cost of TiO_2 (Heather Dylla et al., 2010). It should be noted, TiO_2 content is not frequently reported in photocatalytic pavement studies. Within patents governing this technology TiO_2 content as a percentage of binder ranges from 2-10% (Paz, 2010). Specific values are not available, assumedly to protect competitive advantage. Future stakeholders will need to rely on the research and development process of the patent holders and on available data verifying the products performance.

Material Variables RE: TiO_2 Properties

In addition to the content, the properties of TiO_2 contained within a photocatalytic pavement also impact NO_X removal. TiO_2 occurs in a variety of mineral forms, including anatase, brookite, and rutile. Although each mineral form is photocatalytically active, direct comparison finds that anatase is best-suited for photocatalytic oxidation applications because anatase is superior in both the rate at which electron-hole pairs are generated and has a better ability to adsorb reactants (Sclafani and Herrmann, 1996). Although anatase is a superior photocatalyst, mixtures of rutile and anatase (e.g., Degussa P-25, which contains anatase and rutile at a 3:1 ratio) garner the greatest photoactivity due to interaction between the minerals (Ohno et al., 2001). In addition to an appropriate mixture of mineral forms, high specific surface area values have also been demonstrated to enhance photocatalytic activity (Husken et al., 2009). Further discussion of TiO_2 properties, which enhance photocatalytic activity falls outside of the scope of this review. If of interest to the reader, the following publication would serve as a good starting point: Carp et al. (2004). As noted by the article, particular research needs include development of photocatalysts that can be activated by visible light and are selective in the pollutants that are oxidized. Stakeholders considering use of photocatalytic pavements would be wise to follow developments in TiO_2 photocatalysts and if possible select a catalyst which incorporates worthwhile research developments.

Material Variables RE: Mix Design and Surface Treatment

Even if the most photocatalytically efficient photocatalyst is selected for use in a pavement application, substantial care needs to be taken in designing a mix and surface treatment in order to garner the maximum removal of ambient NO_X. In cementitious systems some pavements can be made photocatalytic with addition of a thin mortar placed on the surface or a non-photocatalytic component. TiO_2 is added to either the cement or water components of the mortar mix. Lab research indicates that TiO2 is more homogeneously distributed, resulting in greater NO_X removal, when TiO2 is mixed with water (Husken et al., 2009). The researchers quality control may not be achievable in ready-mix plants. It is possible a more consistent distribution of TiO_2 in a photocatalytic mortar may be realized by tasking cement suppliers with the supplying photocatalytic cement. A second method to produce a cementitious photocatalytic pavement is to simply substitute photocatalytic cement in place of Type I cement when pouring concrete. With present technology, this practice is expensive. The cost can be reduced to an extent by using a two-lift pavement construction. Using widely accepted construction practice, a top layer could be reduced a 4 cm thickness (Hall et al., 2007). This technique does substantially increase costs (e.g., it requires two paving plants, two paving machines, and additional labor), but opens up

new opportunities to use lower-quality less expensive concrete in the bottom lift. Reportedly, these savings may be sufficient to offset the additional costs (Cable and Frentress, 2004).

Another option to produce photocatalytic pavement is to simply spray a water-based TiO_2 coating on an existing concrete surface (a process developed PURETI). The responsible vendor believes that this process may be economical, and independent lab testing indicates that it produces similar levels of NO_X removal as that of a 5% TiO_2 content (by binder weight) mortar coating (M. M. Hassan et al., 2010b). It would seem probable that a water-based spray coating would dissipate over time with exposure to roadway environments. Simulated weathering did not confirm this expectation (M. M. Hassan et al., 2010b). However given that coating pavement in this fahion is not common additional lab research complemented by field testing is recommended.

Surface treatments also can enable greater NO_X removal. Sand blasting and mixes in which aggregated sized less than 300 µm in diameter were removed, treatments which both increase the pavement specific surface area, each increase NO_X removal (Heather Dylla et al., 2010; Husken et al., 2009; Poon and Cheung, 2007). A rapidly developing advancement holding substantial promise is the development of pervious photocatalytic concrete, which has approximately 6 times more surface area exposure to sunlight (Asadi et al., 2012). Under the same testing conditions, pervious concrete with a TiO_2 depth of 2 inches or greater provided at minimum 11% greater NO removal than non-pervious photocatalytic concrete.

Operational Variables Impacting Photocatalytic TX Active Performance

Operating Variable: Blinding

The air-purifying effectiveness of photocatalytic pavements is hindered by reductions in NO_X PCO rate in comparison to the initial PCO rate (i.e., the rate when the pavement was installed). Pavement-specific literature attributes observed reductions to a decrease in irradiance reaching TiO_2 caused by fine dust and organism adhesion(Beeldens et al., 2011) and interference from roadway contaminants such as dirt, de-icing salt, and motor oil (H. Dylla et al., 2011b). Other TiO_2 studies attributed reductions in photocatalytic activity to blinding by the accumulation of oxidation products and intermediates (Beeldens, 2008; Demeestere et al., 2008; Ibusuki and Takeuchi, 1994; J. Zhao and Yang, 2003). These observed reductions in [NO_X] reduction performance are significant. A study in which photocatalytic paving blocks set in an outdoor environment and then tested in a photoreactor at set intervals observed a 50% decrease in removal efficiency over a 5-month period (Y Murata and Tobinai, 2002). This decrease was attributed to dust and organism adhesion. A similar test reported a 36% to 78% decrease in removal efficiency over 4 months and a 22% to 88% decrease with 12 months of exposure (Yu, 2003). After observing accumulation of particulate matter, oil, and chewing gum, and scratches on the pavement surface, the researchers credited a reduction in photocatalytic surface area as the cause for the decrease. To maximize the air-cleaning performance of photocatalytic concrete the primary factors that cause reductions in [NO_X] reduction must be identified. Dylla et al. (2011) used laboratory tests to determine the influence of dirt, de-icing salt, and motor oil on [NO_X] reduction. Each material significantly reduced oxidation efficiency, but the study did not

compare the amount of material applied to test pieces to amounts observed on installed pavements. This study also did not assess whether the oxidized product, NO_3^-, caused a reduction in oxidation efficiency. To ensure long-term performance of photocatalytic pavement, photoreactor studies must determine the primary factors that cause the field observed decrease in $[NO_X]$ reduction performance.

Operating Variable: Pavement Age

As noted above, materials that interfere with catalytically active sites can cause decreases in $[NO_X]$ reduction performance. Sufficient data does not exist to establish whether photocatalytic activity also decreases with pavement age. One report notes that activity lasts for a least one year, but acknowledges that longer duration tests are not complete (Cassar, 2004). Theoretically, the pavement should maintain photocatalytic activity because TiO_2 is not consumed by the $[NO_X]$ reduction process. Furthermore, any abrasion that results from traffic should expose new TiO_2 particles. Nevertheless, these assertions have not been verified with robust laboratory or field data. United States stakeholders will not progress with any large-scale projects unless research establishes that pavement age does not have a significant impact on activity (Berdahl and Akbari, 2007).

Operating Variable: Wash-off/Regeneration

Efficient use of photocatalytic pavement requires strategies to address the known decrease in $[NO_X]$ reduction rate that occurs over time after the pavement is installed in a near-road environment. Researchers have suggested shearing airflow, burning chemisorbed carbon species, simulated rainfall, and road cleaning (Beeldens et al., 2011; Demeestere et al., 2008; J. Zhao and Yang, 2003). Demeestere et al. (2008) found that airflow was a completely ineffective regeneration mechanism. While, surface burning may be economical for some small-scale applications, it is impractical for pavements. Some sources claim that rain or surface washing is sufficient to regenerate photocatalytic activity (Beeldens, 2008; Beeldens et al., 2011). One source noted the beneficial effect of rain, but still recommended surface washing at an interval of two months (Yu, 2002). However, another researcher found that washing with a brush and deionized water did not cause a statistically significant change (or increase) in the activity of photocatalytic paving blocks that had been partially deactivated by outdoor exposure in a near-road environment for a period of months (Yu, 2003). The conflicts that exist in published literature point to a need for research that determines effective washing mechanisms to regenerate the photocatalytic activity of these pavements. This research must tailor washing mechanisms to the factors that cause $[NO_X]$ reduction rate reductions and estimate the required washing frequency to maintain $[NO_X]$ reduction performance.

Operating Variable: Ecological Impact

Although the NO_3^- product that results from NO_X PCO can be used as a plant nutrient, within the United States, NO_3^- is a water pollutant where excessive concentrations in aquatic environments causes eutrophication (The Cadmus Group, 2009). Research on this possible unintended pollution is limited, but appears to suggest that concentrations are at levels that do not warrant

ecological concern. One example calculation yielded a concentration of 5.3 mg/L NO_3^- (City Concept, 2004). A second publication asserts that NO_3^- becomes bound inside the concrete matrix as calcium nitrate ($CaNO_3$) and that dissolution into runoff water would be at a concentration 10 times less than the first pollution level (PICADA, 2011). Another publication seemingly acknowledges that a water pollution problem is possible by proposing that NO_3^- can be extracted from runoff with a standard sewage plant (Husken et al., 2009). This solution may be practical in the authors country of residence (the Netherlands) but within the United States, the majority of road runoff travels directly to surface water. Potential stakeholders require laboratory and field data that confirms NO_3^- in runoff will not exacerbate current water pollution problems (Berdahl and Akbari, 2007).

Combined Effects of Variables

It warrants noting that the aforementioned individual variables do not operate in discrete fashion, but rather that they are all likely to overlap in terms of impact at any time. As a result, this multi-layered set of variables imposes a highly degree of complication with trying to develop an appropriate model of expected real-world behavior with TX Active pavement performance.

Field Evaluation of Photocatalytic Pavements

Multiple field studies of photocatalytic pavements do exist (see Table 3), but documentation is comparatively less extensive than that of laboratory research. Available field research can be categorized as those that compare photocatalytic and control sections, measure NO_3^- deposition as evidence of photocatalytic activity, and attempt to model observations. These categories of field research are summarized in the sub-sections that follow.

Table 3. Locations of field comparison of photocatalytic and control sections

Location	Installation type	Pavement type	Surface area (m^2)	Traffic volume	NO_X conc. change (%)	Measurement type	Reference
Antwerp, Belgium	Parking lanes of urban road	Paving blocks	10,000		20		Beeldens, 2006
Via Morandi, Segrate, Italy	Urban road	Thin mortar overlay	7,000	1000 veh h^{-1}	60	Max.	Italcementi, 2006; Essroc, 2008; Italcementi, 2009;
					50	Avg.	
Calusco dAdda, Bergamo, Italy	Industrial site road	Paving blocks	8,000		45	Avg.	Italcementi, 2006; Italcementi, 2009
Porpora Street, Milan, Italy	Road within tunnel	Concrete, photocatalytic ceiling paint	728 (concrete)	30,000 veh d-1	23	Min. UV irradiance	Italcementi, 2006
Borgo Palazzo, Bergamo, Italy	Urban	Paving blocks	7,000	400 cars h^{-1}	40	Max.	Italcementi, 2009
					20	Min	
			12,000		66	Max.	Guerrini and Peccati, 2007
					20	Min.	
Rue Jean Bleuzen, Vanves, France	Urban road	Concrete overlay	6,000	13,000 cars d^{-1}	20	Min.	Italcementi, 2009

Table 4. Locations of other photocatalytic pavement field studies

Location	Installation type	Pavement type	Surface area (m^2)	Reference
Hengelo, Netherlands	Urban road	Paving blocks	750-1,200	Overman, 2009
Milan, Italy	Parking garage	Spray coating on asphalt	4,000	Crispino and Vismara, 2010
Forli-Cesena, Italy	Highway	Spray coating on asphalt	2,500	Crispino and Vismara, 2010
Cantù and Monza, Italy	Urban road	Spray coating on asphalt		Crispino and Vismara, 2010
Ferrara, Italy	Urban road	Spray coating on asphalt	13,000	Crispino and Vismara, 2010
Milan, Italy	Road within tunnel	Spray coating on asphalt	11,000	Crispino and Vismara, 2010
Multiple locations, Japan	Sidewalks and urban roads	Paving blocks	25,000	Beeldens and Cassar, 2011
Baton Rouge, LA, United States	Urban road	Spray coating on concrete		Hassan and Okeil, 2011
Den Hoek 3, Wijnegem, Belgium	Industrial site road	Concrete, two-lift construction		Beeldens and Elia, 2012

Field Comparison of Photocatalytic and Control Pavement Sections

Error! Reference source not found. summarizes the field studies that reported a percent change in NO_X concentration between control and photocatalytic sections. For the studies listed, the Borgo Palazzo report provides the most detailed data. The proposed locations for the control and photocatalytic locations were monitored prior to the study, verifying that each section demonstrated similar characteristics for NO_X pollution concentration and variation with time (Guerrini and Peccati, 2007). During low irradiance hours, concentration at each section was not measurably different. For daylight hours, when both irradiance and traffic markedly increased, the change in concentration between the control and photocatalytic sections ranged from 20-66%. The report also noted that soiling caused by construction traffic caused a decreased in photocatalytic activity.

In addition to general observations, which comport well with laboratory data, the report from Guerrini and Peccati (2007) also provided new insights specific to field applications. As evidenced by the 1-hour standard promulgated by the USEAP in 2010, short-term exposure to NO_X is particularly damaging to human health. The control location data displays peaks in NO_X concentration that correspond with high traffic volumes. These peaks are substantially diminished in observations from the photocatalytic section. Furthermore values of percent difference for these instances are substantially above average reports, indicating that photocatalytic pavement is particularly effective as a tool to mitigate short-term spikes in air pollution. Laboratory data has established that photocatalytic pavements oxidize NO_X when a small volume of NO_X is passed over the pavement surface, but it is difficult to extrapolate this lab data to large areas. Observations by Guerrini and Peccati (2007) begin to provide this

extrapolation by providing measurements at 0.3 and 1.8 m. While measurements at the lower observation point indicate greater [NO_X] reduction, even at 1.8 m the photocatalytic section values are on average 20% lower than at the control location.

At the Baton Rouge site, NO_X concentration was also measured simultaneously for a concrete section coated sprayed with a TiO_2 aqueous solution and a control section (M. M. Hassan and Okeil, 2011). To compare the two sections, in one figure the authors reported total daily NO_X reduction in units of ppb. For each data point, the reported value was greater than 1000 ppb. The statistical approach used is difficult to understand and does not facilitate comparisons with other field or laboratory studies. Considering that this value is an order of magnitude greater than the USEPA 1-hour standard, it is highly improbable that the statistic is the difference between locations. Regardless, the report does provide evidence that the pavement oxidizes NO_X in field applications. Hassan and Okiels work also draws correlations between environmental factors and NOx reduction observed. In concert with lab data, the authors observed that NO_X reduction was negatively correlated to relative humidity and wind speed and positively correlated to irradiance.

The authors consideration of wind direction warrants additional discussion. It is anticipated that the majority field applications of photocatalytic pavement will occur in a street canyon where both natural ventilation is reduced and heavy traffic represents the major portion of NO_X pollution. For the geometric configuration of a street canyon, longitudinal winds flush the area, preventing accumulation of NO_X. Under transverse winds, the residence time of the pollutant molecule is increased, permitting more time for photocatalytic oxidation and thereby resulting in increased percent NO_X reduction. This study found that NO_X reduction was higher when winds were in a longitudinal direction than when winds blew transversely. The result can be explained by the sites geometric conditions. Unlike anticipated applications, this study occurred in an area free from buildings which would prevent natural ventilation. Instead of flushing the surface and diminishing NO_X reduction, longitudinal winds are associated with the highest NO_X residence time at this particular location. Of particular interest, the authors found that transverse winds were especially negative. These winds carry the pollutant off of the pavement. Future stakeholders will need to take time to consider where the install pavements. As mentioned previously, a street canyon may be especially good location. Due to a lack of natural ventilation residence time of the pollutant above the photocatalytic surface is increased, enhancing photocatalytic oxidation.

Available field studies that compare photocatalytic and control sections of pavement highlight multiple factors that influence photocatalytic oxidation and the difficulty in providing data that provides sufficient evidence that will persuade stakeholders to adopt this technology. The reported studies are worthwhile, but additional work must provide more detailed data and data that is collected for a longer duration than that of the present work.

Field Measurement of NO_3^- Deposition

The comparative approach, which evaluates photocatalytic pavement with reference to a control section, requires significant expenses of both time and dollars. Furthermore, the data obtained can be difficult to evaluate because of multiple factors influence both the concentration of NO_X

pollution in an area and the effectiveness of photocatalytic oxidation. An alternative approach measures NO_3^-—the final product of NO_X photocatalytic oxidation–that accumulates on the surface of a pavement containing TiO_2. For photoreactor tests, this approach is described by an international standard (ISO, 2007). Osborn et al. (2012) applied this approach in an effort evaluate photocatalytic pavements in the field. A section of the pavement surface was isolated and soaked with water. This water was then analyzed for $[NO_3^-]$. For a 7 day observation period, $[NO_3^-]$ on the photocatalytic section averaged 0.04 mg l-1 as N whereas the control section averaged 0.003 mg l-1 as N. While the method holds promise, deficiencies must be addressed in order to use this approach to evaluate photocatalytic pavements. Foremost, the author does not provide evidence that the procedure removes all NO_3^- from the pavement surface or provide a factor to account for the amount of NO_3^- that remains on the surface following use of the washing technique. Additionally, the author assumes that all NO_3^- oxidized remains on the surface and that water is the only factor that can remove the compound. Without factors that account for these uncertainties, the application is quite limited.

Modeling Efforts to Predict Field Observations

Comparative field studies and studies that measure products of NO_3^- on the photocatalytic surface represent worthwhile steps to validate photocatalytic pavements in the field. However, it is probable that the most useful tool to persuade future stakeholders will be models that can accurately predict NO_X concentration for photocatalytic and non-photocatalytic pavements. This type of model, would then serve as a tool by which a particular area could be evaluated as a candidate for photocatalytic pavement. After determining an expected decrease in NO_X concentration for the area, the stakeholders could then determine whether the cost of constructing a photocatalytic roadway outweighs other pollution mitigation options.

Based on field data, M. M. Hassan and Okeil (2011) provide a nonlinear regression model governed variables of traffic volume, relative humidity, wind speed, temperature, and irradiance factors. Considering the multiple factors involved, the models reported 0.70 R^2 value appears quite high. However application to other test locations is severely limited because upper boundaries are set at values of 52 vehicle h^{-1}, 2.7 m s^{-1}, and 20°C for traffic volume, wind speed, and temperature respectively. Furthermore, the model does not distinguish whether the output result is for the breathing height of an adult or directly at the pavement surface. Although a stakeholder will be regulated by the concentration recorded at a near-road or area-wide monitor, true concern is human welfare. Therefore, models should allow users to determine an estimate of concentration at the breathing heights of both children and adults.

A deliverable from the PICADA project provides a second option to predict the NO_X abatement effectiveness of photocatalytic materials (Barmpass et al., 2006). The fluid dynamics-based model was developed for photocatalytic coatings on buildings, but could be adapted for photocatalytic pavements. A reference scenario is developed with inputs of street and building dimensions, wind speed and direction, and average observed NO_X concentration. The scenario is then adjusted for photocatalytic oxidation of NO_X by inclusion of a deposition velocity variable. Incorporating all environmental factors that influence photocatalytic oxidation into a single

variable severely limits the model. As noted by the authors this model should only be used as a "rough guide".

Overmans two-dimensional model is based on both fluid dynamics and kinetic equations for photocatalytic oxidation and atmospheric reactions (Overman, 2009). The fluid dynamics components are governed by building and street geometry along with wind speed and direction. The photocatalytic oxidation kinetics component is based data obtained by Ballari et al. (2010) and includes inputs to account for irradiance, relative humidity, and NO and NO_2 concentration. In addition, with input of O_3, the model accounts atmospheric photolysis of NO_2 by UV irradiance. This model was applied to a road in Hengelo, Netherlands, with predicted reduction ranging from 2-6% and 10-19% for NO and NO_2 respectively. The two-dimensional component of the model allows for prediction of concentration at varied heights; however, wind direction is always assumed to be transverse. To account for other wind directions, a three-dimensional model would be required. Unfortunately, while calibrated against observations prior to photocatalytic pavement installation, a report is not available that assesses the predicted results after construction. This follow-up modeling effort would provide substantial

Research Gaps

Photocatalytic pavements have generated high interest from researchers and potential stakeholders. With an ever-increasingly stringent regulatory environment, it is highly probable that new approaches will be needed to mitigate NO_X pollution. Furthermore, while this review places focus on photocatalytic reactions with NO_X, benefits exist that cause oxidation of other pollutants detrimental to both the human welfare and the natural environment. At present, multiple areas exist in both laboratory and field research for which additional knowledge is needed. While the body of literature is substantial, future research must use strengthen the link between photoreactor and field studies, determine the environmental variables with the greatest impact on $[NO_X]$ reduction, and develop models to facilitate selection of roadways for which maximum $[NO_X]$ reduction can be achieved. While the field is novel and fascinating to study, the amount of work to be overcome is still significant. Multiple researchers are needed to address this problem and each will only be able to incrementally move the state of knowledge forward. However, it is the authors hope that with collective efforts of researchers in this field, a technology that meaningfully abates NO_X pollution can be developed.

Pervious Concrete Pavement

Pervious concrete is a rigid pavement and is structurally designed as such. Rigid pavement design considerations specific to pervious concrete are lower flexural strength, lower modulus of elasticity, and subgrade design assuming saturated conditions. AASHTO, ACI, or PCA design procedures are appropriate, however fatigue relationships have not been established or field verified so designs should provide a higher design reliability (Delatte, 2007). Results reported in the literature show a linear decrease in modulus of elasticity values for pervious concrete with increased void content, similar to relationships for strength. Reported modulus of elasticity for pervious concretes with 25% voids was around 3.6 million psi (24,800 MPa) and decreased to 1.5 million psi (10,300 MPa) at 40% voids, for mixtures using limestone aggregate (Crouch et

al., 2007). Oftentimes the aggregate base depth is controlled by the required water storage capacity and soil infiltration rate. In cold climates the aggregate base depth can normally be 12 to 18 inches (300-450 mm) or more. In most cases the additional aggregate base required for the hydrologic design will balance the lower modulus of the surface concrete. While standard rigid pavement designs are appropriate conservative inputs for modulus of elasticity and fatigue performance should be used.

The hydrologic design of pervious concrete has the most available guidance since the storage design is basically that of a traditional detention/retention area. The infiltration type depends on soil infiltration capacity and amount of recovery time desired between storm events. Most systems are designed to empty before 48 to 72 hours. Designs can either infiltrate all of the stormwater (full infiltration), some of the stormwater such as the water quality volume (partial infiltration), or be lined to prevent infiltration (no infiltration). For pervious concrete shoulders a drain tile is recommended to prevent any lateral flow of water towards the mainline pavement. The shoulder stormwater design should be either designed for no infiltration or partial infiltration.

The hydraulic design of the surface of pervious concrete is the least researched and most difficult to provide exact values for recommendation purposes. The pervious concrete pore size should be sufficiently large to allow the vast majority of suspended solids to pass through into the detention layer. If the pores are too small or the infiltration rate to low, particles become trapped in the surface and the pavement clogs. The ASTM C1701 test for the infiltration rate of in place pervious concrete has allowed actual testing of pavement capacity over time. The author has tested many pervious concrete pavements in various stages of clogging and has proposed some design targets based on the results (Kevern, 2011). Pervious concrete pavements with infiltration rates greater than 500 in./hr (1,250 cm/hr) tended to have lower instances of clogging than those below 250 in./hr. (600 cm/hr) Pervious concrete pavements with infiltration rates above 1,000 in./hr. (2,500 cm/hr) appeared to have some self-cleaning ability and were able to flush even larger amounts of soil through the surface with time. While there is currently no precision and bias statement for the ASTM C1701 test, consideration of infiltration capacity during the design process will reduce instances of clogging.

Global Breakdown of Academic and Industrial Research Activity Locations

The following two figures (i.e., Figures 6 and 7) respectively provide a visual breakdown of academic and industrial research activities aligned to the use and performance of photocatalytic concrete materials.

Iowa State University
Ames, IA

- Sikkema, JK, Alleman, JE, Ong SK, *et al.* (2012). Photocatalytic Concrete Pavements: Decrease in NOX Removal due to Reaction Product Blinding. *P Int Conf Long-Life Conc Pav-2012.*

Louisiana State University
Baton Rouge, LA

- Hassan, MM, Mohammad L, and Copper, S (2012). Mechanical Characteristics of Asphaltic Mixtures Containing Titanium Dioxide Photocatalyst. *J Test Eval.*
- Osborn, D, Hassan, MM, and Dylla, H (2012). Quantification of NO_X reduction via Nitrate Accumulation on a TiO_2 Photocatalytic Concrete Pavement. *J Transp Res Rec.*
- Asadi, S, Hassan, MM, Kevern, J, *et al.* (2012). Development of Photocatalytic Pervious Concrete Pavement for Air and Stormwater Improvements. *J Transp Res Rec.*
- Dylla, H, Hassan, MM, and Osborn D (2012). Field Evaluation of Photocatalytic Concrete Pavements' Ability to Remove Nitrogen Oxides. *J Transp Res Rec.*
- Dylla, H, and Hassan, MM (2012). Characterization of Nanoparticles Released during Construction of Photocatalytic Pavements using Engineered Nanoparticles. *J Nanopart Res.*
- Hassan, MM, Dylla, H, Asadi, S, *et al.* (2012). Lab evaluation of Environmental Performance of Photo-catalytic Titanium Dioxide Warm-Mix Asphalt pavements. *J Mater Civil Eng.*
- Hassan, MM, Dylla, H, Mohammad L, *et al.* (2012). Methods for Application of Titanium Dioxide coatings to Concrete Pavement. *Int J of Pav Res and Tech.*
- Dylla, H, Hassan, MM, Schmitt, M, *et al.* (2011). Effects of Roadway Contaminants on Titanium Dioxide Photodegradation of NO_X. *J Transp Res Rec.*

U of Missouri–Kansas City
Kansas City, MO

- Kevern, JT (2012). Pervious Concrete Shoulders for Stormwater Management. *P Int Conf Long-Life Conc Pav-2012*
- Asadi, S, Hassan, MM, Kevern, J, *et al.* (2012). Development of Photocatalytic Pervious Concrete Pavement for Air and Stormwater Improvements. *J Transp Res Rec.*

Washington State University
Pullman, WA

- Shen, S, Burton, M, Jobson, B, *et al.* (2012). Pervious Concrete with Titanium Dioxide as a Photocatalyst Compound for a Greener Urban Road Environment. *Trans Res B.*

- Hassan, MM, Mohammad L, Cooper S, *et al.* (2011). Evaluation of Nano Titanium Dioxide Additive on Asphalt Binder Aging Properties. *J Transp Res Rec.*
- Dylla, H, Hassan, MM, Schmitt, M, *et al.* (2011). Laboratory Investigation of the Effect of Mixed Nitrogen Dioxide (NO_2) and Nitrogen Oxide (NO) Gases on Titanium Dioxide Photocatalytic Efficiency. *J Mater Civil Eng.*
- Dylla, H, Hassan, MM, Mohammad L, *et al.* (2010). Evaluation of the Environmental Effectiveness of Titanium Dioxide Photocatalyst coating for concrete pavements. *J Transp Res Rec.*
- Hassan, MM, Dylla, H, Mohammad L, *et al.* (2010). Evaluation of the Durability of Titanium Dioxide Photocatalyst Coating for Concrete Pavement. *J Constr Build Mater.*
- Hassan, MM (2010). Quantification of the Environmental Benefits of Ultrafine/nano Titanium Dioxide Photocatalyst Coatings for Concrete Pavement using Hybrid Life Cycle Assessment. *J Infrastruct Syst.*

Figure 8. US research activity with photocatalytic concrete pavement

UNIVERSITY OF TWENTE.

BRRC

HEIDELBERGCEMENT

Italcementi Italcementi Group

UNIVERSITY OF TWENTE. **University of Twente**
Enschede, Netherlands

- Ballari, MM. Yu, QL, & Brouwers, HJH (2011). Experimental study of the NO and NO2 degradation by photocatalytically active concrete. *Catal Today.*
- Ballari, MM, Hunder, M, Husken, G *et al.* (2010). Modelling and experimental study of the NOx photocatalytic degradation employing concrete pavement with titanium dioxide. *Catal Today.*
- Ballari, MM, Hunger, M, Husken, G, *et al.* (2010). NOx photocatalytic degradation employing concrete pavement containing titanium dioxide. *Appl Catal B-Environ.*
- Hunger, M, Husken, G, & Brouwers, HJH (2010). Photocatalytic degradation of air pollutants – From modeling to large scale application. *Cement Concrete Res*.
- Ballari, MM, Hunger, M, Husken, G *et al.* (2009). Heterogeneous Photocatalysis Applied to Concrete Pavement for Air Remediation. *P 3rd Int Sym Nanotech in Constr.*
- Husken, G, Hunger, M, & Brouwers HJH (2009). Experimental study of photocatalytic concrete products for air purification. *Build Environ*.
- Hunger, M, Husken, G, & Brouwers, HJH (2008). Photocatalysis applied to concrete products: Part 1: Principles and test procedure. *ZKG Int*.
- Hunger, M, Husken, G, & Brouwers, HJH (2008). Photocatalysis applied to concrete products: Part 2: Influencing factors and product performance. *ZKG Int*.
- Hunger, M, Husken, G, & Brouwers, HJH (2008). Photocatalysis applied to concrete products: Part 3: Practical relevance and modeling of the degradation process. *ZKG Int.*
- Husken, G & Brouwers, HJH (2008). Air purification by cementitious materials: Evaluation of air purifying properties. *P Int Conf Constr Build Mater 2008.*
- Husken, G., Hunger, M, & Brouwers HJH (2007). Comparative study on cementitious products containing titanium dioxide as photo-catalyst. *Int RILEM Sym TDP 2007.*

BRRC **Belgium Road Research Centre**
Brussels, Belgium

- Beeldens, A, & Elia, B (2012). A double layered photocatalytic concrete pavement: a durable application with air-purifying properties. *10th Int Conf Conc Pav.*
- Beeldens, A, Cassar, L, & Murata, Y (2011). Applications of TiO2 Photocatalysis for Air Purification In Y. Ohama & D. Van Gemert (Eds.), *Application of Titanium Dioxide Photocatalysis to Construction Materials* (1st ed.): Springer.
- Beeldens, A (2008). Air purification by pavement blocks: final results of the research at the BRRC. *Transport Res Arena Eur.*
- Beeldens, A (2007). Air purification by road materials: Results of the test project in Antwerp. *Int RILEM Sym TDP 2007*.
- Beeldens, A (2006). Envrionemtnal friendly concrete pavement blocks: Air purification in the centre of Antwerp. *8th Int Conf Conc Block Pav.*
- Beeldens, A (2006). An environmental friendly solution for air purification and self-cleaning effect: the application of TiO2 as photocatalyst in concrete. *Transport Res Arena Eur.*

Italcementi Italcementi Group **Italcementi**
Bergamo, Italy

- Crispino, M, Brovelli, C, Guerrini, GL, *et al.* (2011). Innovation materials for road construction: Photocatalytic road pavements. *24th World Road Congress.*
- Beeldens, A, Cassar, L, & Murata, Y (2011). Applications of TiO2 Photocatalysis for Air Purification In Y. Ohama & D. Van Gemert (Eds.), *Application of Titanium Dioxide Photocatalysis to Construction Materials* (1st ed.): Springer.
- Guerrini, GL & Peccati, E (2007). Photocatalytic cementitious roads for depollution. *Int RILEM Sym TDP 2007.*
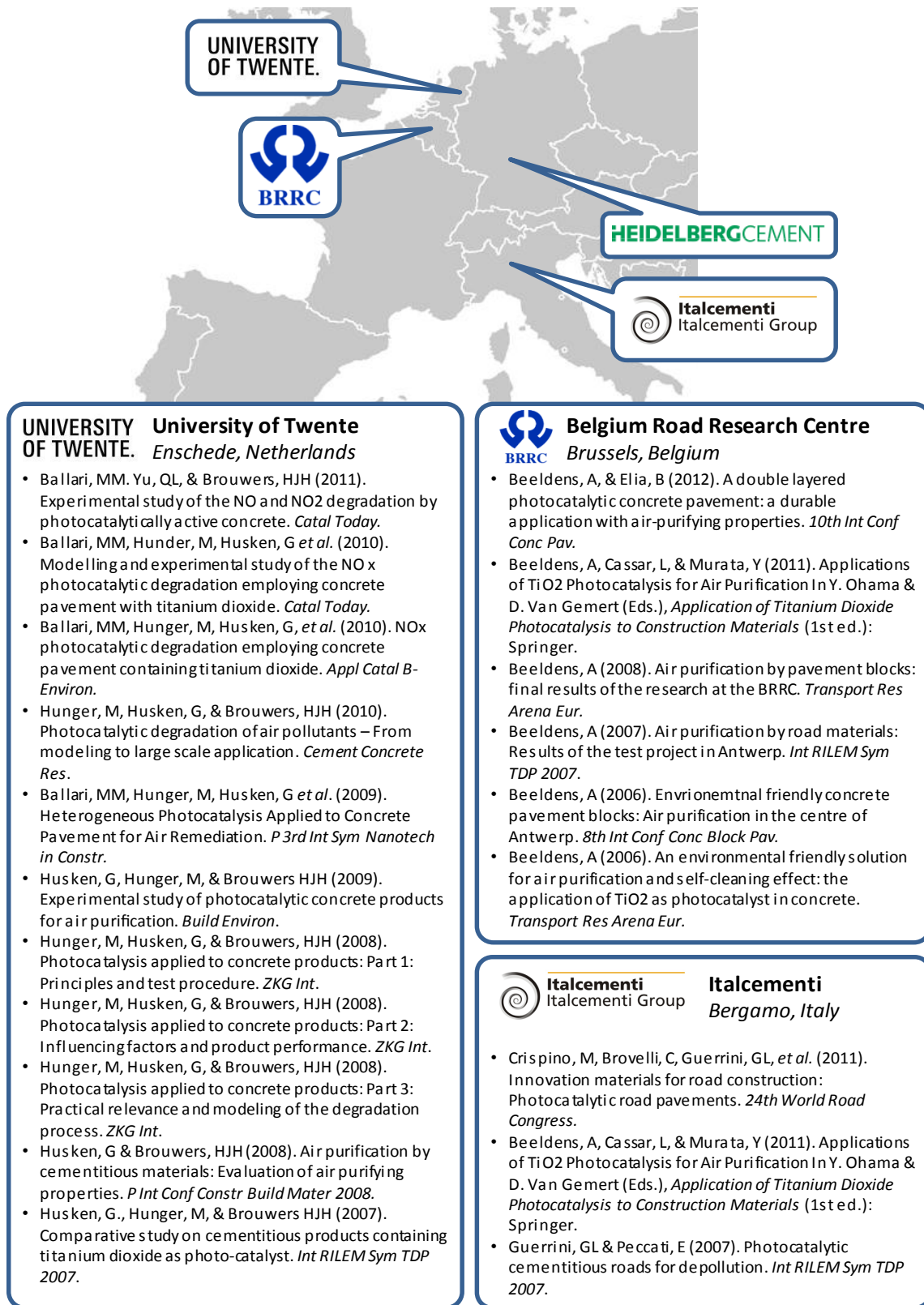
Figure 9. Non-US research activity with photocatalytic concrete pavement

MATERIALS AND METHODS

General Site Location Details

Highway Siting, Expected Traffic Density, and Test Section Size

Highway 141 is situated within the western St. Louis metropolitan region. The general north-south alignment of this project site is bounded on its north and south ends by intersecting Olive (Rt 340) and Ladue Roads, respectively. This stretch of highway was originally known as Woods Mill Road, where the original alignment of the road was located approximately one-quarter mile to the west (see adjacent Figure 10).

Figure 10. General Highway 141 project siting overview at St. Louis, Missouri

Construction of this new highway section, therefore, significantly improves north-south traffic flow through this area, prospectively enhances ambient air and water quality, and improves vehicular safety for adjacent community vehicles still using the original Woods Mill Road. Both the TX Active and conventional pavement test sections were situated on the southbound side of this highway.

MoDOT has projected that the average daily traffic (AADT) for this newly installed section will be approximately 46,000. When originally evaluating prospective new highway locations with which this research project would be completed, it was believed that this traffic density would be acceptable in terms of the correspondingly expected NO_2 concentration. As reported in Cape *et al.,* 2004, NO_2 concentrations can be expected to increase dramatically between an ADT of 0 and 26,000. However, above 26,000, NO_2 concentration increases only slightly with increases in ADT. The data from Cape et al., 2004, was compiled into a figure (i.e., see Figure 11) by HEI, 2009. At the projected AADT, our paving selection falls on the portion of the graph where the slope of the NO_2 concentration vs. distance to highway line is quite low.(Cape et al., 2004).

NO$_2$ Concentration (Hg/m^3)
vs
Distance to Highway (m)
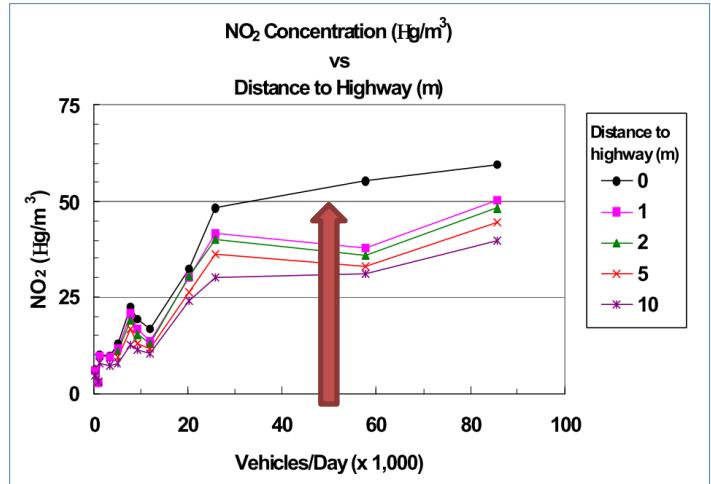
Figure 11. NO$_2$ levels as a function of distance to roadway and total vehicle density. Note: concentration was measured in µg/m3 not Hg/m3. (Adapted from data reported by Cape et al. 2004) (HEI, 2009)

The site test section paved with TX Active material, as well as the complementary control section paved with conventional concrete, was designed and constructed with a linear run of 1,500 ft (457 m), with an overall area of ~5,300 m^2. This length and area is somewhat smaller than the European TX Active paving study in Segrate, Italy and Vanves, France [7000 and 6000 m^2 respectively with respective ADTs of 24,000 and 13,000 (Essroc, 2009; Italcementi, 2009)]. However, given the wind-blocking sound wall siting and orientation (see following section narrative), these test section length and area was considered appropriate for the projects intended assessment.
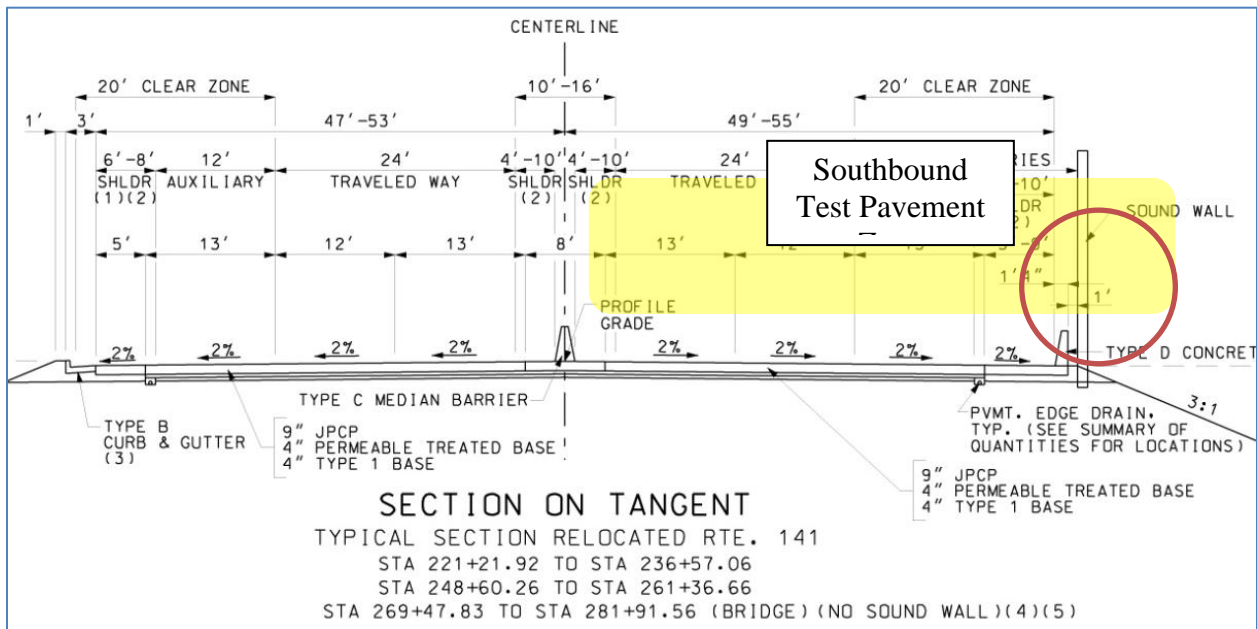
Figure 12. Highway 141 design profile view

Intent on matching wind conditions, sunlight incidence angles, sound wall shading impacts, etc., we situated both pavement test sections at the more northern end of the new Highway 141 section, immediately south of the southbound ramp leaving Olive Rd on the north side of the project area. Figure 13 shows the southbound perspective of this highway section within the TX Active test zone, with the adjacent sound all seen on the right side of this view.

Figure 13. Southbound Highway 141 perspective immediately after access ramp from Oliver Road (Rt 340)

Admittedly, our team did have a related concern about variable vehicle speeds (i.e., escalating) for traffic heading south away from the Olive Rd. ramp, where there would be an inherent change in engine efficiency and varied release of NO_2 emissions. However, we concluded that vehicles have reached a near-steady speed by the time they enter our first set of environmental testing stations approximately 2000 ft beyond the end point of the Olive Road ramp.

In turn, all air, water, and test coupon samples secured during our study were obtained on the western side of these pavement sections, within the shoulder region of these test pavement sections (i.e., again, see red circled zone in the preceding Figure 12).

Conventional Concrete Mixture Proportions

The mainline two-lift pavement mixtures were developed by Fred Weber Inc. with guidance from Essroc/Italicementi regarding use of the TX Active material. The coarse aggregate used was St. Louis formation limestone with a MoDOT "D" gradation. The coarse aggregate specific gravity was 2.64 with an absorption of 1.08%. The aggregate gradations along with the coarse aggregate specifications are shown in Figure 14. The fine aggregate was Missouri River sand with a specific gravity of 2.63 and absorption of 0.40%.
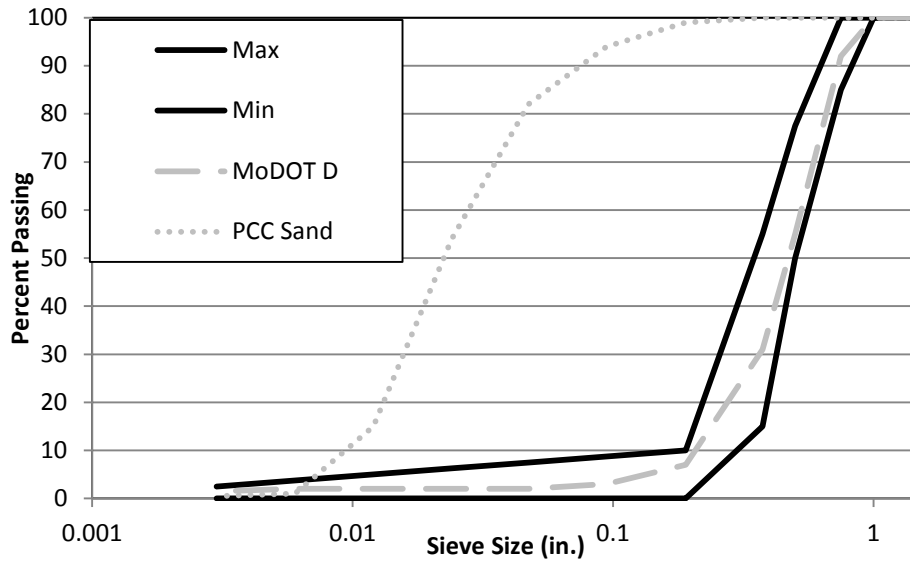
Figure 14. Impervious concrete aggregate gradations

The concrete mixture proportions are shown in Table 5. The bottom lift was a lean concrete with 25% Class C fly ash. The top lift only contained TX Active cement as to not dilute the photoreactive properties.

Table 5. Concrete mixture proportions

Material	Bottom Lift (pcy)	Top Lift (pcy)
Type I/II Cement	345	0
TX Active Cement	0	541
Fly Ash "C"	115	0
Coarse Agg.	1888	1882
Fine Agg.	1369	1226
Water	193	227
Air	6%	6%

Pervious Concrete Mixture Proportioning

Pervious concretes are a hybrid of a traditional pavement surface, a stormwater detention basin, and a filter. Consequently, successful designs should address all three aspects. The requirements for pervious concrete for use as a shoulder are as follows:

- Strong enough to function as a shoulder pavement
- Durable enough to prevent excessive concrete material-related maintenance
- High enough permeability to minimize clogging maintenance
- Proper hydrologic design to minimize lateral water movement

- Rapid aggregate base draining for subgrade protection
- Rapidly constructible
- Able to be cured without plastic

Pervious concrete mixture development was based on lessons learned from the pervious concrete overlay construction and performance at MnROAD (Kevern et al. 2011) and the previously mentioned requirements. Other controlling factors in the design were placed by the contractor, 1) limited coarse aggregate gradations were available, and 2) placement would be performed by discharging concrete from an agitator truck directly onto the shoulder and finished with a roller-screed. One additional condition placed on the mixture, by the author, to ensure the selected mixture could be used for wide-spread shoulder applications was the elimination of curing under plastic.

A super absorbent polymer (SAP) was investigated to hold additional curing water in the cement paste, provide sacrificial water for evaporation, and improve hydration. A crushed crystalline partial sodium salt of cross-linked polypromancic acid rated at 2000 times absorption for pure water was included in the mixture development (Kevern and Farney 2012).

The available aggregate gradations are shown in Figure 15.
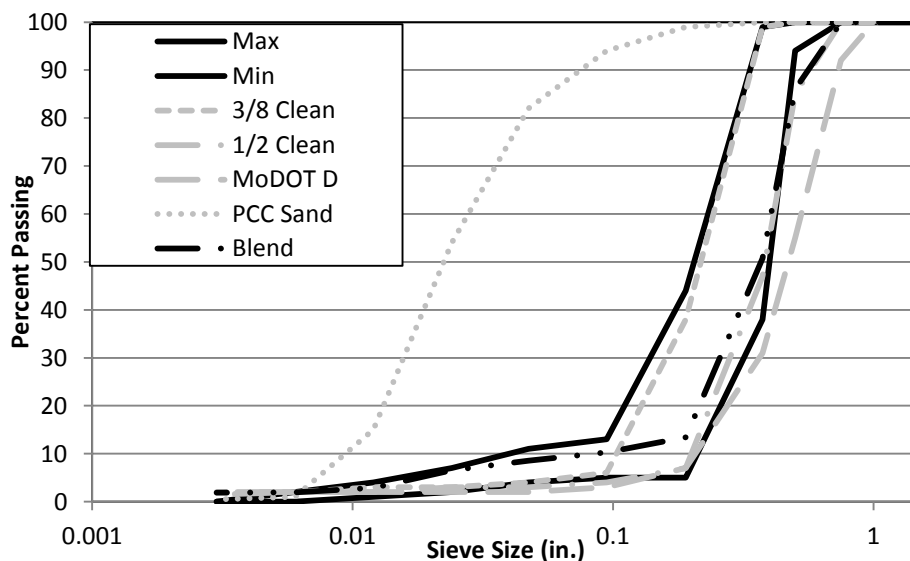
Figure 15. Potential and selected aggregate gradations

The gradation limits shown for pervious concrete were suggested in a report by the Portland Cement Association (PCA) (Kevern et al. 2010). Three limestone coarse aggregate were available. Two were clean aggregates available for asphalt production and one used for the conventional concrete paving. While many different aggregate gradations can create pervious concrete, excessively large aggregates create an uneven and rough surface. The available concrete aggregate was deemed too coarse. The 3/8 inch clean aggregate met gradation criteria but trended toward the fine limit. Simultaneously considering future maintenance, generally

pervious concretes with large pores and high permeability have less clogging than finer mixtures (Kevern 2011). Consequently the ½ inch (12.5 mm) clean gradation was selected. Since the coarse aggregate contained a large portion of voids, a relatively high sand content (22% by mass) was used to provide sufficient strength.

The selected mixture proportions are shown in **Error! Reference source not found.**. The water content shown includes a water-to-cement ratio (w/c) of 0.35 and an additional 0.05 required for internal curing (RILEM 2007). The extra water is absorbed into the SAP, which swells. Balancing the desired amount of voids required decreasing the cement content to maintain appropriate mortar volume. Compared to most other pervious concrete mixtures, the mixture shown in **Error! Reference source not found.** has a lower cement content and higher w/c ratio.

Admixtures include SAP at 1.5 oz/cwt (1 mL/kg) , polycarboxylate water reducer at 4 oz/cwt (3 mL/kg) , hydration stabilizer at 4 oz/cwt (3 mL/kg), and air entrainer at 1 oz/cwt (0.7 mL/kg). One additional benefit of the SAP is better admixture efficiency provided by lubrication of the hydrated SAP gel. Typically a one-third to one-half reduction of the admixtures used for conventional pervious concrete produce the same results with the SAP mixtures.

At equal void contents a baseline pervious concrete mixture without SAP would contain 575 pcy (341 kg/m^3) of cement and a w/c of 0.30. When the extra cost of SAP combined with the reductions in cement content and admixtures are factored, the SAP mixture costs $1.70 extra per cubic yard. Additional cost savings from eliminating plastic materials and labor are highly specific, but generally result in savings versus the control mixture.

Table 6. Selected pervious concrete mixture proportions

Material	Amount (pcy)
TX Active Cement	510
Coarse Agg.	2030
Fine Agg.	360
Fibers	1.5
Water	200
Design Voids	24%
Design UW	114.75 pcf

Specific Details with Field-Scale Air Sampling, Instrumentation, and Analyses

Both short-term active and long-term passive air monitoring methods were used during this study, by which we might quantify the benefits to the urban environment using concrete produced with photocatalytic cement through NO_2 abatement. Of course, nitrogen dioxide levels were measured in each case alongside pavements both with and without TX Active materials.

The latter passive method used a time-integrative diffusion $\rightarrow$ reaction method for NO_X, NO_2, and NO analysis, commonly referred to as an Ogawa- or Palmes-type method. Our research team

felt that passive samplers were well-suited to this type of performance assessment, and published results for passive testing have validated that the obtained results have been comparable to reference methods (Hagenbjörk-Gustafsson et al., 2009; Mukerjee et al., 2009; Sather et al., 2007).

The following four figures depict Ogawa samplers used at the 141 site, as were affixed to the crash barriers adjacent to each pavement test section.

Figure 16. Ogawa sampler

Figure 17. Ogawa sampler with protective shroud

Figure 18. Ogawa analyzers mounted on adjacent crash barrier wall (i.e., including three upper and three lower samplers per each location)

Upper crash barrier
Ogawa samples
(~0.8 meter elevation)

Lower crash barrier
Ogawa samples
(~0.2 meter elevation)
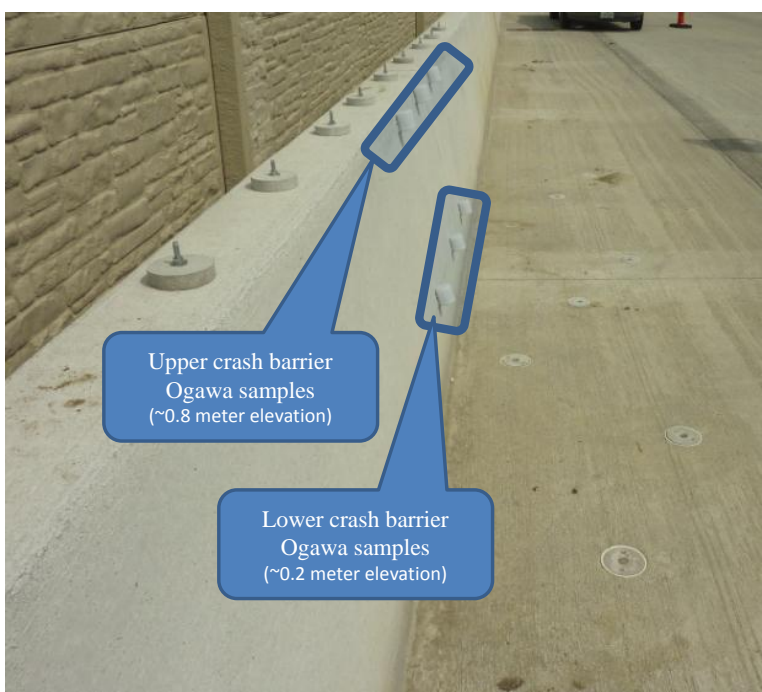
Figure 19. Upper (~100 cm height) and lower (~30 cm height) Ogawa sample unit layout per each test location

Further details regarding the Ogawa hardware and the associated application of these passive devices can be found at their web site (www.ogawausa.com/passive.html). The Ogawa analysis employs two types of chemically treated reactant capture pads housed within these samplers, which essentially act as sponges to sorb nitrogen oxides from the adjacent atmosphere over an extended multi-day to multi-week time period.

This studys passive analytical approach represented one of the unique aspects of our research effort. Prior testing of the TX Active concept for NO_2 removal, largely documented by technical

personnel involved with the involved industries (i.e., Italcementi or Essroc), focused on the use of real-time on-site chemiluminescent analysis (Scott, 2010). No doubt this method has advantages, but our research team believed that the Ogawa-type approach offered a better analytical perspective by way of its time-integrative approach. Ogawa- or Palmes-type sampling has, in fact, been extensively applied for near-road NO_2 testing in Europe of the past several years, and the Ogawa-type sampling method has been used in the United States during extensive road-related NO_2 testing in relation to nearby school systems (i.e., Mukerjee, et al., 2004, 2009a and b). Related validation of the utility of this passive diffusion testing strategy has been provided by Nash and Leith, 2010.

On-site NO and NO_2 testing, using an ozone titration instrument was also used for active testing on intermittent, seasonal intervals (see Figure 20).

Figure 20. On-site use of Active NOx 2B Technologies tnstrumentation

This 2B Technologies Inc. ozone depletion instrument includes a molybdenum pre-processor which enables the device to individually quantify both NO and NO_2 values. Two different sampling strategies are involved, measuring both ambient air immediately adjacent to the sound wall, as well as air at the interface between travelled and shoulder zones at a near-surface elevation. The latter, near-surface pavement sampling zone has been arranged using a rubber sampling line…which is analogous to a traffic counter tube commonly placed across highway for monitoring traffic counts…affixed to the pavement and extending across the shoulder to the edge if the adjacent travel lane.

While active chemiluminescent testing was not conducted on-site, an invitation has been extended to the US Environmental Protection Agency to bring their mobile NO_2 lab resources (and, assumedly, using chemiluminescent methods) to this site, such that their testing efforts verifies our own NO and NO_2 removal findings via both passive Ogawa and active ozone-titration protocols.

In both instances, the air sampling equipment was situated in the near-road zone, either affixed to the Type D barrier adjacent to the tested highway sections (i.e., as in the case of our Ogawa testing units) or sitting just behind the crash barrier (i.e., as in the case of our active NOx instrument) and sniffing air immediately adjacent to this barrier in direct proximity to the nearby travel lane. Our air sampling locations were positioned at each of the one-thirds length points along their respective 1,500 foot TX Active and control pavement zones so that diluting effects of unreacted vehicle exhaust pulled into the zone from the preceding un-reactive pavement, or crossing over from the opposing lane, could be accounted for. In order to improve the statistical quality of the results, triplicate sets of Ogawa samplers were mounted at each of these third-point sampling locations at two different heights, approximately 30 and 100 cm, on the Type D barrier, which itself is situated approximately 2 meters off the travelled pavement edge. These samplers are being left in place for a consistent sequence of fourteen-day testing periods throughout the duration of our study. At the end of each such two-week period, the samplers are removed for analysis and replaced with a fresh new set of sorbent test pads.

Specific Details with Bench-Scale Air Sampling, Instrumentation, and Analyses

Bench-Scale Photoreactor Testing and Related Mortar Slab Preparations

Mortar slabs measuring 152 mm (6 in) × 152 mm (6 in) × 25 mm (1 in) were constructed. The proportions of the cement (TX Active or Type I), water, and fine aggregate (ASTM C778 standard sand, U.S. Silica Co.) were recorded as 624 kg m^{-3} (1052 lb yd^{-3}), 262 kg m^{-3} (442 lb yd^{-3}), and 1412 kg m^{-3} (2380 lb yd^{-3}) respectively. Given the small size of the slabs constructed, the mix did not include coarse aggregate. Except for the coarse aggregate, the proportions used for the laboratory mortar slabs were similar to the photocatalytic concrete paved on Route 141 near St. Louis, Missouri, where field tests are conducted **Error! Reference source not found.** The slab pour used a two-lift procedure with equal volumes of a Type I cement bottom lift followed by a TX Active photocatalytic cement top lift. Following the pour, a damp cloth and plastic sheet were laid over the slab surface for a 24-hr period while the slab cured. In an attempt to remove excess calcium hydroxide, the top surface was immersed in water containing approximately 0.5% carbonic acid (i.e., carbonated water) and rigorously scoured with a plastic bristle brush. Following this treatment the slabs were fully immersed in water (Type I reagent grade) for 2 hours and oven-dried at 60°C (140°F) for 24 hr.

Experimental Apparatus

A bench-scale flow-through poly(methyl methacrylate) (PPMA) photoreactor served as the primary component of the experimental apparatus. Figure 21 shows the photoreactor, along with the NO test gas supply system, UV-A light source, and NO$_X$ analyzer.
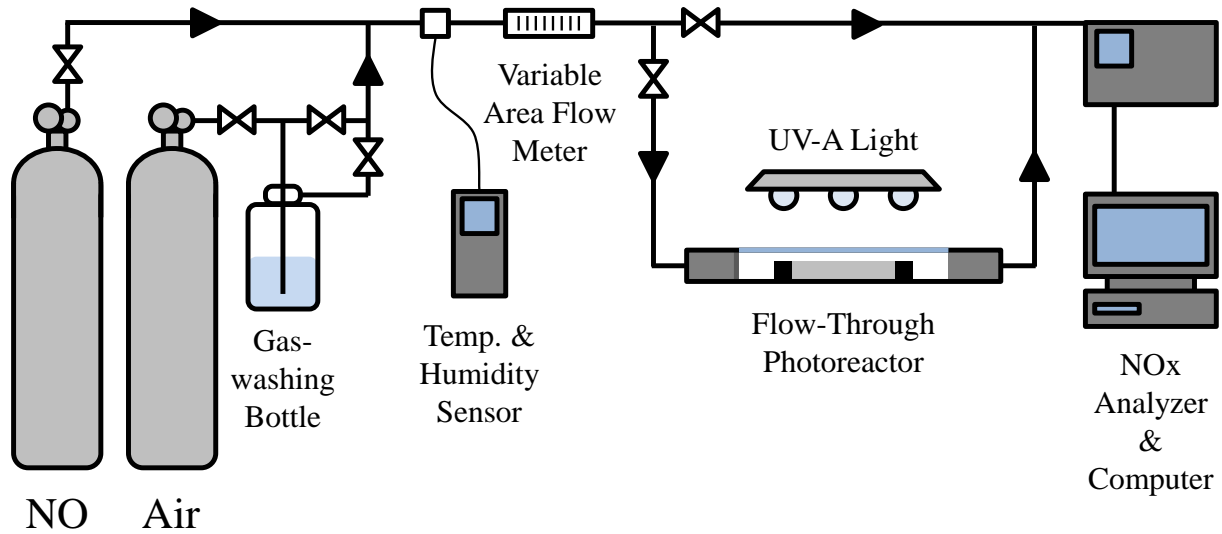
Figure 21. Diagram of experimental apparatus (adapted)

The international standard, ISO 22197-1:2007(E), provided information on the construction and operation of the set-up (ISO, 2007). The test gas supplied to the photoreactor was a mixture of breathing air (grade D, Airgas, Inc.) and $51.6 \pm 1\%$ ppmv NO balanced in nitrogen (EPA protocol gas, Praxair, Inc.) adjusted to obtain a desired NO concentration of 100-1500 ppbv, relative humidity between 20-25%, and a flow rate of 3 L min^{-1} (0.8 gal min^{-1}). A UV-A light (XX-15BLB, Ultra-Violet Products, LLC), directed at the quartz optical window located at the top of the photoreactor, activated the photocatalytic properties of the mortar slab. The measured irradiance on the slab surface was 16 W m^{-2} (1.1 ft lbf s^{-1} ft^{-2}). Within the reactor, 25 mm (1 in) wide PMMA spacers secured the slabs position and were set at a height flush with the slab surface. The gas flowed over the slab through a cross section with a width of 152 mm (6 in) and a height of 6.35 mm (0.25 in). Turbulent airflow over the slab would introduce additional variability in the test. Using the approach detailed in Husken et al. ((2009). Reynolds number was calculated to be 42.6 using an air kinematic viscosity of 1.54×10^{-5} m^{2} s^{-1} (1.66×10^{-5} ft^{2} s^{-1}) and an air flow rate of 3 L min^{-1} (0.8 gal min^{-1}). The length (L_d) for a parabolic velocity profile to develop in the photoreactor was estimated to be approximately 27.1 mm (1.1 in) by the following equation:

$$L_d = 0.1 \cdot Re \cdot H$$

The estimated length was slightly longer than the length of the PMMA spacers, which means that about only 1.1% of the slab surface did not have a fully developed parabolic velocity profile.

A NO$_X$ analyzer, 2B Technologies Model 410 Nitric Oxide Monitor with a Model 401 NO$_2$ Converter, completes the experimental apparatus. The monitor recorded the gas concentrations at 10 s intervals and cycled between NO and NO$_X$ measurements at 5 min intervals. Unlike chemiluminescence instruments, which detect the light produced when NO reacts with ozone (O$_3$), the Model 410 measures the change in UV absorbance at 254 nm when O$_3$ is consumed

upon reaction with NO. UV absorbance is an absolute method; therefore, the analyzer requires calibration annually to correct for non-linearity that exists in the photodiode response and associated electronics.

Bench-Scale Photoreactor Testing Procedure and Program

Figure 22 shows a typical set of results of the testing procedure for an airflow of 3 L min^{-1} (0.8 gal min^{-1}) and a relative humidity of 23%.
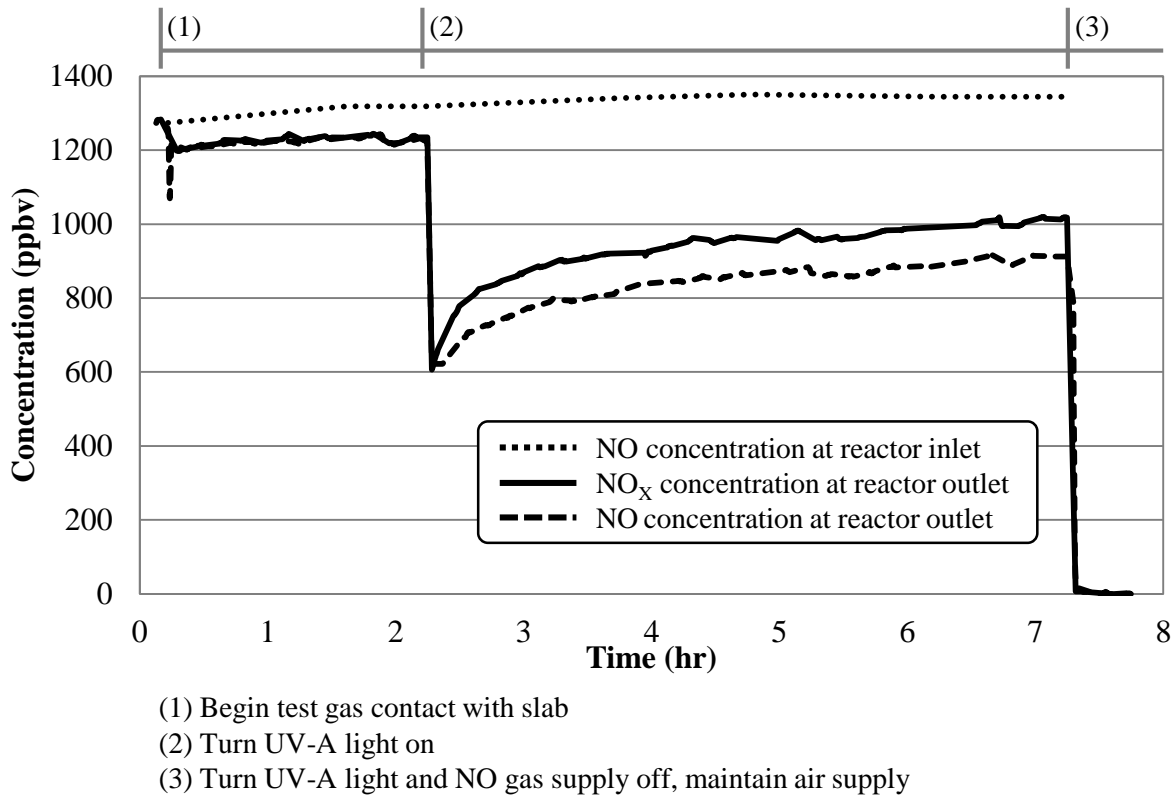

(1) Begin test gas contact with slab
(2) Turn UV-A light on
(3) Turn UV-A light and NO gas supply off, maintain air supply

Figure 22. Representative results from experimental bench-scale testing of photocatalytic mortar specimens

Initially, the supplied test gas was bypassed directly to the NO$_X$ monitor without passing through the photoreactor. After adjusting parameters to desired values, the gas supply was redirected through the photoreactor (see point 1 in Figure 22). Flow was maintained through the photoreactor for a period sufficient to reach steady-state conditions (typically 2 h for the researchers apparatus). Testing of the slabs photocatalytic properties began when the UV-A light was turned on (at point 2 in Figure 20) and continued for a 5-h period. To finish the test, the UV-A and NO gas supply were turned off and air supply was maintained for a 30 min period (see point 3 in Figure 22). The inlet NO concentration was tracked by bypassing the airflow directly to the NO$_X$ monitor at intermittent periods.

Of note, because the experimental apparatus was constructed using high-precision valves (as opposed to a gas calibrator or mass flow controllers) inlet NO concentration increased with time during each test but this gradual increase did not interfere with evaluation of the decrease in NO_X removal.

Following completion of these tests, percent NO_X removal was calculated for various times throughout each test as follows:

$$NO_X \ removal \ (\%) \ = \frac{C_{NOi} - C_{NO_X}}{C_{NOi}} \times 100\%$$

where,

$C_{NOi} = NO \ concentration \ at \ the \ reactor \ inlet \ (ppbv) \ and$

$C_{NO_X} = NO_X \ concentration \ at \ the \ reactor \ outlet \ (ppbv).$

Analysis of Bench-Scale Sample Specimens Using Scanning Electron Microscope-Energy Dispersive Spectroscopy

Following the photo-reactor tests, a FEI Quanta 250 was used to collect Scanning Electron Microscope-Energy Dispersive Spectroscopy (SEM-EDS) data from a subsection of mortar separated from each slab. Investigation of the removal of reaction products from the slab surface was facilitated by using the microscope to collect data from a subsection of each slab that was washed by multiple one hour immersions in water (Type I reagent grade).

Table 7. Synopsis of bench-scale photoreactor research tests

Date	Investigative question	Unique conditions	NO_X removal (%)	Outcome
Oct, 2011	What is the relationship between NO_X inlet concentration and NO_X removal?		27-50	Confirmed inverse relationship between NO_X removal and inlet concentration.
Oct, 2011	What is the relationship between relative humidity and NO_X removal?		50-76	Confirmed inverse relationship between NO_X removal and relative humidity.
Oct, 2011	What is the relationship between test gas flow rate and NO_X removal?		39-50	Confirmed inverse relationship between NO_X removal and flow rate.
Nov-Feb, 2011	Does N removed from test gas balance with N eluted by immersion of slab in water?	Post-test water elution (3 times 1-hour each).	25-50	Results were variable. N in elution water tended to account for less than 80% of N removed from test gas. Entire data set ranged from 60-120%.
Jan, 2012	Are reaction products observable by SEM-EDS?	Post-test SEM-EDS analysis.	NR	Observed N- and C-rich gel-like substance.
Jan-Mar, 2012	Do reaction products blind the surface and reduce NO_X removal?	Tracked NO_X removal over 5- and 20-hour periods	31-85	Formation of reaction products did reduce NO_X removal, but over time removal stabilized at an asymptotic value.
Jan-Mar, 2012	Will immersion in water removal all reaction products?	Post-test water elution (5 times 1-hour each).	NR	N-rich gel observed following elution on all slabs.
Feb, 2012	Will surface treatments impact reaction product removal?	Pre-test surface treatments of acetic acid, hydrochloric acid, and surface sanding. Post-test water elution and SEM-EDS analysis.	NR	N-rich gel observed following elution on all slabs.
May-Jul, 2012	What is source of C in reaction product?	Substituted CO2-free gas for photoreactor test. Post-test SEM-EDS analysis.	NR	Reaction product remained C-rich. Source of C still under investigation.
NR	= not relevant			

Specific Details with Field-Scale Water Quality Instrumentation and Analyses

The water-quality related objective of this research project was intended to quantify the benefits to the urban environment of concrete produced with photocatalytic cement through stormwater runoff testing and temperature measurements. Representative stormwater runoff samples are collected from a standard roadway control section, the section containing photocatalytic two-lift concrete, after additional treatment through a photocatalytic pervious concrete shoulder section, and compared with treatment through a conventional pervious concrete shoulder section. Embedded temperature sensors and determination of actual material thermal capacities are used to model heat storage and release using multiphysical modeling.

Urbanization allows concentrated centers for societal development. Unfortunately, urbanization also negatively changes the environment and is impacting the global climate. Large areas of impervious surfaces are needed for buildings and roadways to allow society to flourish. However, runoff from urban areas is a leading cause of surface water impairment. Impervious surfaces increase stormwater runoff volume and rates, concentrates pollutants, raises air temperatures causing the urban heat island, and decreases air quality. Cool pavements and most recently research on pervious concrete pavements are technologies to help mitigate the urban heat island. TX Active concrete containing titanium dioxide which acts as a catalytic surface for degradation of affixed pollutants. The white color reduces energy absorbed by the surface and the photocatalyst degrades the pollutants before being washed off in the stormwater runoff. The high exposed surface area of pervious concrete allows more contact with air pollutants, possibly further cleaning the stormwater.

The stormwater collection and monitoring of the TX Active travel lane section is shown in Figure 23.
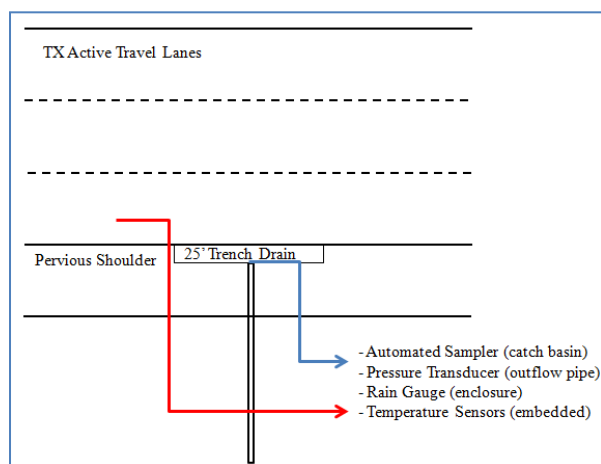
Figure 23. Collection and monitoring for TX Active section, representative of both sections (not to scale)

A 25 ft trench drain was installed at the edge of pavement. Water is directed to a center catch basin which drains to a 6 inch pipe day-lighted to the ditch. An additional conduit was installed

as a wire chase back to the monitoring equipment. The automated sampling tube was installed at the bottom of the catch basin. A pressure transducer determines the water height above a V-notch weir while a conductivity sensor initiates sampling. A rain gauge and air temperature sensor were mounted at the location of the TX Active runoff autosampler equipment.

An additional wire chase conduit was installed between the TX Active surface collection and the pervious concrete shoulder subsurface collection for routing temperature sensor wires. Temperature sensors were hand-installed into the travel lane pavement section just prior to, and during, paving. Temperature sensors were installed in the aggregate base, at aggregate base/base concrete lift interface, at base concrete lift/TX Active interface, and at mid-level in the TX Active overlay.

Figure 24 shows the typical trench drain section. Figure 25 shows the selected product and installation prior to concrete paving.
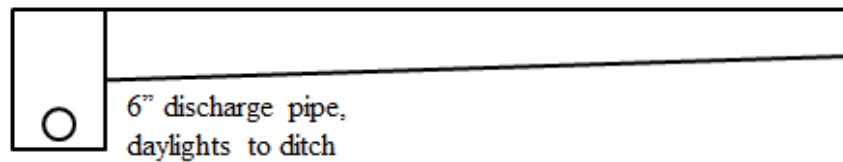
Figure 24. Typical trench drain section (not to scale)
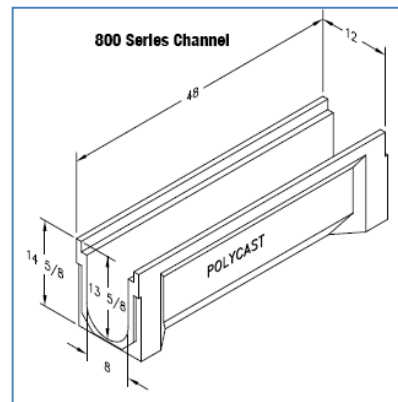
Figure 25. Polycast trench drain information

The molded polycarbonate sections are attached to the underlying soil. The grates are ductal iron mounted slightly lower than the pavement surface and attached with flush bolts to prevent snow plow damage. The side sections drain to a center catch basin with knockout for a 6 in. discharge pipe to the ditch.

TX Active with Water Collection after Pervious Shoulder System

The installation configuration for the pervious concrete shoulder section is shown in Figure 26.

TX Active Travel Lanes

Pervious Shoulder   25' Trench Drain

- Automated Sampler (catch basin)
- Pressure Transducer (outflow pipe)
- Rain Gauge (enclosure)
- Temperature Sensors (embedded)
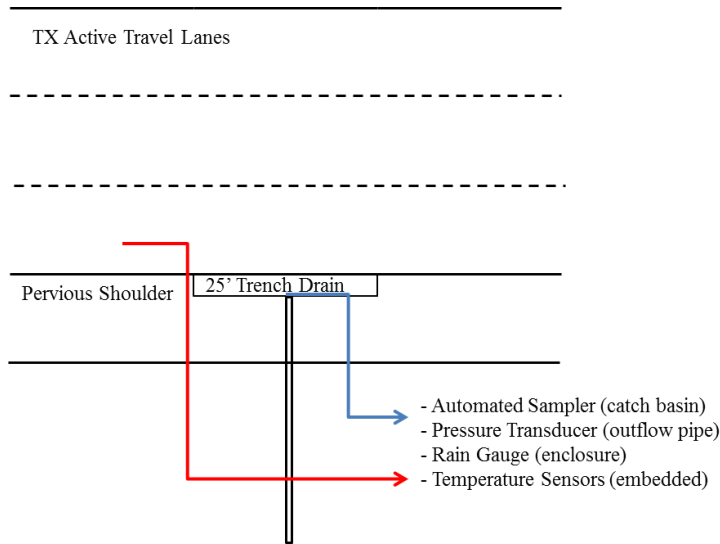
Figure 26. Pervious concrete shoulder collection and monitoring (not to scale)

The pervious concrete test section was located 25 ft from the surface runoff section to minimize impacting stormwater volume. A 6 in. slotted PVC standpipe was installed into the aggregate base/soil interface to the pavement surface for sensor access (see Figure 27).

Slotted PVC standpipe with brass screw cap

8" Pervious Concrete

18" Clean Aggregate Base w/ 40% voids

6" discharge pipe, daylights to ditch

25' slotted pvc pipe

3" (WQV – 1.14")

Non-Woven Geotextile

6" discharge pipe, daylights to ditch
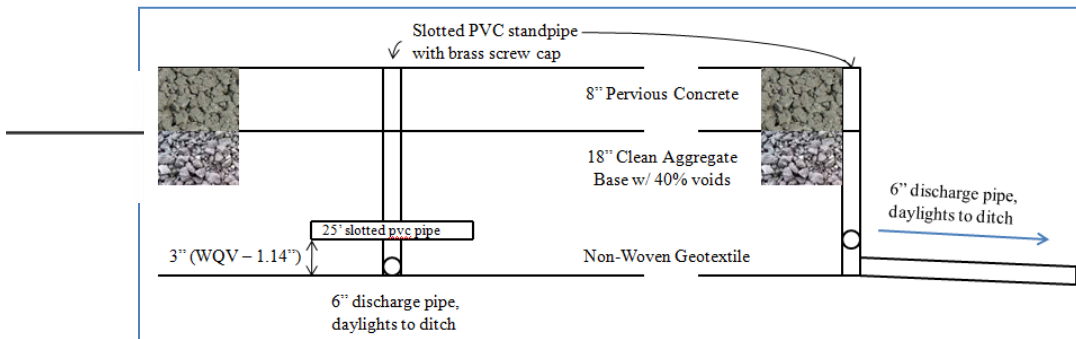
Figure 27. TX Active testing layout

A 25 ft 6 in. pvc tile pipe was installed horizontally at 3 in. above the natural soil level allowing infiltration of the water quality volume, but preventing water being held against the roadway subgrade. The standpipe/tile section was discharged to the ditch. The standpipe top was installed slightly lower than final grade with a removable screw cap to ensure the pipe will not interfere with snowplowing operations. A conduit pipe chase was installed between the standpipe and the sensor vault.

Temperature sensors were installed throughout the pervious concrete TX Active section and routed to the standpipe conduit. Temperature sensors were hand-installed into the pervious pavement section just prior to, and during, paving.

Figure 27 shows the layout of the test sections and location of monitoring equipment. The shoulder and pavement test sections are 25 ft long separated by a 25 ft section which contains the pavement temperature sensors. The monitoring equipment is centrally-located on the outside of the soundwall.

Control Pavement Section with Standard Shoulder

Control values for stormwater runoff volume, rate, and pollutant concentration will be obtained from a nearby standard pavement section located at STA 223+50. A trench drain setup was installed adjacent to the shoulder as detailed for section 1. The control and TX Active sections are 300 ft apart. All equipment installed and described for the TX Active section was installed in the control section, except the weather station. Only one site weather station was installed at the location of the TX Active test site.

Analytical Testing

The sections will be monitored for stormwater volume, stormwater pollutant concentration, and thermal behavior. Automated samplers will obtain water samples for collecting representative stormwater samples. The primary pollutants of concern in relation to pavement runoff are hydrocarbons (i.e., vehicle fuels and lubricant grease and oils) and suspended solids. Since autosamplers are not particularly suited to the collection of hydrocarbon or grease-oil samples, chemical oxygen demand (COD) will be used as surrogate indicators of their presence. Should hydrocarbons levels be lower than the COD test limit, COD testing will be discontinued. Other water quality indicators will include total suspended solids (TSS), turbidity, and pH. The pressure sensors for water quantity will also determine water temperature. Another unique aspect of this water-quality testing effort is that nitrate testing will also be conducted with these runoff samples, as a secondary indication of NO_2 removal as mentioned in relation to air-quality benefits. Nitrate content will be determined using a cadmium reduction technique.

Water quality concentrations are affected by antecedent dry days, and total rainfall and ADT. The testing plan is anticipated to encompass all significant influencing factors over the project duration. Traffic counters will be installed at the site, immediately south of the ramp and north of the two test sections to allow collection of traffic count, composition, and vehicle speed. Temperature will also be monitored at each boundary layer in the concrete systems and at the center of the TX Active overlay and the pervious concrete shoulder. Surface temperature will be manually-collected on days samples and data are downloaded from the site. It is expected that the site will be visited at least every two-weeks. No rainfall occurred during construction and prior to opening and there was no opportunity for background data collection.

Since pavement albedo and solar reflectance index (SRI) are important for green building certification and urban heat island modeling, SRI are being measured throughout the project. Typical concrete pavement initially has a high SRI and then decreases with usage. The self-cleaning aspect of the TX Active should be demonstrated using SRI values over time. The raw energy balance used to calculate SRI will also be used in the multi-physical model for heat transfer.

Initial field infiltration was measured on the pervious concrete shoulder using a randomized testing plan. Additional testing will be performed every 3 months afterward to determine the reduction in permeability over time.

Additional Site Meteorological Testing

The project site has been equipped with a weather station, with wind speed, wind direction, solar irradiation, and temperature gauge (i.e., see Figure 28). The instruments included within this weather station are a thermometer/relative humidity sensor (Campbell Scientifics CS215), pyranometer (Campbell Scientifics CS300), wind speed and direction sensor (RM Young 03002-5), and a tipping bucket rain gauge (Hydrological Services TB4).

Figure 28. Sensor vault and temporary weather station installation

Pavement Coupon Sampling and Analyses

Bulk slab specimens were created for both the TX Active overlay and the pervious concrete shoulder. Actual specific heat capacity is being measured using a semi-adiabatic setup developed for quantifying actual construction material thermal capacities. Samples will also be treated with various levels of pollutants and exposed to UV light. Albedo and simulated stormwater runoff water quality will be measured.

Complementary Lab Assessment of TX Active Coupons

Photo-reactive conversion of NO_2 and deposition of ionic nitrate onto the TX Active surface will be further quantified and characterized with use of sample coupons. These coupons will be mounted on top of the concrete barrier (approximately 1 m above the roadway) and set in wells cut into the concrete shoulder. Figure 29 offers an approximate sense of this mounting approach.
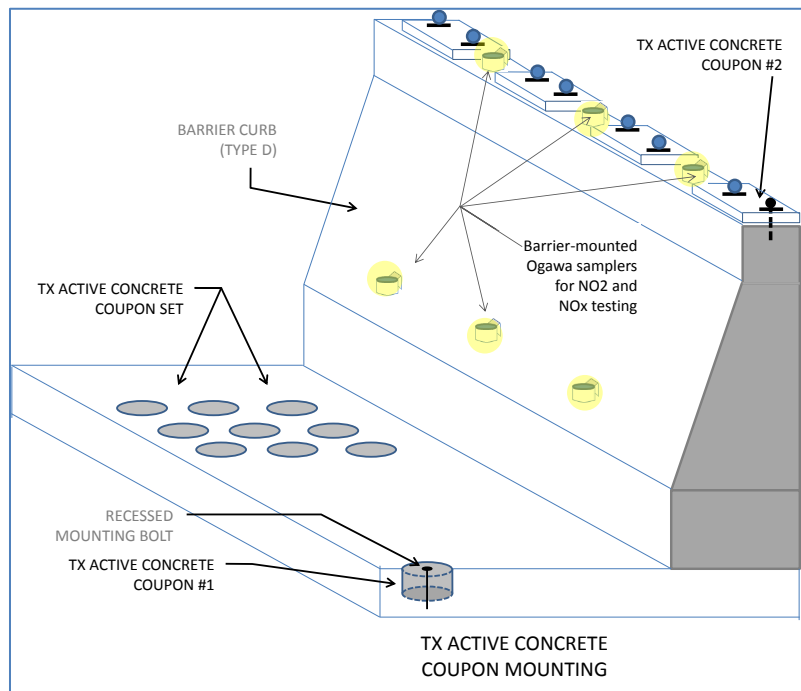
Figure 29. Paving overview with top TX Active layer in foreground

When installed in, the coupons will be flush with the pavement to minimize any change in the shoulder safety performance. At each Ogawa sampling point, 40 to 50 coupons will be placed. These coupons can be exchanged at various intervals to document NO_2 removal effectiveness of both fresh and aged materials. This strategy that directly measures nitrate formation and adhesion will provide the study with direct procedures for quantifying NO/NO_2 removal and conversation to bound nitrate by way of photo-reactive conversion.

As mentioned previously, following invitation, active chemiluminescent testing will be conducted in parallel with a second, active ozone-titration method, such that both sets of results can be directly compared. This parallel testing scheme will then validate our use of the active ozone-titration method for on-site field testing in lieu of the more commonly employed chemiluminescent method.

CONSTRUCTION CHRONOLOGY AND HIGHLIGHTS

October 24, 2011

- The southbound 141 mainline two-lane section was paved on this day using a two-lift placement with a top TX Active section at a depth of approximately 2 inches (~5 cm).

- Representatives from MoDOT, FHWA, Essroc, Iowa State University, and University of Missouri-Kansas City were present for this initial pour.

- A schematic overview of this location is given on the following page.

- Google Earth or Bing Maps coordinates for this location are as follows: 38°4026.25"N 90°2938.39"W

- Approximately 1,500 linear feet of the southbound two-lane mainline paving was placed at this time.

- Representative photographs taken during this paving activity are provided on the following pages. Web archived photographs and video *(including alternative *.WMV, MPG, and MTS video formats)* taken this day are also available at the following Web URL: http://home.eng.iastate.edu/~jea/TX-Active-Project

Figure 30. Paving overview with top TX Active layer in foreground

Text boxes on figure:

TX Active Travel Lanes
Paved 24 October 2011
Southbound, 1500' length, 24'width

TX Active Auxiliary Lane
Paved 1 November 2011
Southbound, 1500' length, 12' width

TX Active Pervious Shoulder
Paving scheduled for early Spring 2012
Southbound, 75' length, 5' width
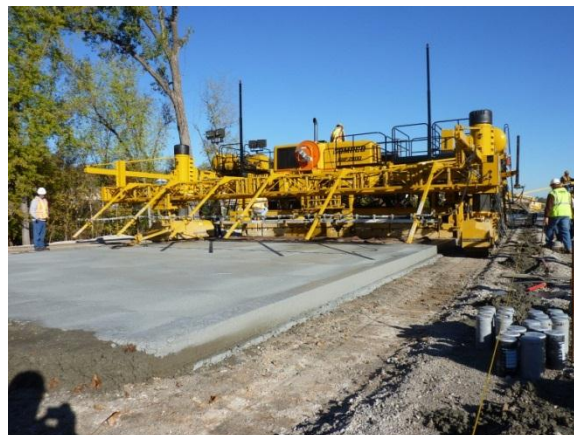
Figure 31. Initial placement of TX Active mix ahead of Gomaco paver

Figure 32. Dr. John Kevern (University of Missouri – Kansas City) collecting TX Active mix samples
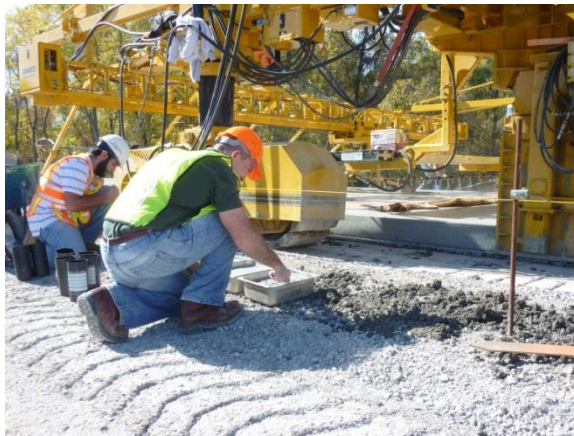
Figure 33. Jim Grove – FHWA Office of Pavement Technology

Figure 34. Jim Grove – FHWA Office of Pavement Technology

November 1, 2011

- Another mainline single-lane section was paved on this day, again using a two-lift placement with a top TX Active section at a depth of approximately 2 inches (~5 cm).

- The location of this section is also shown on the preceding schematic.

- Approximately 1,500 linear feet of this two-lane mainline paving was placed at this time.

Winter 2011-2012

- Instrumentation used for meteorological and solar radiation monitoring immediately adjacent to the TX Active pavement area will be mounted to this sound wall and activated.

- Paving of the remaining control and non-research highway sections was started.

Spring 2012

- The final TX Active paving section featuring a pervious concrete shoulder was poured in the spring.

- Paving of the remaining control and non-research highway sections was completed.

- The sound wall adjacent to the west side of the new road section was built during the late Spring 2012.

- Runoff collection lines used to capture representative pavement and shoulder storm-water samples was installed during the Spring 2012 in conjunction with the latter shoulder paving activity.

- Field evaluation of NO_2 and NO_X presence was started in May 2012, using both Ogawa passive samplers and 2BTechnologies active testing (i.e., based on ozone depletion protocol).

- Ogawa testing was then continued on a monthly basis from May 2012 through mid August 2012.

July 14, 2012

- The new highway was placed into operation.

Figure 35. Operating Highway 141 perspective along southbound Olive Road ramp

Figure 36. Operating Highway 141 perspective within TX Active paving zone and showing adjacent crash barrier and sound wall

Figure 37. Highway 141 Opening Day festivities (July 14, 2012: S.K. Ong)

EXPERIMENTAL RESULTS

Materials Characterization

Pervious Concrete

The standard hardened pervious concrete properties are shown in Table 8. Voids were determined according to ASTM C1754 *Standard Test Method for Density and Void Content of Hardened Pervious Concrete* (ASTM, 2012). Measured voids were higher than designed most likely due to the edge effects caused by poor particle packing of the large aggregate along the walls of the relatively small (4 in. by 8 in.) cylinders. The compressive strength was tested according to ASTM C39 on sulfur-capped specimens. Sample density was fixed to control variability. Permeability was tested using a falling-head device on 4 inch (100 mm) diameter and 6 inch (150 mm) length specimens using the procedure developed for the American Concrete Institute (ACI) pervious concrete student competition, where specimens are covered in heat shrink plastic and confined in a rubber membrane before testing from a water height of 9 inches (200 mm). The high permeability was desirable for long maintenance cycles between cleaning and for resistance to clogging.

Table 8. Hardened testing results

Property	Results
Voids	28%
Unit Weight	114.75pcf
Permeability	2050 in./hr
7d Comp. Str.	3200 psi
28d Comp. Str.	3355 psi

Results from SAP testing in pervious concrete showed a 16% increase in the degree of hydration for sample cured at 50% relative humidity. Moisture loss testing showed the SAP mixtures including the additional water had similar evaporation. When the extra water was considered sacrificial, the SAP mixtures had significantly less evaporation. When ring shrinkage was tested the SAP mixtures developed higher strength, had increased time to cracking, and retained higher residual strength than the control mixtures. Additional information on using internal curing to improve pervious concrete performance can be found in the author's 2012 TRB paper "Reducing Curing Requirements for Pervious Concrete Using a Superabsorbent Polymer for Internal Curing" (Kevern and Farney, 2012).

Figure 38 A, B, and C shows a demonstration of the self-cleaning ability of the pavement using a red rhodamine dye. For testing 1 mL of a 5% solution of rhodamine dye was applied to a 3 in^2 (20 cm^2) area. Figure 38A shows the sample before application. Figure 38B shows the sample after the dye was applied and allowed to dry overnight. After drying the samples were placed outside in sunlight for five hours per day from 10am to 3pm. Figure 38C shows the sample after 4 days of testing. One area of concern for future use of photocatalytic concrete is unwanted interactions with curing compounds. Membrane-forming curing compounds prevent the air

pollution and other dirt particles from physically contacting the concrete surface, eliminating any photocatalytic effects. One area of investigation was to locate a curing compound that would not reduce the self-cleaning or air cleaning properties. Since the photocatalytic reaction is able to degrade hydrocarbons, a hydrocarbon-based material was investigated. Soybean oil has been successfully used to cure pervious concrete, reduce moisture loss, and protect surfaces against deicer salt scaling (Kevern, 2010). Figure 39 shows a red color image analysis of the rate of color degradation on samples with and without soybean oil curing applied at 200 sf/gallon (4900 m^2/m^3). Soybean oil was applied and allowed to dry 24 hours before applying the rhodamine dye. No difference in self-cleaning ability was observed for the samples cured with soybean oil.
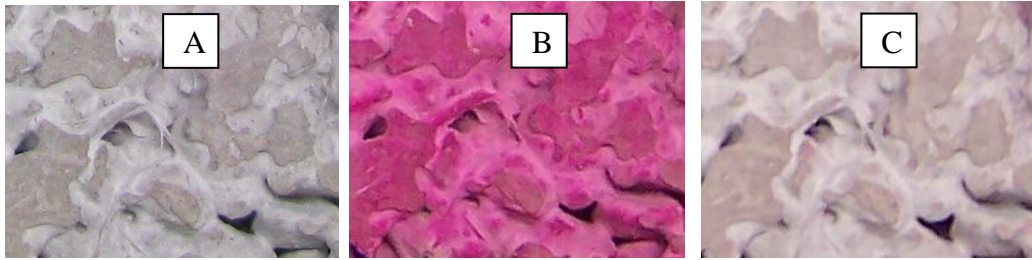
Figure 38. Demonstration of self-cleaning ability
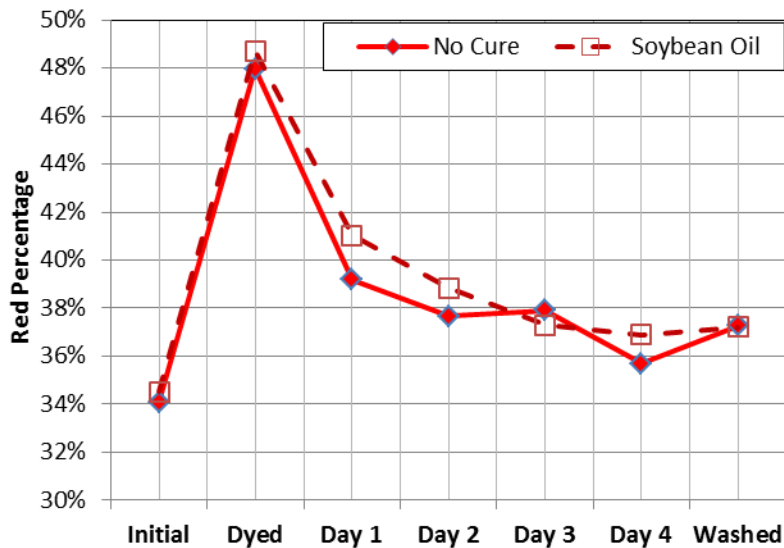
Figure 39. Self-cleaning ability as measured by rodamine red degredation

Bench-Scale Assessment of Pervious Concrete Air Quality Reactivity

After the initial mixture proportions were selected, samples were tested for air pollutant reduction ability. Samples sized 12 in. by 12 in. by 3 in. (250mm x 250mm x 75mm) were created at several void contents possible on the project. The pollutant removal ability was measured using nitrogen oxide species reduction according to ISO standard 22197-1 (JIS, 2010). Samples were tested at 30% relative humidity, a pollutant flow rate of 3 L/min., and UV

intensity of 2.4 mW/cm^2. In Figure 40, the error bars represent 1 standard deviation from the mean.
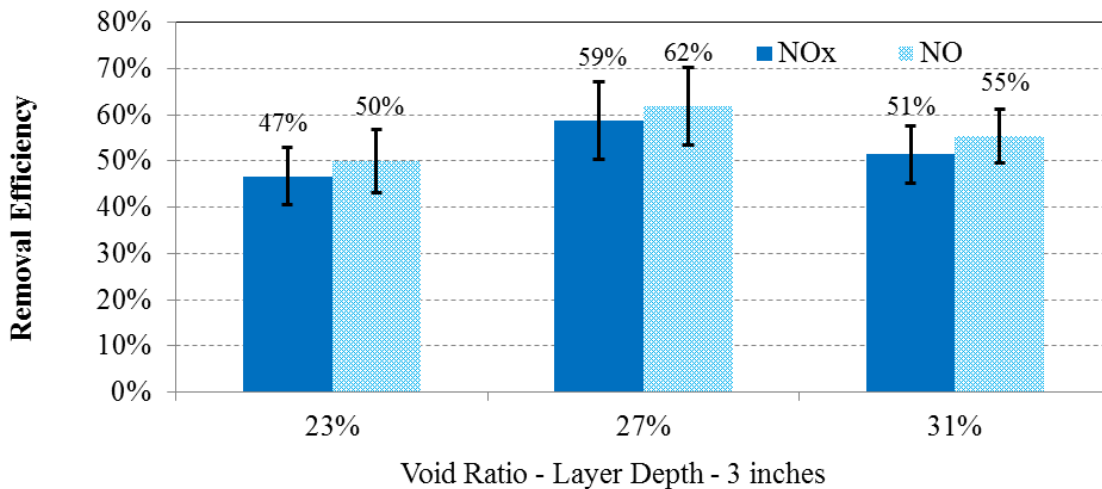
Figure 40. Pollutant Removal Ability

Photocatalytic pervious concrete selected for this project had higher removal rates than impervious photocatalytic concrete. Across the range of voids expected on the project there was no difference in removal capacity. More information on the ability of photocatalytic pervious concrete to remove air pollutants can be found in the Transportation Research Board paper by Hassan (Asadi et al., 2012).

Initial testing confirmed the relationships between NO_X inlet concentration, relative humidity, and flow rate with the work of other researchers (e.g., Murata et al., 2000, Hüsken and Brouwers, 2008, Dylla et al., 2010, Ballari et al., 2011). Testing also attempted to demonstrate that N removed from the gas stream balanced with N that has adsorbed on the slab and was converted to a reaction product (i.e., NO_3^- and HNO_2). These balances ranged between 60 and 120%; however, in the great majority of cases the balance fell below 80%. This finding indicates that either not all N from reaction products was removed by the water elution procedure or that one of the systems N outlets was not accounted for. In a separate investigation, analysis by SEM-EDS found that the reaction products were observable on the slab surface. With this knowledge, the elution procedure was tested to determine whether immersing the slab in water for additional 1-hour periods would remove all reaction products from the slab surface. When tested by SEM-EDS, the reaction products were observable even on the slabs immersed in water for a total of 5 hours (1 hour each immersion). Various pre-photoreactor test surface treatments were also tested to determine if the reaction product would be completely eluted if the sample was prepared in a different fashion. SEM-EDS analysis also revealed that the reaction product was rich in C. Although N-based reaction products should not have a strong association with the product surface, the researchers considered that the C in the product may have a different interaction with the slab and may be more difficult to remove. Prepared slabs were quite fresh (i.e., formed less than 1 month before the photoreactor test); therefore, the surface carbonation reaction [CO_2 + $Ca(OH)_2 \rightarrow CaCO_3 + H_2O$] had not gone to completion. The researchers attempted to speed up carbonation by treating the surface with acetic acid (CH_3CO_2H). Slabs treated with acetic acid

also exhibited both the same reaction products and incomplete removal of reaction products following immersion in water.

In the on-going field study the researchers will measure the amount of NO_3^- and NO_2^- eluted from coupons placed in the field for time periods ranging from 1 to 12 months. Knowledge that all of the reaction products cannot be removed from the surface will be used to upwardly adjust our estimate of NO_X removed by the concrete.

The fact that not all of the reaction products was removed by elution also raises concerns that these reaction products will blind photocatalytically active sites and either eliminate or dramatically reduce the pavements air-cleaning properties. Photoreactor testing at an average inlet concentration of 1500 ppbv found that due to reaction product blinding NO_X removal decreased by 20% over a 20-hour period. Although percent removal initially decreased in comparison to a reference measurement, as time progressed removal stabilized asymptotically. Hence, it is probable that reaction product formation will not result in the complete loss of the pavements air-cleaning property.

As observed by SEM-EDS analysis, the N-rich gel-like reaction product was also high in C. This observation was unexpected and led to various hypotheses of Cs source. One hypothesis proposed CO_2 in the test gas as the C source. To investigate this proposition, a photoreactor test was run with a CO_2-free test-gas. Following the test, SEM-EDS analysis of the slab found that the reaction product remained C-rich. Instead, it appears probable that C in the reaction product is due to photocatalytic reactions of VOCs. The particular VOC has not been identified, but with the materials used to construct the photoreactor, numerous sources exist.

Extrapolation of Bench-Scale Air Quality Testing Results to Field-Scale Performance Assessment

Testing at low NO_X concentration provides the best comparison to NO_X removal that may be observed in the field. As part of the photoreactor tests used to evaluate reaction product blinding, two tests were run with an inlet concentration of 100-ppb. These tests showed NO_X removal between 76 and 85%. As a percentage this removal is impressive, but this result does not inform what level of NO_X removal may be observed in the field. A more useful approach calculates NO_X removed per surface area over a specific time period. For the purposes of this report the estimate will be made using the following units: mmol m^{-2} hr^{-1}. NO_X removal averaged 82% for the referenced test and the slab measures 0.023 m^2, this converts the following:

$$\frac{n_{NO_X\ removed}}{a\ t} = \frac{Q}{22.4l\ mol^{-1}}\left(\phi_{NO_{Xi}} - \phi_{NO_X}\right)\frac{1}{a}$$
$$= \frac{3.0l\ min^{-1}}{22.4l\ mol^{-1}}(0.0100\mu l\ l^{-1} - 0.0013\mu l\ l^{-1})\frac{1}{0.023m^2}$$
$$= 5.07 \times 10^{-8} mol\ m^{-2}\ min^{-1}$$

The surface area of the photocatalytic pavement at the field site near St. Louis measures 5000 m^2. Assuming 12 hours of daylight (when the pavement is photocatalytically active), the calculation below determines possible daily NOX removal:

$$n_{NO_X \ removed \ daily} = 5.07 \times 10^{-8} mol \ m^{-2} \ min^{-1} 5000 m^2 12h = 0.18 mol$$

As a rough extrapolation, consider a 5000 m^3 volume of air (i.e., the pavement surface area and a 1 m upper boundary) that is highly polluted (i.e., the NO_X concentration is at the 1-hour NO_2 NAAQS, 100 ppbv). If one mole of a gas occupies 0.0224 m^3, this volume of air contains 0.022 moles of NO_X. A multitude of other factors will also influence the actual amount of NO_X removed by the pavement, but given that these two numbers differ by an order of magnitude, the pavement does hold promise as an air pollution mitigation technology.

Field Water Quality Testing

Water analysis consisted of water quantity measurement and water sampling for quality analysis. V-notch weir boxes were constructed out of schedule 40 sheet PVC, with a 30 degree V-notch for each of the four pipes day lighted from the pervious concrete sections. A pressure transducer was installed at the bottom of weir box, directly behind V-notch as shown in Figure 41 for water height and temperature measurements.
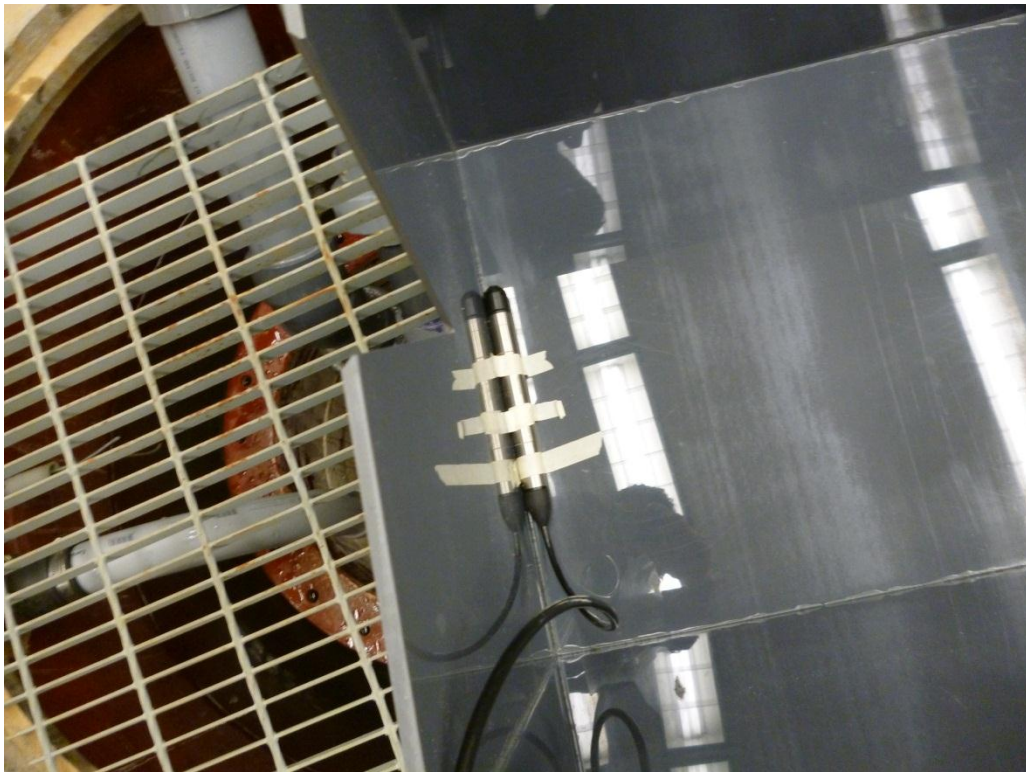
Figure 41. Pressure transducer placement in weir box

The pressure transducers (Campbell Scientific Instruments, Model Number PS440) measure height of water above the mid-diameter of the sensor as well as the temperature. To ensure accuracy, the V-notch weir box was calibrated in the hydraulics lab at UMKC by simulating flow into the box and determining the corresponding head of water above the V-notch. The actual calibration and testing of the weir box is shown in Figures 42 and 43.

Figure 42. Pressure transducer placement in weir box
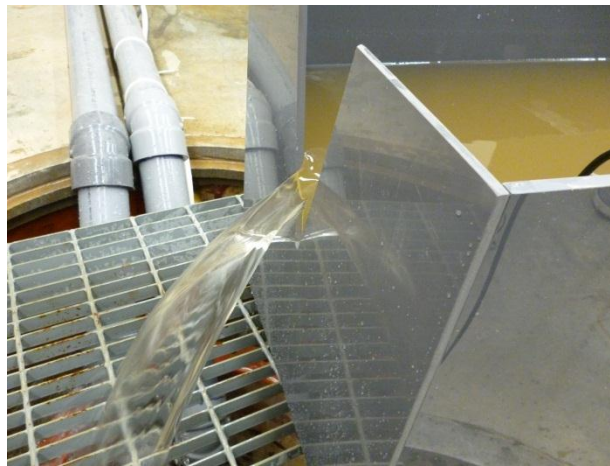
Figure 43. Weir box lab testing

The pressure transducer data was recorded the data logger (Campbell Scientific CR1000) used in the field installation. After determining the head of water above the V-notch, results were calculated using the standard weir discharge equation for flow. Calculated flow was then compared to the flow provided by the laboratory Venturi tube. Calibration results are shown in Figure 44.
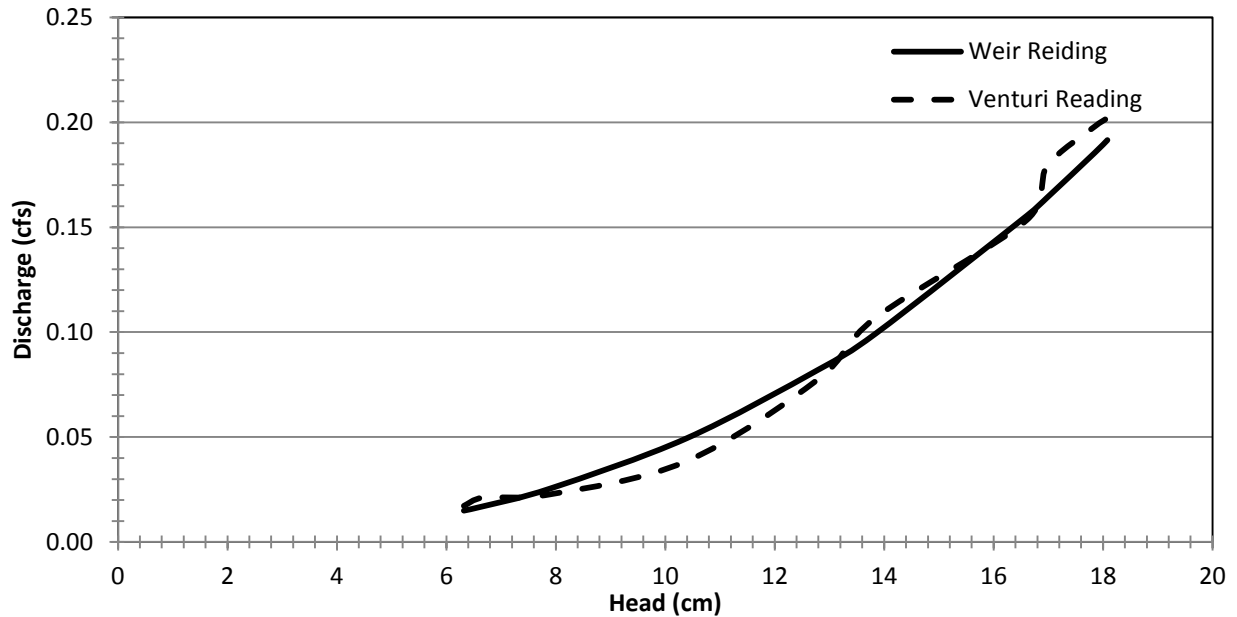
Figure 44. Weir box calibration results

Four weir boxes were placed in total. Figure 45 depicts a plan view of each site showing the locations as well as the respective effective watersheds of two weir boxes. Both sections had the same plan view, thus the figure is representative of both the photocatalytic pavement section as well as the control section. The diagram does not show the sound wall or the barrier curb, and is not to scale. Figures 45 show the base, the placement with support, and the final locations of the boxes. The weather stations shown in Figure 47 were temporarily installed on the concrete vault prior to soundwall installation. The wind speed and direction equipment were relocated to the top of the soundwall.
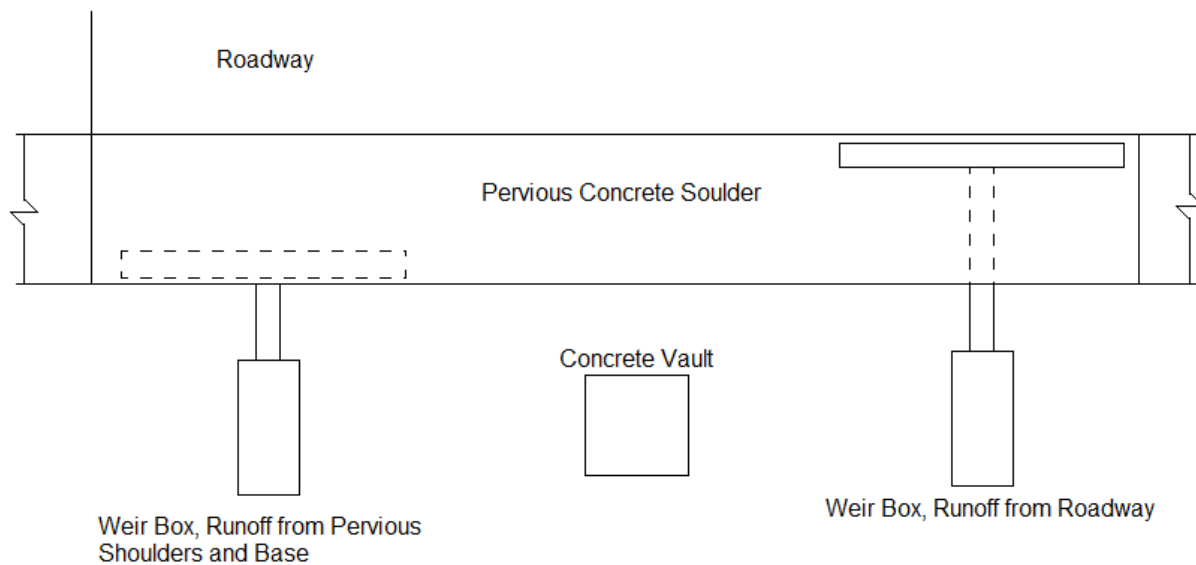
Figure 45. Plan view of weir box locations (not to scale)

Figure 46. Base for weir box

Figure 47. Weir box with base and supports

Figure 48. Final locations of weir boxes in the control section

Figure 49. Final locations of weir boxes in the TX Active section

Each of the vaults contain two water samplers (Global Water WS700, WS750) with the intake hose located adjacent to the pressure transducer in the weir box. The weir box from the pervious concrete base was connected to the WS700 that has a single two gallon container (Figure 50). The WS700 samplers are programmed to capture the first flush. Under actual conditions the WS700 sampler is filled in approximately 35-40 minutes, with a 1000 milliliter sample collected every five minutes. The weir box collecting the runoff from the roadway were connect to the WS750 samplers which have two one gallon containers (Figure 51). Sampling from the roadway surface captures both the first flush and the entire storm event. For the entire storm event a 50 milliliter sample is collected every five minutes, while first flush is 600 milliliters every five minutes.

Figure 50. Two-gallon automated water sampler

Figure 51. Two one-gallon automated samplers

Water quality testing consists of determining the total suspended solids (TSS), pH, turbidity, and nitrate concentrations. Electronic sensors are used to measure pH and turbidity. Nitrate is determined using cadmium reduction. TSS is determined by mass retained on a glass filter. At this time no water samples have been collected due to lack of electricity on the site.

Also, pressure sensors (CS450) were installed at the bottom of the pervious concrete aggregate base to determine the water level within the pervious concrete shoulders. The pressure sensors will be used to measure the rate of water level change over time for infiltration and water balance calculations. Figure 52 shows the perforated standpipe in the aggregate base, pressure sensor, and thermocouple wires.

Figure 52. Perforated stand pipe within aggregate base showing pressure sensor and thermocouple wires

Traffic Safety Management

The Missouri DOT has been extremely helpful during all phases of this project. Most recently, the MoDOT Maintenance Division has provided an outstanding level of traffic management and safety support, as depicted within the following two figures.

Figure 53. Traffic safety in place during sampling with truck-mounted TMA

Figure 54. Traffic safety in place during sampling

Field-Scale Air Quality Testing

Ogawa testing was started on both the TX Active and control pavement sections approximately two months in advance of the highway being opened to traffic (i.e., starting in mid-May 2012) in order to ascertain background performance. Once the highway was opened, this testing has been continued on a monthly basis…and will be continued for a period of twelve months following the date of this current report. All future data will then be compiled into an addendum final report with an estimated publication date of ~late Summer 2013.

Figure 55. Ogawa sample collection underway

The Ogawa results obtained as of this reports late August 2012 timeframe are presented in the following sets of figures (i.e., extending from Figure 56 at May 15, 2012 to June 14, 2012 through Figure 61 at August 1, 2012 to August 14, 2012). For the first two such sampling periods (May 14, 2012 to June 14, 2012 and June 14, 2012 to July 13, 2012), only lower level (i.e., 30 cm sampling height) results were identified.
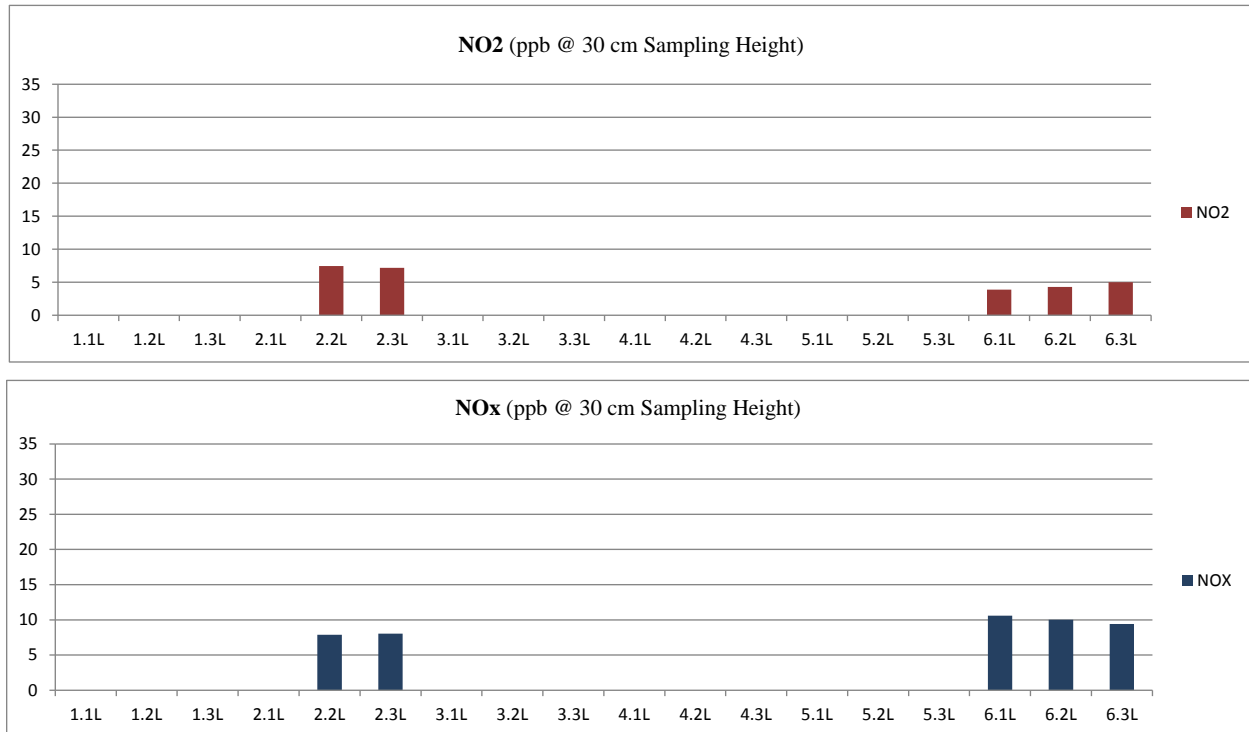
Figure 56. Ogawa sampling results at lower 30 cm height for May 14, 2012 to June 14, 2012
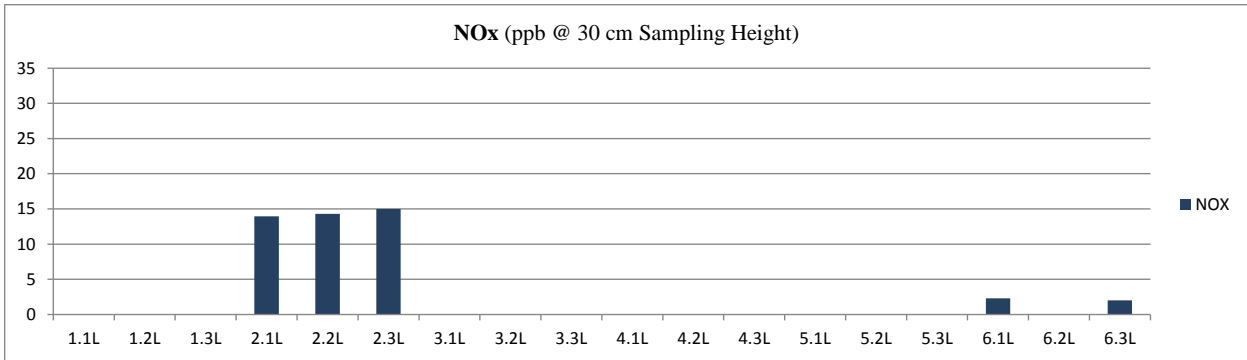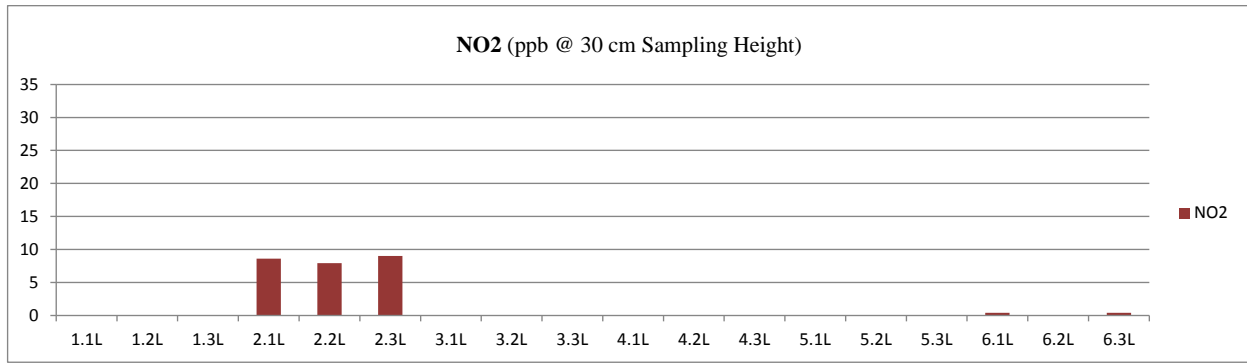
Figure 57. Ogawa sampling results at lower 30 cm height for June 14, 2012 to July 13, 2012
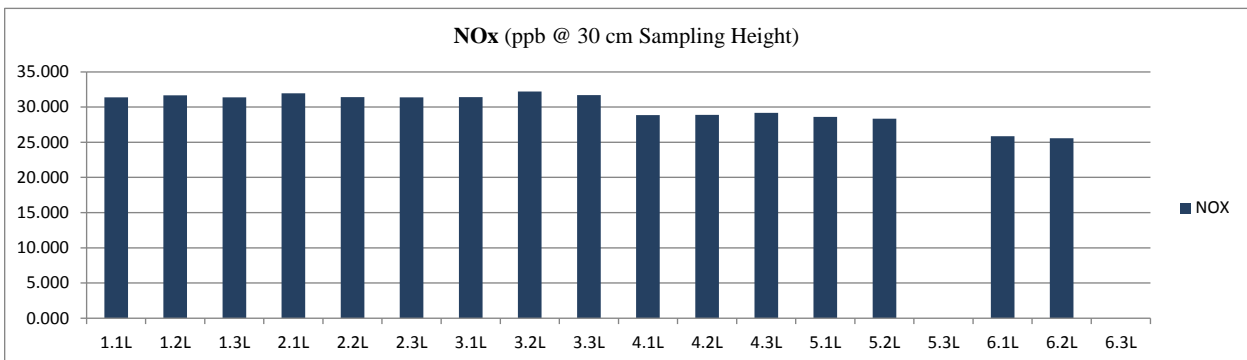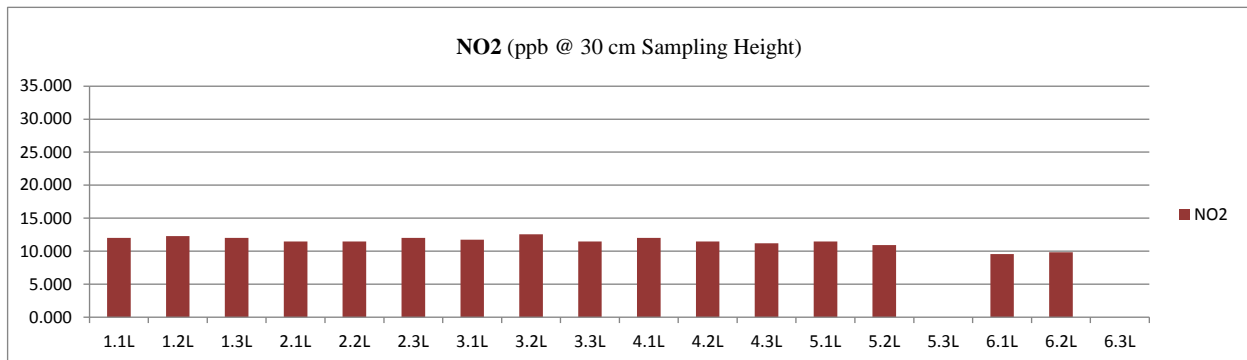
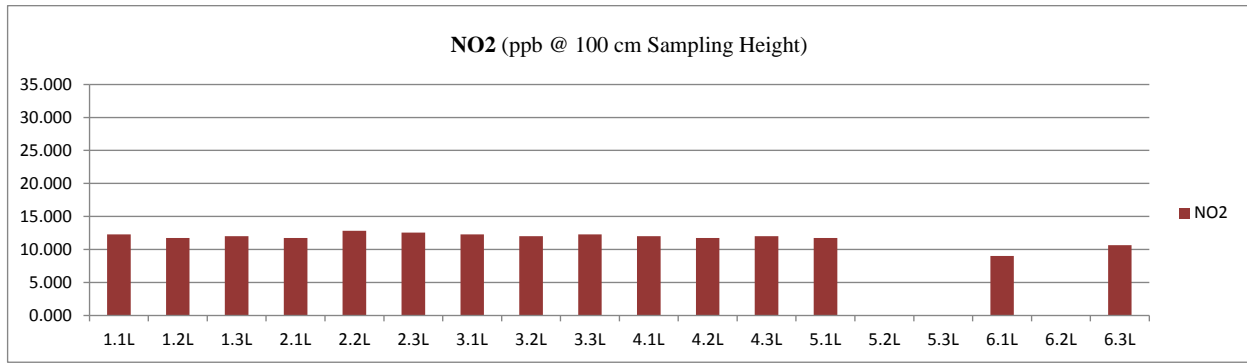**Figure 58. Ogawa sampling results at lower 30 cm height for July 13, 2012 to August 1, 2012**
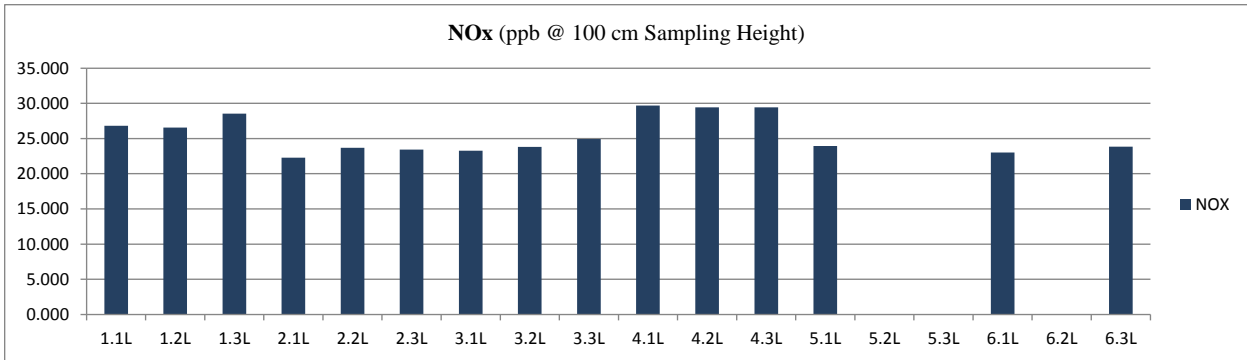
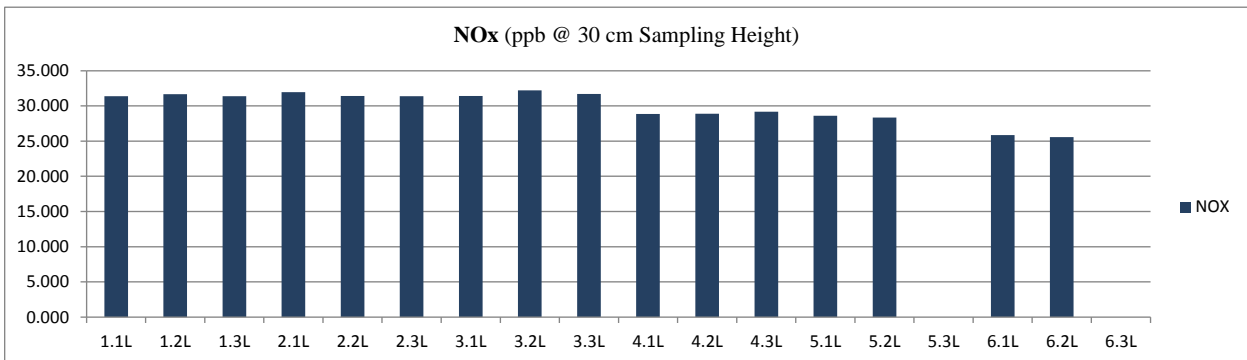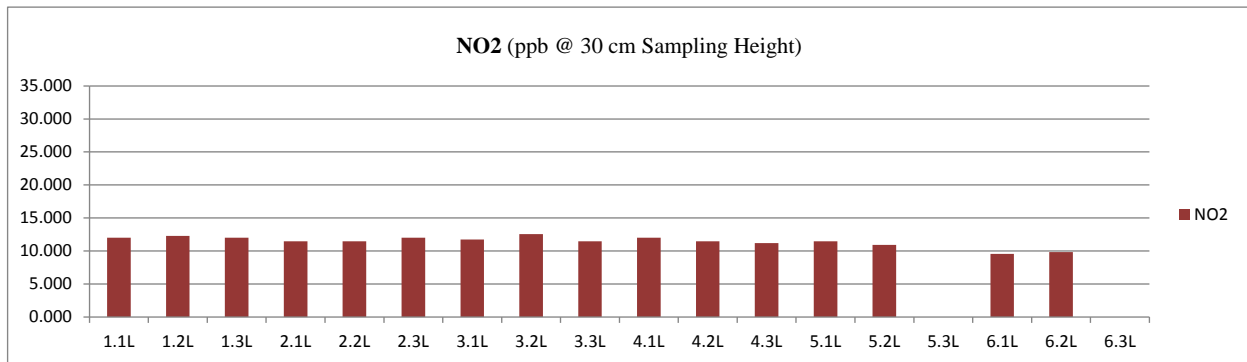**Figure 59. Ogawa sampling results at upper 100 cm height for July 13, 2012 to August 1, 2012**

Figure 60. Ogawa sampling results at upper 100 cm height for August 1, 2012 to August 14, 2012
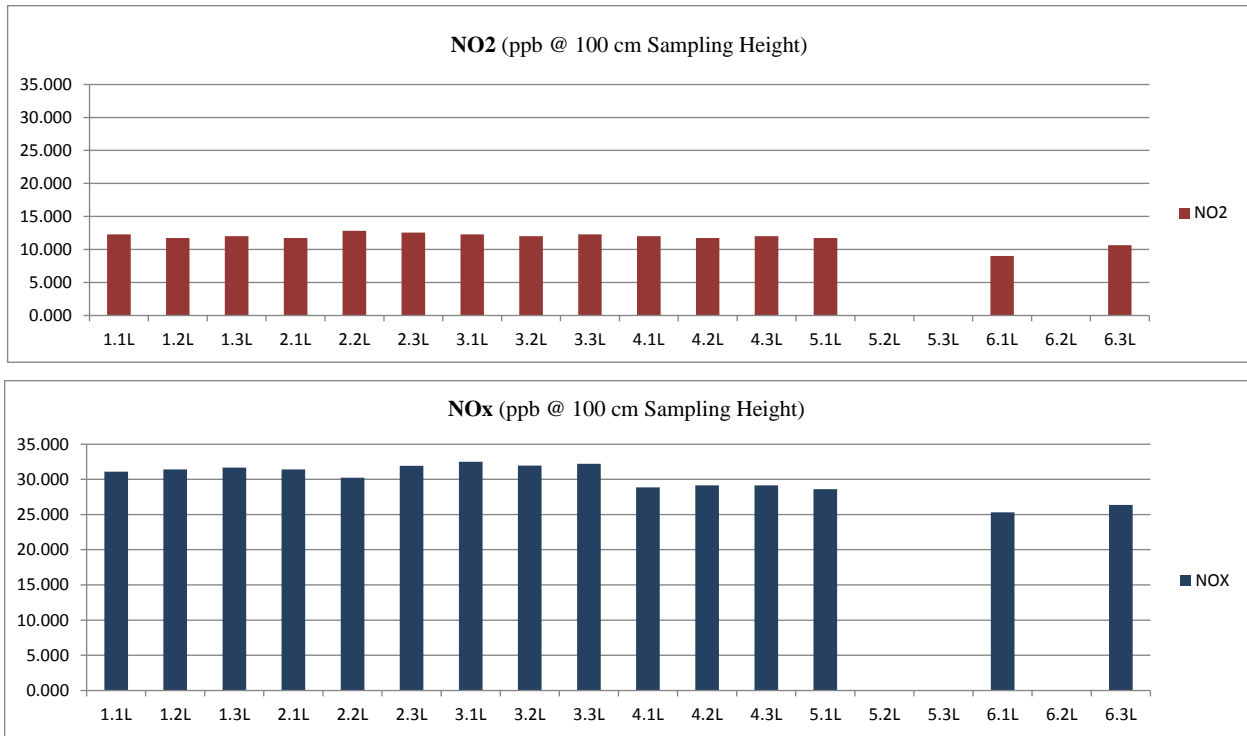
73

Figure 61. Ogawa sampling results at upper 100 cm height for August 1, 2012 to August 14, 2012

Table 9 provides a narrative overview of what these schematic results are believed to show.

Table 9. Narrative summary of Ogawa results recorded from May 14, 2012 through August 14, 2012

Sampling Timeframe	Upper NO2 Results	Lower NO2 Results	Upper NOx Results	Lower NOx Results
May 14, 2012 to June 14, 2012	- No measurements	- The lower NO2 values were ~3-4 ppb	- No measurements	- The lower NOx values ranged from ~7 ppb to 10 ppb
	Conclusions: - Without any traffic on the highway at this time, the NO2 and NOx values were low, as expected - Given the low level NOx levels, given the low level NOx levels, these results did not show NO2 depletion for sampling sites 1, 2, and 3 (i.e., with TX Active pavement) *versus* 4, 5, and 6			
June 14, 2012 to July 13, 2012	- No measurements	- The lower NO2 values were ~7-8 ppb	- No measurements	- The lower NOx values ranged from ~3 ppb to 15 ppb

	Conclusions: - Without any traffic on the highway at this time, the NO2 and NOx values were low, as expected - Again, given the low level NOx levels, given the low level NOx levels, these results did not show NO2 depletion for sampling sites 1, 2, and 3 (i.e., with TX Active pavement) *versus* 4, 5, and 6			
July 13, 2012 to August 1, 2012	- The upper NO2 values were ~9 ppb to13 ppb	- The lower NO2 values were ~9 ppb to12 ppb	- The upper NOx values were ~22 ppb to 30 ppb	- The lower NOx values were ~25 ppb to 30 ppb
	Conclusions: - With traffic on the highway at this time, the NO2 and NOx values were somewhat higher, although still below expected levels due to lower AADT density - Yet again, given the low level NOx levels, these results did not show NO2 depletion for sampling sites 1, 2, and 3 (i.e., with TX Active pavement) *versus* 4, 5, and 6			
August 1, 2012 to August 14, 2012	- The upper NO2 values were ~11 ppb to12 ppb	- The lower NO2 values were ~9 ppb to12 ppb	- The upper NOx values were ~22 ppb to 30 ppb	- The lower NOx values were ~25 ppb to 32 ppb
	Conclusions: - With traffic on the highway at this time, the NO2 and NOx values were higher, although essentially the same as had been seen for the last two weeks in July and still below expected levels due to continued lower AADT density - Once again, given the low level NOx levels, these results did not show NO2 depletion for sampling sites 1, 2, and 3 (i.e., with TX Active pavement) *versus* 4, 5, and 6			

Field Pavement Coupon Assessment

As mentioned within the Materials and Methods section, a set of test TX Active coupons were both embedded into the paved shoulder as well as fastened to the top of the adjacent crash barrier. In turn, intermittent, seasonal-based sampling of these coupons allows for a temporal characterization of aging, blinding, etc. impacts on the TX Active surface by which its photocatalytic reactivity is expected to decline with time. The following figures show these coupons as well as depicting the process by which they are physically embedded on a temporary, removable basis into the paved shoulder. Coupons removed in this fashion are then wrapped in protective foil to negate further photocatalytic reaction prior to subsequent bench-scale analysis to determine their current reactivity rates.

Figure 62. Coupon placement at both paved shoulder (nine each) and top of crash barrier locations (nine each)
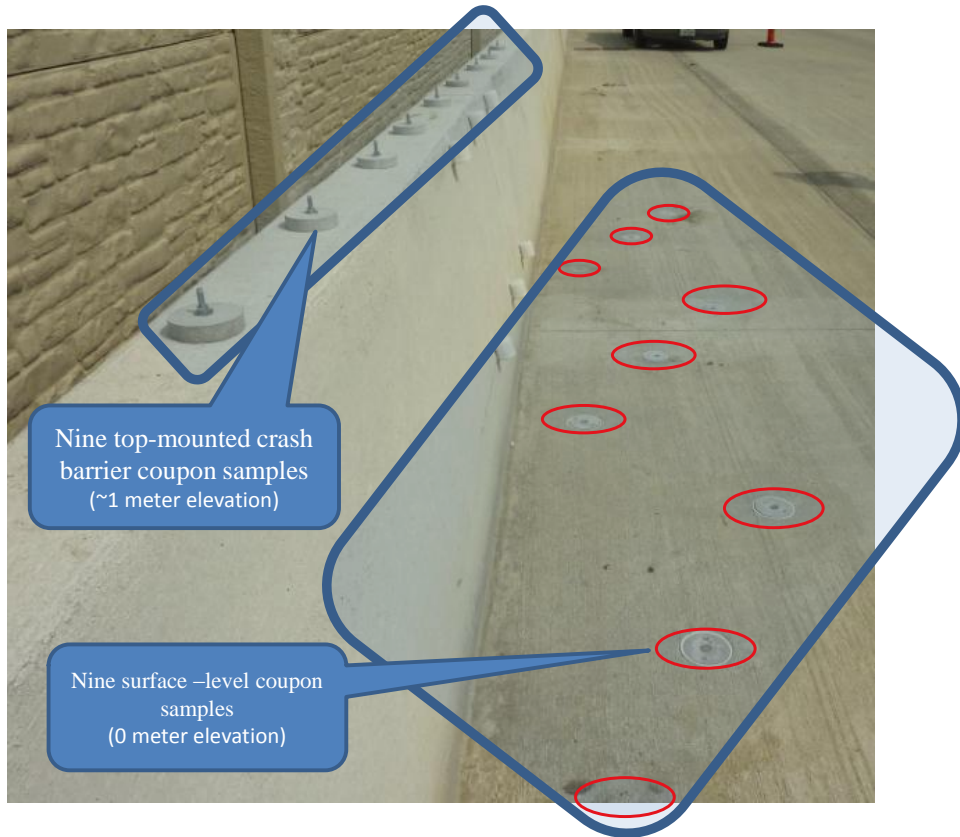
Figure 63. Coupon placement at both paved shoulder (nine each) and top of crash barrier (another nine each) locations

Figure 64. Closeup of coupon samples removed from paved shoulder locations

Figure 65. Coupon sample collection underway showing open pavement coupon mounting hole with accompanying mounting bolt

Figure 66. View of embedded coupon holder with mounting bolt

Figure 67. Preservative foil wrapping of coupon samples

Urban Heat Island Testing

Urban heat island instrumentation is a combination of thermocouples installed throughout the pavement systems, albedo measurements, and a full weather station. The instruments included within this weather station are a thermometer/relative humidity sensor (Campbell Scientifics CS215), pyranometer (Campbell Scientifics CS300), wind speed and direction sensor (RM Young 03002-5), and a tipping bucket rain gauge (Hydrological Services TB4). This sentry is shown attached to the vault behind the TX active section in Figure 68.

Figure 68. Tipping bucket rain gauge (left) and weather station (right)

All pressure sensors, including those in the weir boxes measure temperature which will be used to monitor water temperature through the installation. Figure 69 shows the thermocouple wire locations in the TX Active concrete pavement and shoulder and Figure 70 shows the control section thermocouple wire locations. The wires used were T-wire thermocouple wire.
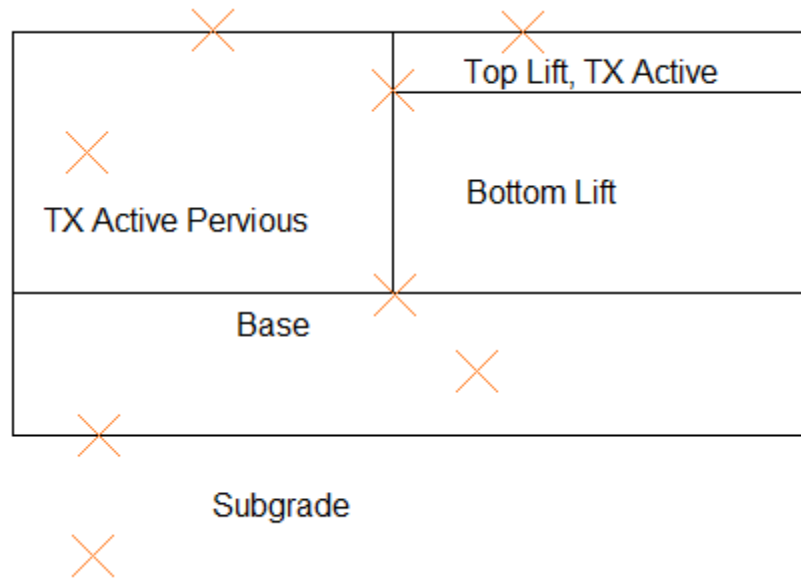
Figure 69. Cross section of TX Active section with locations of thermocouple wires, denoted by X (not to scale)
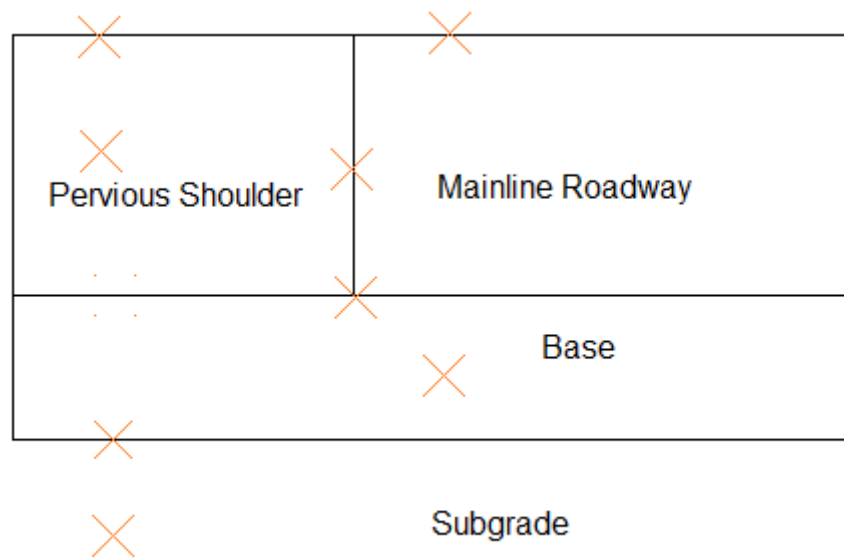

Figure 70. Cross section of TX Active section with locations of thermocouple wires, denoted by X (not to scale)

Initial solar reflectance was determined according to ASTM E1918 using the dual pyranometer (Campbell Scientific CMP3) setup (Figure 71). Initial testing was performed just prior to the road opening and visually the surface contained a significant amount of soil from construction. It is anticipated that all albedo values will increase after a flushing rain event. The initial albedo

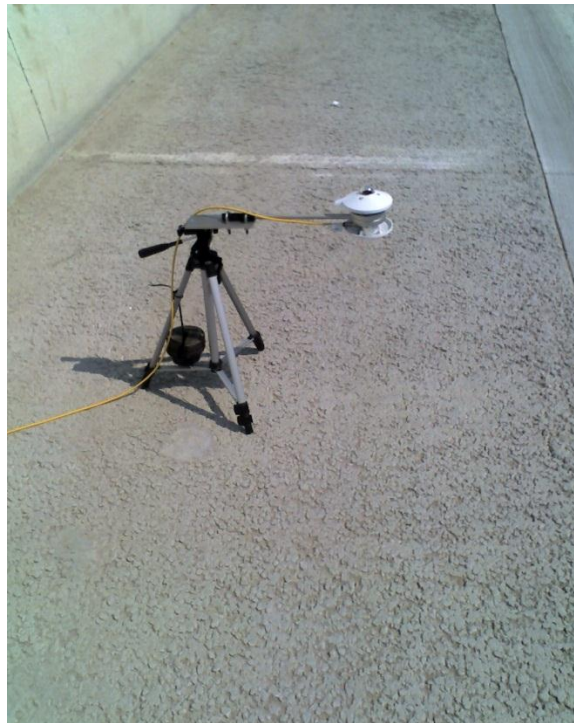results are shown in Table 10. Both TX Active sections had higher reflectance than the control section.

Figure 71. Albedometer used for initial reflectance measurements

Table 10. Albedometer measurements

Location	Albedo
TX Active Roadway	0.33
Control Roadway	0.31
TX Active Pervious Shoulder	0.33
Control Pervious Shoulder	0.29

SUMMARY

The following narrative details cover the summary highlights for this project:

1. Construction with this innovative highway has been finished, and the road was opened for public use on 14 July 2012.

2. Our extensive setup with field water sampling equipment is in place, such that leachate and runoff sample collection from both the TX Active and control pavement sections is ongoing.

3. Our similarly extensive set of field air sampling equipment is also in place, such that both passive and active air monitoring of NOx levels from both the TX Active and control pavement sections is ongoing.

4. Our similarly extensive set of field pavement and meteorological sampling equipment is also in place to capture site temperature, rainfall, wind speed and direction, etc. conditions.

5. Field results are now being collected which track water, air, and test coupon performance. Two months of passive Ogawa air quality testing has been completed prior to opening the highway, where this data serves as a baseline for comparison with findings observed during highway operation.

6. Extensive lab testing has also been completed, and also continues in support of incoming new coupon tests. Multiple tests have been completed with lab-scale photoreactor studies. These latter lab tests were used to quantify the expected photoreactivity of the employed TX Active materials on a specific basis (i.e., rate of NOx removal per unit surface area). In addition, these lab tests have involved fundamental assessments of related photocatalytic mechanisms in terms of reactant consumption relative to product formation under standard and non-standard (e.g., reduced temperature) environmental conditions.

7. As of the date of this Final Report I publication, the speed limit along the highway temporarily remains limited to 30 MPH…at which point traffic density on the highway remains low.

8. Commensurate with the latter, reduced AADT levels, current vehicle emission and ambient NO_2 levels (i.e., measured with the Ogawa samples) during the first month of highway operation have been sizably lower than expected, in the neighborhood of ~10 ppb, and NOx levels of ~30 ppb.

9. With these low AADT and low vehicle NOx emission levels, therefore, the observed TX Active reactivity has been similarly reduced to this point.

10. The latter circumstance of lower AADT, lower vehicle emission, and nominal TX Active reactivity will shortly change in sequential fashion, where escalating AADT will generate a substantial increase in NOx emission and, in turn, a far higher reactivity of the TX Active due to the higher reactant concentration gradient.

11. Placement and data collection with field traffic counters to obtain AADT levels is currently being started.

12. Parallel bench-scale testing of reactivity rates with representative TX Active specimens well suggests that the full-scale 141 highway will exhibit a significant level of NO_2 removal once traffic AADT levels escalate to expected levels and NO_2 emissions correspondingly increase.

13. In fact, lab-scale assessment of the potential reactivity rate of the employed TX Active material (i.e., at ambient NO2 levels in the 100 ppb range) *versus* expected vehicular emission rate essentially showed a ten-fold difference.

14. Only limited active testing of NO and NO_2 has as yet been conducted at the full-scale site using the 2B Technologies ozone depletion instrument. These results, though, were quite similar (i.e., with NO_2 levels in the single-digit level) to the previously observed field Ogawa results.

15. Testing of aged, on-site coupons is currently being started, for the first such set of six aged couples collected two weeks ago.

Lastly, the findings presented within this current (August 2012) Final Report I publication will be augmented with a forthcoming, August 2013 Final Report II edition which covers additional lab- and field-scale testing results for an upcoming additional year.

Appendices

The following appendices are included within this report:

A   Wind-Rose Patterns for St. Louis, Missouri and Related Project
    Site Selection Perspectives
B   Project National Steering Committee

REFERENCES

Asadi, S., Hassan, M. M., Kevern, J. T., and Rupnow, T. (2012). Development of Photocatalytic Pervious Concrete Pavement for Air and Stormwater Improvements. Transportation Research Record.

ASTM, Standard C-1754/1754M, "Standard Test Method for Density and Void Content of Hardened Pervious Concrete," Annual Book of ASTM Standards Vol. 4(2), ASTM International, West Conshohocken, PA: ASTM International, 2012.

Ballari, M. M., Hunger, M., Husken, G., and Brouwers, H. J. H. (2009). Heterogeneous Photocatalysis Applied to Concrete Pavement for Air Remediation. Nanotechnology in Construction 3, Proceedings, 409-414.

Ballari, M. M., Hunger, M., Husken, G., and Brouwers, H. J. H. (2010). NOx photocatalytic degradation employing concrete pavement containing titanium dioxide. Applied Catalysis B-Environmental, 95(3-4), 245-254. doi: 10.1016/j.apcatb.2010.01.002

Ballari, M. M., Yu, Q. L., and Brouwers, H. J. H. (2011). Experimental study of the NO and NO2 degradation by photocatalytically active concrete. Catalysis Today, 161(1), 175-180. doi: 10.1016/j.cattod.2010.09.028

Barmpass, P., Moussiopoulos, N., and Vlahocostas, C. (2006). De-Pollution Prediction Tool and Integrated Economic Assessment PICADA Project.

Beeldens, A. (2007, October 8-9). Air Purification by Road Materials: Results of the Test Project in Antwerp. Paper presented at the International RILEM Symposium on Photocatalysis, Environment and Construction Materials - TDP 2007, Florence, Italy.

Beeldens, A. (2008). Air purification by pavement blocks: final results of the research at the BRRC. Ljubljana, Slovenia.

Beeldens, A., Cassar, L., and Murata, Y. (2011). Applications of TiO2 Photocatalysis for Air Purification In Y. Ohama and D. Van Gemert (Eds.), Application of titanium Dioxide Photocatalysis to Construction Materials (1st ed.): Springer.

Berdahl, P., and Akbari, H. (2007). Evaluation of Titanium Dioxide as a Photocatalyst for Removing Air Pollutants

Bigi, A., and Harrison, R. M. (2010). Analysis of the air pollution climate at a central urban background site. Atmospheric Environment, 44(16), 2004-2012. doi: 10.1016/j.atmosenv.2010.02.028

Brauer, M., Hoek, G., Van Vliet, P., Meliefste, K., Fischer, P. H., Wijga, A., Brunekreef, B. (2002). Air pollution from traffic and the development of respiratory infections and asthmatic and allergic symptoms in children. American Journal of Respiratory and Critical Care Medicine, 166(8), 1092-1098. doi: DOI 10.1164/rccm.200108-007OC

Brunekreef, B., Janssen, N. A. H., deHartog, J., Harssema, H., Knape, M., and vanVliet, P. (1997). Air pollution from truck traffic and lung function in children living near motorways. Epidemiology, 8(3), 298-303.

Cable, J. K., and Frentress, D. P. (2004). Two-Life Portland Cement Concrete Pavements to Meet Public Needs. Ames, IA: Center for Portland Cement Concrete Pavement Technology.

Cape JN, Tang YS, van Dijk N, Love L, Sutton MA, Palmer SCF. Concentrations of ammonia and nitrogen dioxide at roadside verges, and their contribution to nitrogen deposition. Environmental Pollution 2004; 132: 469-478.

Carp, O., Huisman, C. L., and Reller, A. (2004). Photoinduced reactivity of titanium dioxide. [Review]. Progress in Solid State Chemistry, 32(1-2), 33-177. doi: 10.1016/j.progsolidstchem.2004.08.001

Cassar, L. (2004). Photocatalysis of cementitious materials: Clean buildings and clean air. [Article]. Mrs Bulletin, 29(5), 328-331.

Chen, M., and Chu, J. W. (2011). NO(x) photocatalytic degradation on active concrete road surface - from experiment to real-scale application. [Article]. Journal of Cleaner Production, 19(11), 1266-1272. doi: 10.1016/j.jclepro.2011.03.001

City Concept. (2004). D-NOx: The concrete paving block for atmospheric purification Tessenderlo, Belgium.

Clean Air Act, 42 U.S.C. § 7401 et seq. (2008).

Crouch, L., Pitt, J., and Hewitt, A. "Aggregate Effects on Pervious Portland Cement Concrete Static Modulus of Elasticity," Journal of Materials in Civil Engineering, Vol. 19, No. 7, 2007.

Dalton, J. S., Janes, P. A., Jones, N. G., Nicholson, J. A., Hallam, K. R., and Allen, G. C. (2002). Photocatalytic oxidation of NOx gases using TiO2: a surface spectroscopic approach. Environmental Pollution, 120(2), 415-422. doi: 10.1016/s0269-7491(02)00107-0

Delatte, N. "Structural Design of Pervious Concrete Pavements," Transportation Research Board Annual Meeting, TRB 2007 Annual Meeting CD, 16pg.

Demeestere, K., Dewulf, J., De Witte, B., Beeldens, A., and Van Langenhove, H. (2008). Heterogeneous photocatalytic removal of toluene from air on building materials enriched with TiO2. Building and Environment, 43(4), 406-414. doi: 10.1016/j.buildenv.2007.01.016

Dylla, H., Hassan, M. M., Mohammad, L. N., Rupnow, T., and Wright, E. (2010). Evaluation of Environmental Effectiveness of Titanium Dioxide Photocatalyst Coating for Concrete Pavement. Transportation Research Record(2164), 46-51. doi: 10.3141/2164-06

Dylla, H., Hassan, M. M., Schmitt, M., Rupnow, T., and Mohammad, L. N. (2011a). Laboratory Investigation of the Effect of Mixed Nitrogen Dioxide and Nitrogen Oxide Gases on Titanium Dioxide Photocatalytic Efficiency in Concrete Pavements. Journal of Materials in Civil Engineering, 23(7), 1087-1093. doi: 10.1061/(asce)mt.1943-5533.0000248

Dylla, H., Hassan, M. M., Schmitt, M., Rupnow, T., Mohammad, L. N., and Wright, E. (2011b). Effects of Roadway Contaminants on Titanium Dioxide Photodegradation of NOx. Paper presented at the Transportation Research Board 90th Annual Meeting, Washington, DC.

Essroc. TX Active, Photocatalytic Concrete Technology. Essroc, Italcementi Group, Bergamo, Italy, 2009.

Finkelstein, M. M., Jerrett, M., and Sears, M. R. (2004). Traffic air pollution and mortality rate advancement periods. American Journal of Epidemiology, 160(2), 173-177. doi: Doi 10.1093/Aje/Kwh181

Frank, S. N., and Bard, A. J. (1977). Heterogeneous Photocatalytic Oxidation of Cyanide Ion in Aqueous-Solutions at Tio2 Powder. Journal of the American Chemical Society, 99(1), 303-304.

Fujishima, A., and Honda, K. (1972). Electrochemical Photolysis of Water at a Semiconductor Electrode. [10.1038/238037a0]. Nature, 238(5358), 37-38.

Fujishima, A., and Zhang, X. T. (2006). Titanium dioxide photocatalysis: present situation and future approaches. Comptes Rendus Chimie, 9(5-6), 750-760. doi: DOI 10.1016/j.crci.2005.02.055

Fujishima, A., Hashimoto, K., and Watanabe, T. (1999). TiO2 photo catalysis: fundamentals and applications. Tokyo: BKC, Inc.

Fujishima, A., Rao, T. N., and Tryk, D. A. (2000). Titanium dioxide photocatalysis. Journal of Photochemistry and Photobiology C: Photochemistry Reviews, 1(1), 1-21. doi: 10.1016/s1389-5567(00)00002-2

Fujishima, A., Zhang, X. T., and Tryk, D. A. (2008). TiO(2) photocatalysis and related surface phenomena. [Review]. Surface Science Reports, 63(12), 515-582. doi: 10.1016/j.surfrep.2008.10.001

Garshick, E., Laden, F., Hart, J. E., and Caron, A. (2003). Residence near a major road and respiratory symptoms in US veterans. Epidemiology, 14(6), 728-736. doi: DOI 10.1097/01.ede.0000082045.50073.66

Grant, R. H., and Slusser, J. R. (2005). Estimation of ultraviolet-A irradiance from measurements of 368-nm spectral irradiance. Journal of Atmospheric and Oceanic Technology, 22(12), 1853-1863. doi: 10.1175/jtech1823.1

Guerrini, G. L., and Peccati, E. (2007, October 8-9). Photocatalytic Cementitious Roads for Depollution. Paper presented at the International RILEM Symposium on Photocatalysis, Environment and Construction Materials - TDP 2007, Florence, Italy.

Hagenbjörk-Gustafsson A, Eriksson K, Forsberg B. Field Evaluation of the Ogawa Diffusive Sampler for NO2/ NOX in a Cold Climate. Epidemiology 2009; 20: S161 10.1097/01.ede.0000362548.83420.d7.

Hall, K., Dawood, D., Vanikar, S., Tally, R., Cackler, T., Correa, A, Voigt, G. (2007). Long-Life Concrete PAvements in Europe and Canda: Federal Highway Administration.

Hassan, M. M., and Okeil, A. (2011). Field and Laboratory Investigation of Photocatalytic Pavements: Final Report. Baton Rouge, LA: Gulf Coast REsearch Center for Evacuation and Transportation Resiliency.

Hassan, M. M., Dylla, H., Mohammad, L. N., and Rupnow, T. (2010a, April). Durability of Titanium Dioxide Photocatalytic Layer for Pavement Surfaces. Paper presented at the 46th Annual Conference of the Associated Schools of Construction, Boston, Massachusetts.

Hassan, M. M., Dylla, H., Mohammad, L. N., and Rupnow, T. (2010b). Effect of Application Methods on the Effectiveness of Titanium Dioxide as a Photocatalyst Compound to Concrete Pavement. Paper presented at the Transportation Research Board 89th Annual Meeting, Washington, D.C.

Hagenbjörk-Gustafsson A, Eriksson K, Forsberg B. Field Evaluation of the Ogawa Diffusive Sampler for NO_2/ NO_X in a Cold Climate. Epidemiology 2009; 20: S161 10.1097/01.ede.0000362548.83420.d7.

Hassan, M. M., Dylla, H., Mohammad, L. N., and Rupnow, T. (2010c). Evaluation of the durability of titanium dioxide photocatalyst coating for concrete pavement. Construction and Building Materials, 24(8), 1456-1461. doi: 10.1016/j.conbuildmat.2010.01.009

HEI. Traffic-Related Air Pollution: A Critical Review of the Literature on Emissions, Exposure, and Health Effects. Health Effects Institute, Boston, MA, 2009.

Herrmann, J. M. (1999). Heterogeneous photocatalysis: fundamentals and applications to the removal of various types of aqueous pollutants. Catalysis Today, 53(1), 115-129.

Herrmann, J. M., Péruchon, L., Puzenat, E., and Guillard, C. (2007, October 8-9). Photocatalysis: from fundamentals to self-cleaning glass applications. Paper presented at the International RILEM Symposium on Photocatalysis, Environment and Construction Materials - TDP 2007, Florence, Italy.

Husken, G., and Brouwers, H. J. H. (2008, June 16-20). Air purification by cementitious materials: Evaluation of air purifying properties. Paper presented at the International Conference on Construction and Building Technology, Kuala Lumpur, Malaysia.

Husken, G., Hunger, M., and Brouwers, H. J. H. (2009). Experimental study of photocatalytic concrete products for air purification. Building and Environment, 44(12), 2463-2474. doi: 10.1016/j.buildenv.2009.04.010

Hwang, S., Lee, M. C., and Choi, W. (2003). Highly enhanced photocatalytic oxidation of CO on titania deposited with Pt nanoparticles: kinetics and mechanism. Applied Catalysis B-Environmental, 46(1), 49-63. doi: 10.1016/s0926-3373(03)00162-0

IADOT. Traffic Flow Map of Ames C Story County, 2007 Annual Average Daily Traffic. Iowa Department of Transportation, Ames, IA, 2007. [Cited: May 4, 2011] http://www.iowadot.gov/maps//msp/traffic/2007/cities/amesc.pdf.

Ibusuki, T., and Takeuchi, K. (1994). Removal of Low Concentration Nitrogen Oxides Through Photoassisted Heterogenous Catalysis. Journal of Molecular Catalysis, 88(1), 93-102. doi: 10.1016/0304-5102(93)e0247-e

ISO. (2007). Fine ceramics (advanced ceramics, advanced technical ceramics)--Test method for air-purification performance of semiconducting photocatalytic materials--Part 1: Removal of nitric oxide. (ISO 22197-1:2007(E)). Geneva, Switzerland.

Italcementi. TX Active, The Photocatalytic Active Principle, Technical Report. Italcementi, Bergamo, Italy, 2009.

Jacoby, W. A., Blake, D. M., Noble, R. D., and Koval, C. A. (1995). KINETICS OF THE OXIDATION OF TRICHLOROETHYLENE IN AIR VIA HETEROGENEOUS PHOTOCATALYSIS. Journal of Catalysis, 157(1), 87-96. doi: 10.1006/jcat.1995.1270

JIS. (2010). Fine ceramics (advanced ceramics, advanced technical ceramics)--Test method for air-purification performance of semiconducting photocatalytic materials--Part 1: Removal of nitric oxide. (JIS R 1701-1:2010). Tokyo, Japan.

Kevern, J. T., Wang, K., and Schaefer, V. R. "Evaluation of Pervious Concrete Workability Using Gyratory Compaction." American Society of Civil Engineers Journal of Materials in Civil Engineering, Vol.21, No. 12, Dec, 2009.

Kevern, J.T. "Using Soybean Oil to Improve the Durability of Concrete Pavements," International Journal of Pavement Research and Technology, Sustainable Concrete Pavements Special Edition, V.3, No. 5, Sept. 2010.

Kevern, J.T. "Operation and Maintenance of Pervious Concrete Pavements," 90th Annual Transportation Research Board Annual Meeting, Washington D.C., Jan 23-27, 2011.

Kevern, J.T. and Farney, C. "Reducing Curing Requirements for Pervious Concrete Using a Superabsorbent Polymer for Internal Curing." Transportation Research Record: Journal of the Transportation Research Board (TRB), Construction 2012, Transportation Research Board of the National Academies, Washington D.C. (accepted for publication)

Kim, J. J., Smorodinsky, S., Lipsett, M., Singer, B. C., Hodgson, A. T., and Ostro, B. (2004). Traffic-related air pollution near busy roads - The East Bay childrens respiratory health study. American Journal of Respiratory and Critical Care Medicine, 170(5), 520-526. doi: DOI 10.1164/rccm.200403-2810C

Kumar, P., Dushenkov, V., Motto, H., and Raskin, I. (1995). Phytoextraction – The Use of Plants to Remove Heavy Metals from Soils. Environmental Science and Technology, 29(5), 1232-1238. doi: 10.1021/es00005a014

Lim, T. H., Jeong, S. M., Kim, S. D., and Gyenis, J. (2000). Photocatalytic decomposition of NO by TiO2 particles. Journal of Photochemistry and Photobiology a-Chemistry, 134(3), 209-217. doi: 10.1016/s1010-6030(00)00265-3

MECA. (2007). Frequently Asked Questions about the Installation of Emission Control Technology on Existing Diesel Engines Washington, D.C.: Manufacturers of Emission Controls Association Retrieved from http://www.meca.org/galleries/default-file/diesel%20retrofit%20FAQ%200507.pdf.

Mukerjee S, Oliver KD, Seila RL, Jacumin Jr HH, Croghan C, Daughtrey Jr EH, et al. Field comparison of passive air samplers with reference monitors for ambient volatile organic compounds and nitrogen dioxide under week-long integrals. Journal of Environmental Monitoring 2009; 11: 220-227.

Murata, Y., and Tobinai, K. (2002). Influence of various factors on NOx removal performance of permeable interlocking block based on photocatalysis. Journal of Structural and Construction Engineering(Transactions of AIJ)(555), 9-15.

Murata, Y., Kamitani, K., and Takeuchi, K. (2000). Air Purifying Blocks Based on Photocatalysis. Paper presented at the Japan Interlocking BLock Pavement Engineering Association World Congress 2000, Tokyo, Japan.

Murruni, L., Conde, F., Leyva, G., and Litter, M. I. (2008). Photocatalytic reduction of Pb(II) over TiO(2): New insights on the effect of different electron donors. [Article]. Applied Catalysis B-Environmental, 84(3-4), 563-569. doi: 10.1016/j.apcatb.2008.05.012

Obee, T. N., and Brown, R. T. (1995). TIO2 Photocatalysis for Indoor Air Applications – Effects of Humidity and Trace Contaminant Levels on the Oxidation Levels of the Oxidation Rates of Formaldehye, Toluene, and 1,3-Butadiene. Environmental Science and Technology, 29(5), 1223-1231. doi: 10.1021/es00005a013

Ohama, Y., and Van Gemert, D. (2011). Introduction. In Y. Ohama and D. Van Gemert (Eds.), Application of titanium Dioxide Photocatalysis to Construction Materials (1st ed.): Springer.

Ohno, T., Sarukawa, K., Tokieda, K., and Matsumura, M. (2001). Morphology of a TiO2 photocatalyst (Degussa, P-25) consisting of anatase and rutile crystalline phases. [Article]. Journal of Catalysis, 203(1), 82-86. doi: 10.1006/jcat.2001.3316

Osborn, D., Hassan, M. M., and Dylla, H. (2012). Quantification of NOX reduction via Nitrate Accumulation on a TiO2 Photocatalytic Concrete Pavement. Transportation Research Record(??), ??

Overman, H. T. J. (2009). Simulation model for NOX distributions in a street canyon with air purifying pavement. (Master: Civil Engineering and Management), University of Twente, Eschede, Netherlands.

Paz, Y. (2010). Application of TiO2 photocatalysis for air treatment: Patents overview. Applied Catalysis B-Environmental, 99(3-4), 448-460. doi: 10.1016/j.apcatb.2010.05.011

Peral, J., and Ollis, D. F. (1992). Heterogenous Photocatalytic Oxidation of Gas-Phase Organics for Air Purification – Acentone, 1-Butanol, Butyraledhyde, Formaldehyde, and Meta-Xylen Oxidation. Journal of Catalysis, 136(2), 554-565. doi: 10.1016/0021-9517(92)90085-v

PICADA. (2011). Guideline for end-users, GROWTH Project GRD1-2001-40449.

Poon, C. S., and Cheung, E. (2007). NO removal efficiency of photocatalytic paving blocks prepared with recycled materials. Construction and Building Materials, 21(8), 1746-1753. doi: 10.1016/j.conbuildmat.2006.05.018

Primary National Ambient Air Quality Standards for Nitrogen Dioxide: Final Rule, 75 Fed. Reg. 6474 (2010), (to be codified at 40 C.F.R. pts. 50 and 58).

Rousseau, P., Drouadaine, I., Maze, M., Vaton,G., Souprayen, C., and Tripathi, A. (2009). Impact du procédé NOxer sur la dispersion atmosphérique de NOx issus du trafic routier, EUROVIA Centre de Recherche Poster Presentation, Saint-Denis, France.

Sather M, Slonecker E, Mathew J, Daughtrey H, Williams D. Evaluation of ogawa passive sampling devices as an alternative measurement method for the nitrogen dioxide annual standard in El Paso, Texas. Environmental Monitoring and Assessment 2007; 124: 211-221-221.

Sclafani, A., and Herrmann, J. M. (1996). Comparison of the photoelectronic and photocatalytic activities of various anatase and rutile forms of titania in pure liquid organic phases and in aqueous solutions. Journal of Physical Chemistry, 100(32), 13655-13661. doi: 10.1021/jp9533584

Sikkema, J. K., Alleman, J. E., Ong, S. K., Koziel, J. A., Taylor, P. C., and Bai, H. (2012, September 18-21). Photocatalytic Concrete Pavements: Decrease in NOX Oxidation due to Reaction Product Blinding. Paper presented at the International Conference on Long-Life Concrete Pavement-2012, Seattle, Washington.

Stone, W., Jonas, J., Grytza, S.P., Alleman, J., Kevern, J.T., Brooks, J.L., and Hilton, N.R. Route 141 Environmentally Friendly Project: MoDOT Green Road Initiative Project. Presented at MO/KS Chapter, ACPA 32nd Annual Portland Cement Concrete Paving Conference, Kansas City, MO, 2012.

Strini, A., Cassese, S., and Schiavi, L. (2005). Measurement of benzene, toluene, ethylbenzene and o-xylene gas phase photodegradation by titanium dioxide dispersed in cementitious materials using a mixed flow reactor. Applied Catalysis B-Environmental, 61(1-2), 90-97. doi: 10.1016/j.apcatb.2005.04.009

The Cadmus Group, I. (2009). Nutrient Control Design Manual: State of Technology Review Report.

Thoma, E. D., Shores, R. C., Isakov, V., and Baldauf, R. W. (2008). Characterization of near-road pollutant gradients using path-integrated optical remote sensing. Journal of the Air and Waste Management Association, 58(7), 879-890. doi: Doi 10.3155/1047-3289.58.7.879

Tompkins, D. T., Lawnicki, B. J., Zeltner, W. A., and Anderson, M. A. (2005). Evaluation of photocatalysis for gas-phase air cleaning - Part 1: Process, technical, and sizing considerations. Ashrae Transactions 2005, Vol 111, Pt 2, 111, 60-84.

UNI. (2007). (UNI 1247:2007). Milan, Italy.

USEPA. (1994). Environmental Fact Sheet: Air Toxics from Motor Vehicles. (EPA400-F-92-004). Washington, D.C.

USEPA. (2001). National Air Quality and Emissions Trends Report, 1999. (EPA 454/R-01-004). Washington, D.C.

USEPA. (2006). The Master List of Compounds Emitted by Mobile Sources - 2006. (EPA420-B-06-002).

USEPA. (2007). Summary of Current and Historical Light-Duty Vehicle Emission Standards. Washington, D.C.: Retrieved from http://www.epa.gov/greenvehicles/detailedchart.pdf.

USEPA. (2009). National Primary Drinking Water Regulations. (EPA 816-F-09-004). Washington, D.C.

USEPA. (2010a). Design Values (Average 1-Hour 98th Percentiles over 3 Years) by County for Nitrogen Dioxide Research Triangle Park, NC: Retrieved from http://www.epa.gov/oaqps001/nitrogenoxides/pdfs/NO2_final_designvalues_0608_Jan22.pdf.

USEPA. (2010b). Fact Sheet: Final Revisions to the National Ambient Air Quality Standards for Nitrogen Dioxide. Research Triangle Park, NC: Retrieved from http://www.epa.gov/oaqps001/nitrogenoxides/pdfs/20100122fs.pdf.

USEPA. (2010c). Final Regulatory Impact Analysis (RIA) for the NO2 National Ambient Air QUality Standards (NAAQS). Research Triangle Park, NC: Retrieved from http://www.epa.gov/ttnecas1/regdata/RIAs/FinalNO2RIAfulldocument.pdf.

USEPA. (2011a, July 6). Ground-level Ozone: Basic Information Retrieved September 27, 2011, from http://www.epa.gov/groundlevelozone/basic.html

USEPA. (2011b, July 6). Nitrogen Dioxide: Health Retrieved September 27, 2011, from http://www.epa.gov/air/nitrogenoxides/health.html

USEPA. (2012a, July 20). Green Vehicle Guide: Frequent Questions Retrieved July 20, 2012, from http://www.epa.gov/greenvehicles/Faq.do

USEPA. (2012b, July 5). Heavy-Duty Highway Compression-Ignition Engines And Urban Buses -- Exhaust Emission Standards Retrieved July 19, 2012, from http://epa.gov/oms/standards/heavy-duty/hdci-exhaust.htm

USEPA. (2012c). "Polluted Runoff (non-point source pollution)" Basic Information Retrieved March 16, 2012, from http://www.epa.gov/owow_keep/NPS/whatis.html

Vardoulakis, S., Fisher, B. E. A., Pericleous, K., and Gonzalez-Flesca, N. (2003). Modelling air quality in street canyons: a review. Atmospheric Environment, 37(2), 155-182. doi: 10.1016/s1352-2310(02)00857-9

Wang, Y. J., DenBleyker, A., McDonald-Buller, E., Allen, D., and Zhang, K. M. (2011). Modeling the chemical evolution of nitrogen oxides near roadways. Atmospheric Environment, 45(1), 43-52. doi: 10.1016/j.atmosenv.2010.09.050

Watts, M. J., and Cooper, A. T. (2008). Photocatalysis of 4-chlorophenol mediated by TiO(2) fixed to concrete surfaces. Solar Energy, 82(3), 206-211. doi: 10.1016/j.solener.2007.08.001

Yu, J. C. (2002). Ambient Air Treatment by Titanium Dioxide (TiO2) Based Photocatalyst in Hong Kong Hong Kong.

Yu, J. C. (2003). Deactivation and Regeneration of Environmentally Exposed Titanium Dioxide (TiO2) Based Products Hong Kong.

Zhao, J., and Yang, X. D. (2003). Photocatalytic oxidation for indoor air purification: a literature review. Building and Environment, 38(5), 645-654. doi: 10.1016/s0360-1323(02)00212-3

Zhao, Y., Han, J., Shao, Y., and Feng, Y. (2009). Simultaneous SO(2) and NO removal from flue gas based on TiO(2) photocatalytic oxidation. Environmental Technology, 30(14), 1555-1563. doi: 10.1080/09593330903313786

APPENDIX A

**Wind-Rose Patterns for St. Louis, Missouri
and Related Project Site Selection Perspectives**

Overview:

Matching the directional alignment of the project paving sections with the regional wind rose patterns was originally considered while evaluating how the air-sample collection effort might be optimized. As can been seen in the wind-rose data given below, however, the prevailing winds in the St. Louis area change considerably in both their direction and speed during the course of a year…to the point where there really is not an optimal road alignment for this upcoming sampling effort.
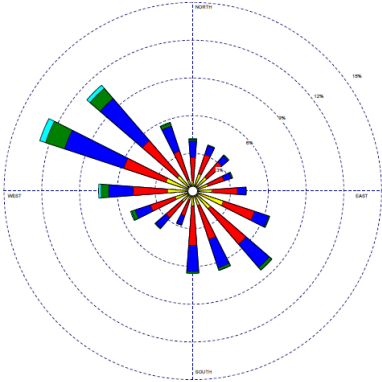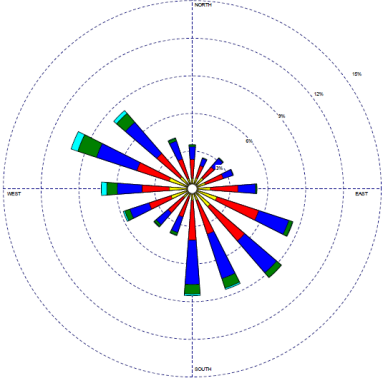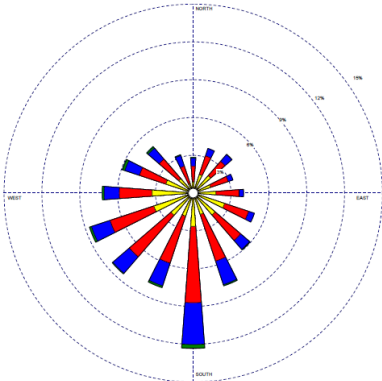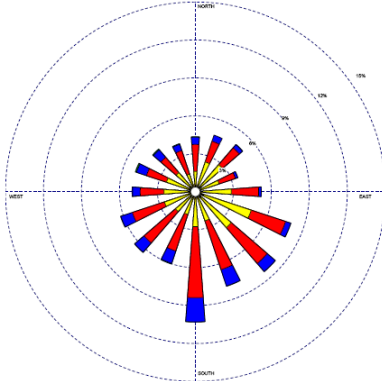
During cold weather months (e.g., see February below), it would appear that the wind typically passes from the northwest to the southeast, and that there is less directional variation throughout the month. The colder months also appear to have the highest wind speeds.

During warmer months (i.e., see August on the following page), wind speeds tend to be lower and more spread out in terms of direction. The dominant wind direction during warmer summer months appears to be from the south.

Prior near-road NO_2 testing conducted by the US EPA, has also shown that there is considerable traffic-induced turbulence of the air mass, and contaminants, immediately overlying a high-traffic urban highway (Baldauf, 2009). Taking into account this vehicle-induced turbulence with the seasonal variability of wind direction and speed, and also factoring in the time-integrative nature of Ogawa-type passive NO_2 sampling, the concluding sense of this issue is that factoring wind direction into a decision about road alignment is probably an unnecessary step. Even then, there is little if any precedent in the literature where other researchers have made attempts to match the placement or on-off manipulation of air sampling equipment with ambient wind direction,

Wind Rose Plots: (see URL:
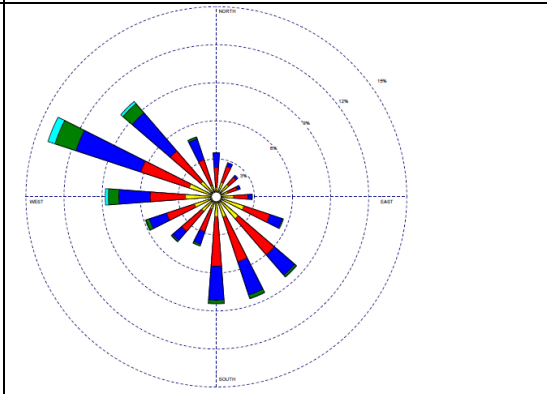*http://www.isws.illinois.edu/atmos/statecli/Roses/wind_climatology.htm*)

Month	Wind-Rose Plot	Prevailing Wind Direction
February		Predominantly from the northwest
April		From the northwest…but also from the southeast
June		Predominantly from the south
August		Predominantly from the south to southeast
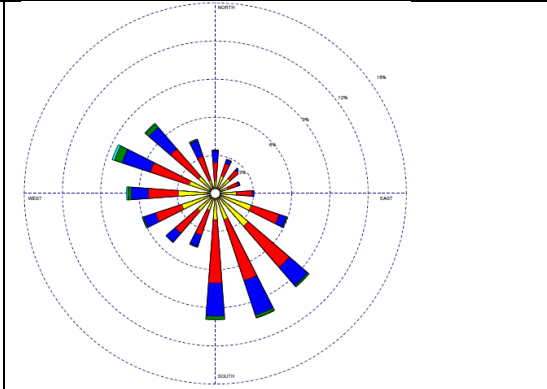
October		Predominantly from the south to southeast
December		Predominantly from the west-northwest

APPENDIX B

_____

<center>

Project National Steering Committee

</center>

_____

<center>

(24 current members)

</center>

FHWA (4 each):	• **Suneel Vanikar**, Office of Pavement Technology FHWA Office of Pavement Technology HIPT-20, Washington, DC 20590 Phone: 202- 366-0120 Email: suneel.vanikar@dot.gov • **Gina Ahlstrom**, Office of Pavement Technology Email: gina.ahlstrom@dot.gov • **Victoria Martinez**, Office of Natural Environment Email: victoria.martinez@ dot.gov • **Dawn Perkins**, Missouri Division Email: dawn.perkins@dot.gov	_suneel.vanikar@dot.gov;_ _gina.ahlstrom@dot.gov;_ _victoria.martinez@dot.gov;_ _dawn.perkins@dot.gov_
US EPA (3 each):	• **Laura Bachle** bachle.laura@epamail.epa.gov • Dr. **Rich Baldauf**, US EPA – Risk Management Air Research, EPA Office of Research and Development, National Risk Management Laboratory, Air Pollution Prevention and Control Division (APPCD), Emissions Characterization and Prevention Branch (ECPB) Office: 919-541-4386 Email: baldauf.richard@epa.gov • **Lisa Hair, PE** Room 7333E EPA West **Mailing address for items sent via US Mail:** US EPA Office of Water (4503-T) 1200 Pennsylvania Avenue, N.W. Washington, D.C. 20460	_bachle.laura@epamail.epa.gov;_ _baldauf.richard@epa.gov;_ _hair.lisa@epa.gov;_

<center>

97

</center>

	Actual address: USEPA Office of Water (4503-T) 1301 Constitution Avenue, N.W. Room 7424 Washington, D.C. 20004 Phone: 202-566-1043 Fax: 202-566-1332 Email: hair.lisa@epa.gov	
Missouri DOT (3 each):	• **Bill Stone, PE** Organizational Performance Administrator, MoDOT Phone: 573-526-4328 Email: william.stone@modot.mo.gov • **Nancy Leroney** Email: *nancy.leroney@modot.mo.gov* • **Brett Trautman** Email: brett.trautman@modot.mo.gov	*william.stone@modot.mo.gov;* *brett.trautman@modot.mo.gov;* *nancy.leroney@modot.mo.gov*
Missouri DNR (2 each)	• **Steven Hall** Air Quality Monitoring Phone: 573-751-8406 Email: stephen.hall@dnr.mo.gov • **Jerry Downs** Near Roadway NO_2 Ambient Air Monitoring Email: jerry.downs@dnr.mo.gov • **Curtis Gately**, Chief NPDES Permits Unit Water Protection Program Phone: (573) 526-1155 Email: curtis.gateley@dnr.mo.gov	*stephen.hall@dnr.mo.gov;* *jerry.downs@dnr.mo.gov;* *curtis.gateley@dnr.mo.gov;*
Essroc Italcementi Group (3 each)	• **Dan Schaffer** Email: dan.schaffer @essroc.com • **Steve Grytza**, Territory Manager Email: steven.grytza@essroc.com • **Gian Luca Guerrini**, Direzione Innovazione, Italcementi Group Email: g.guerrini@itcgr.net	*dan.schaffer@essroc.com;* *steven.grytza@essroc.com;* *g.guerrini@itcgr.net;*
Lehigh Hanson (Heidelberg	• **Lori Tiefenthaler**, VP Sustainability and Marketing Communications Email: lori.tiefenthaler@lehighhanson.com	*lori.tiefenthaler@lehighhanson.com;* *mojohnson@lehighcement.com;*

Cement Group) (3 each)	• **Morgan Johnson**, Technical Services Representative Email: mojohnson@lehighcement.com • **Wolfgang Dienemann**, Director Global Research and Development Heidelberg Cement Technology Center Email: Wolfgang.Dienemann@htc-gmbh.com;	*wolfgang.dienemann@htc-gmbh.com;*
Fred Weber, Inc.	• **Justin Brooks**, Senior Project Manager Construction Services Phone: 314-792-6931 Email: jlbrooks@fredweberinc.com	*jlbrooks@fredweberinc.com*
Iowa State University and CP Tech Center (InTrans) (5 each)	• Dr. **James Alleman**, ISU Email: jea@iastate.edu • Dr. **Say Kee Ong**, ISU Email: skong@iastate.edu • Dr. **Peter Taylor**, National Concrete Pavement Technology Center, ISU Email: ptaylor@iastate.edu • **Tom Cackler**, National Concrete Pavement Technology Center, ISU Email: tcackler@iastate.edu • **Joel Sikkema**, ISU Doctoral Candidate Email: jsikkema@iastate.edu	*jea@iastate.edu;* *skong@iastate.edu;* *ptaylor@iastate.edu;* *tcackler@iastate.edu;* *jsikkema@iastate.edu;*
University of Missouri – Kansas City School of Computing and Engineering	• Dr. **John Kevern** UMKC School of Computing and Engineering University of Missouri – Kansas City 370H Flarsheim Hall, 5100 Rockhill Road Kansas City, MO 64110 Phone: 816-235-5977 Email: kevernj@umkc.edu	*kevernj@umkc.edu*